UNIVERSITY OF CALIFORNIA SAN DIEGO

Comparing Different Formulations for Delivering Arginine Deiminase Drug

A dissertation submitted in partial satisfaction of the
requirements for the degree Doctor of Philosophy

in

NanoEngineering

by

Li-Chang Chen

Committee in charge:

Professor Sadik Esener, Chair
Professor Yi Chen
Professor Michael Heller
Professor Yu-Hwa Lo
Professor Shankar Subramaniam

2019

The Dissertation of Li-Chang Chen is approved, and it is acceptable in quality and form for publication on microfilm and electronically:

_____

_____

_____

_____

_____

Chair

University of California San Diego

2019

DEDICATION

I dedicate this dissertation to my mother, my father, and my sister for their endless support, encouragements, and love. To my grandpa, Aunt Angel, and Uncle Kenny for always believe in me and support my decisions. Lastly, to my future wife and family.

EPIGRAPH

There's Plenty of Room at the Bottom
-Richard Feynman

TABLE OF CONTENTS

LIST OF FIGURES

ACKNOWLEDGEMENTS

I would like to acknowledge Professor Sadik Esener for his guidance and support throughout my graduate career. He gave me the opportunity to pursue a PhD in his group, while working at Polaris Pharmaceuticals, Inc. His willingness to allow me to collaborate with a pharmaceutical company is something that not all professors are willing to do. With his busy traveling schedule, he always made time to discuss any issues with the project that I was working on. The freedom he provided encouraged me to lead, design, and resolve any issues with my project. This was truly a tough experience that taught me to be an independent researcher. Professor Esener was always supportive of me in what I want to do in both academic and industry settings.

I would also like to thank the members of my committee: Professors Yi Chen, Michael Heller, Yu-Hwa Lo, and Shankar Subramaniam. They have provided invaluable suggestions and advice for my project and future career.

I would like to thank Polaris Pharmaceuticals, Inc. and their R&D team for their support. First and foremost, Bor-Wen Wu gave me the opportunity to work on this collaboration project and provided majority of the funding. Jim Thomson was always guiding and helping me with every aspect of my project, bringing his biophysics and biochemistry expertise. My team, Richard Showalter, Wei-Jong Shia, PhD, Wes Sission, and Derek Lee for their knowledge on biology, biochemistry, and the ADI drug. Bob Almassy for providing his expertise in the structure of enzymes. Richard Hickey for running all my animal study samples. Lastly, my co-workers at Polaris who made my work experience unforgettable.

I would like to acknowledge lab members in the Esener Lab: Ya-San Yeh, Mukanth Vaidyanathan, and Negin Mokhtari for being great mentors and teaching me all the ins and outs.

They also gave me lots of tips on surviving graduate school. Grace Chang, my undergraduate/intern, for helping me with many of my nanoparticle synthesis and comparison experiments.

Special thanks to Dana Jimenez for staying on top of all the administrative work that was involved throughout my graduate career, and for always reminding me and checking in on me. Dana truly made my graduate career at UCSD go smoothly. I want to thank Faith Buckley for always tracking down Professor Esener for me and working out all the logistics during my visit to OHSU. I do not think I could finish graduate school this smoothly without all the administrative work that Dana and Faith have done for me.

Of course, my high school friends and my San Diego friends for their support and encouragement throughout my graduate career. Listening to all the complaints, going through all the ups and downs with me. Thank you all for the laughter and fun the past 5 years. My tennis buddies for always being down to play tennis to de-stress. This has been a long journey, a memorable and unforgettable journey.

Last but not least, my family and relatives in Taiwan. Even though we are split by an ocean, thank you for your endless love and support throughout my life and the past 5 years. I could not have finished this dissertation without you guys!

Chapter 2, and its methods were developed and owned by Polaris Pharmaceuticals, Inc., San Diego, California. Collaborators for this development: Jason (Li-Chang) Chen, Richard Showalter, Wei-Jong Shia, Wes Sisson, Derek Lee, Bob Alamassy, and Jim Thomson. The dissertation author was the primary investigator and author of this material.

Chapter 3, and its methods were developed and owned by Polaris Pharmaceuticals, Inc., San Diego, California. Collaborators for this development: Jason (Li-Chang) Chen, Richard

Showalter, Wei-Jong Shia, Wes Sisson, Derek Lee, Bob Alamassy, and Jim Thomson. The dissertation author was the primary investigator and author of this material.

Chapter 4, and its methods are developed and owned by Ortac and Esener *et al*. from the University of California San Diego, La Jolla, California with a co-development with Polaris Pharmaceuticals, Inc., San Diego, California. Collaborators for this development: Jason (Li-Chang) Chen, Ya-San Yeh, Negin Mokhtari, Jim Thomson, and Sadik Esener. The dissertation author was the primary investigator and author of this material.

Chapter 5, and its methods are developed and owned by Vaidyanathan and Esener *et al*. from the University of California San Diego, La Jolla, California with a co-development with Polaris Pharmaceuticals, Inc., San Diego, California. Collaborators for this development: Jason (Li-Chang) Chen, Grace (Ting-Yu) Chang, Mukanth Vaidyanathan, Ya-San Yeh, Negin Mokhtari, Jim Thomson, and Sadik Esener. The dissertation author was the primary investigator and author of this material.

Chapter 6, and its methods were developed and owned by Polaris Pharmaceuticals Inc., San Diego, California. Collaborators for this development: Jason (Li-Chang) Chen, Grace (Ting-Yu) Chang, Richard Hickey, Ya-San Yeh, Mukanth Vaidyanathan, Jim Thomson, and Sadik Esener. The dissertation author was the primary investigator and author of this material.

VITA

2010 – 2013 Bachelor of Science, University of California San Diego

2013 – Polaris Pharmaceuticals, Inc.

2014 – 2015 Master of Science, University of California San Diego

2015 – 2019 Doctor of Philosophy, University of California San Diego

PUBLICATIONS

Brin, E.; Wu, K.; Dagostino, E.; Kuo, M. M.; He, Y.; Shia, W.; **Chen, L.**; Stempniak, M.; Hickey, R.; Almassy, R.; Showalter, R.; Thomson, J. TRAIL stabilization and cancer cell sensitization to its pro-apoptotic activity achieved through genetic fusion with arginine deiminase. *Oncotarget*. **2018**, *9(97)*, 36914-36928.

PATENT

R. Almassy, R. E. Showalter, J. A. Thomson, W. Sisson, W. Shia, **L. Chen**, Y. Lee, "Arginine deiminase with reduced cross-reactivity toward ADI-PEG 20 antibodies for cancer treatment," Int. Patent WO/2014/151982, 2014.

ABSTRACT OF THE DISSERTATION

Comparing Different Formulations for Delivering Arginine Deiminase Drug

by

Li-Chang Chen

Doctor of Philosophy in NanoEngineering

University of California San Diego, 2019

Professor Sadik Esener, Chair

Cancer remains one of the most difficult diseases to treat. In the past half century, cancer treatment has heavily relied on small molecule drugs, which are very potent on killing cancer cells, but lacks the tumor specificity which brings high toxicity against normal cells. For this reason, the improvement and development of new therapeutics that target cancer cells specifically is critical so that toxicity can be minimized for normal cells.

One potential targeting strategy is to exploit the alterations in amino acid synthesis, or salvage pathways displayed by cancer cells. The goal is to target tumors that are sensitive to one

of the conditionally essential or the nonessential amino acids. This allows the normal cells to remain unaffected because they have the ability to synthesize sufficient amounts of necessary amino acids to survive. Unfortunately, most enzymes with the potential for amino acid depletion therapy are derived from nonhuman sources, which makes them highly immunogenic. Therefore, for these enzymes to have clinical efficacy, they must be formulated to be delivered in a way that can avoid or delay the immune response. Arginine deiminase (ADI) is a great example of a nonhuman enzyme that depletes a semi-essential amino acid, arginine, in the human body. ADI has shown some potential in treating hepatocellular carcinoma, melanoma, and some mesotheliomas cancer patients.

The scientific significance of this dissertation is to engineer the recombinant native ADI, PEGylated ADI, and nanoparticle platform to encapsulate ADI so that it can be a better drug candidate compared to its native and PEGylated ADI by assessing their pharmacodynamics and pharmacokinetics properties. PEGylating ADI or other enzymes is the current standard formulation that delivers a nonhuman enzyme by creating a shielding layer around the molecule to delay its immune response. If the proposed silica coated liposome encapsulated ADI nanoparticle platform can be synthesized to avoid the immune response completely, it will out-compete the PEGylation strategy. Finally, the comparison between the different formulations will be tested *in vitro* and *in vivo* settings to prove this concept.

Chapter 1: Introduction

Cancer, the second leading cause of death worldwide, has remained one of the most difficult diseases to treat. One main feature of cancer is its ability to rapidly replicate abnormal cells that can survive the body's immune system and then invade other parts of the body, causing them to spread to different organs. The spreading of cancer cells is known as metastasis, which is the major cause of death from cancer. In the past half a century, cancer treatment has heavily relied on low molecular weight drugs, also known as small molecule drugs. This class of drugs is very potent in its ability to kill cancer cells, but lacks tumor specificity and therefore, brings high levels of toxicity against normal cells. Killing healthy cells creates side effects that reduce the effectiveness of therapeutic treatments in a patient. For this reason, the improvement and development of new therapeutics are needed to overcome some of these issues. At the same time, a deeper knowledge of tumor cell formation is needed [1].

Proliferating cells process metabolites to fulfill their biosynthetic demands of replication, while maintaining energy and redox homeostasis [2]. For this reason, there are metabolic challenges within the tumor microenvironment, which is poorly vascularized and depleted of nutrients. To compensate, cancer cells will use different strategies to obtain necessary nutrients from the body to help maintain viability and build new biomass. This was recently described as cancer metabolism [3]. In the 1920s, Otto Warburg discovered cancer metabolism, where he observed that tumor tissues consume glucose much more rapidly than the surrounding healthy tissues, and convert glucose to lactate regardless of oxygen availability, which is known as the aerobic glycolysis or the Warburg effect [4]. Later, Harry Eagle discovered that the optimal proliferation of certain cultured mammalian cells requires a several fold molar excess of

glutamine compared to any other amino acids [5]. Both glucose and glutamine are the most rapidly consumed nutrients by many cultured cancer cell lines [6, 7], although altered metabolism of fatty acids, nucleotides, folate, acetate, proteins, and several other amino acids besides glutamine have also been reported [3].

According to Teixeira *et al.*, there are 20 amino acids that are identified in cells, and among those are 9 that the human body cannot produce; therefore, they must be obtained from diet. The essential amino acids include L-histidine, L-isoleucine, L-leucine, L-lysine, L-methionine, L-phenylalanine, L-threonine, L-tryptophan, and L-valine. There are 6 amino acids that are considered conditionally essential, which means that they can be synthesized by humans. However, synthesis can be limited due to prematurity as an infant or severe catabolic distress. These amino acids are L-arginine, L-cysteine, L-glycine, L-glutamine, L-proline, and L-tyrosine. The remaining 5 amino acids are considered nonessential, which means they can be synthesized in the body, and they are L-alanine, L-asparagine, L-aspartic acid, L-glutamic acid, and L-serine [1].

The best circumstances for utilizing amino acid depletion therapies are when tumors are sensitive to one of the conditionally essential or the nonessential amino acids, and also when a patient has underlying metabolic problems. This will ensure that only tumor cells are affected by the treatment, whereas normal cells remain unaffected because they have the ability to synthesize sufficient amounts of necessary amino acids to survive. Unfortunately, depletion through dietary restriction is generally insufficient to attain a level that is therapeutically relevant. Because enzymes have high affinity and specificity, enzymatic depletion of amino acids has become the main approach. However, the human genome does not encode enzymes with the required affinity and specificity for therapeutic purposes [8]. Therefore, the most successful instance of enzymatic

amino acid depletion therapy utilizes an enzyme synthesized by *E. coli* bacteria. This is the remarkable Asparaginase, also known under the brand name Oncaspar manufactured by Enzon Pharmaceuticals, which is used for treatment of childhood acute lymphoblastic leukemia (ALL) and non-Hodgkins lymphoma [9]. Another example is the use of arginine deiminase (ADI), which has been tested in clinical trials treating hepatocellular carcinoma (HCC), melanoma, and other urea cycle deficient cancer cells that rely on L-arginine to survive [10]. Less common is the use of the essential amino acids in amino acid depletion therapies. These therapies will only work when the normal metabolism of the essential amino acid is disrupted or when there is defect in the ability to use a certain amino acid. A good example is L-methionine, which have shown to be detrimental for tumor tissue survival, including colon, breast, prostate, ovary, lung, brain, kidney, stomach, and bladder cancers, as well as larynx melanoma, sarcoma, leukemia, and lymphomas [1]. In this case, the enzyme methionase, also known as methionine-γ-lyase, is currently in clinical trials to treat some of the cancers listed.

L-arginine is a precursor and mediator of a series of biological pathways, some of them involved in important cellular functions, such as nitrogen metabolism [11], creatine, agmatine, and polyamine synthesis [12]. The enzyme argininosuccinate synthetase (ASS) catalyzes the condensation of L-citrulline and L-aspartic acid to argininosuccinate which is subsequently converted to L-arginine and fumaric acid by argininosuccinate lyase (ASL) [13]. In healthy adults, endogenous synthesis of L-arginine is sufficient to make it a nonessential amino acid [14]. However, under catabolic stress, such as inflammation, infection, etc., the levels of L-arginine from endogenous synthesis may not be sufficient to meet metabolic demands and L-arginine then becomes an essential amino acid. Therefore, L-arginine is often considered as a conditional or semi-essential amino acid [15].

Certain types of tumor cells, such as prostate carcinoma, metastatic melanoma, and hepatocellular carcinoma are frequently ASS deficient, while lung and colon carcinomas are almost always ASS positive. However, some other human cancers, such as renal cell carcinoma, sarcomas, and invasive breast carcinoma are sometimes ASS deficient [10]. The ASS deficient cancer cells have an elevated requirement for arginine, which causes arginine autotrophy. Therefore, these tumor cells rely only on exogenous arginine to proliferate and grow. For this reason, deprivation of arginine is being investigated as a novel strategy for cancer therapy and has been showing promising efficacy against ASS deficient tumors, or arginine auxotrophic tumors [16, 17, 18].

Arginine can be degraded by several methods: (1) using enzymes in the cell, like L-arginase (ARGase) or L-arginine decarboxylase (ADC), (2) using human recombinant arginase I (ARGase-I), or (3) using parasite enzymes from a bacterial source, such as arginine deiminase (ADI). Of these enzymes, ARGase-I and ADI have the most therapeutic potential. L-arginine decarboxylase, on the other hand, is relatively toxic to normal cells and therefore, not used for therapeutic purposes [19]. According to Dillon *et al.*, at physiological pH, ADI has a higher enzyme activity compared to arginase. In addition, ADI has more than 1000 fold higher affinity for arginine, which allows the enzyme to lower arginine levels to a much greater extent than arginase. As shown in the results by Dillon *et al.*, K_m or Michaelis constant for ADI is about 30 μM, whereas K_m for arginase is about 45 mM [20]. Therefore, ADI is a much better enzyme to use for therapeutic applications based on its biochemical characteristics as an enzyme.

Despite all of the promising biochemical properties of ADI for cancer therapy, the application of these treatments presents some limitations. The therapeutic efficiency of ADI is limited to tumors that do not express ASS, referred to as ASS negative (-), and/or have an

inactivated citrulline to arginine recycling pathway [21, 22]. Additionally, ADI has a short serum half-life and when injected into humans for prolonged treatments, ADI becomes highly immunogenic. To overcome some of these limitations, a PEGylated form of ADI was formulated, ADI-PEG 20 (molecular weight of 20 kDa), that serves to reduce the immunogenicity of the enzyme while greatly improving its pharmacokinetic half-life in serum [23, 24, 25]. This PEGylated enzyme revealed a similar efficiency in *in vitro* assays with melanomas and HCC as compared with native ADI, however, it shows a better effectiveness in *in vivo* assays [21]. Currently, the antitumor activity of Polaris Pharmaceuticals' ADI-PEG 20 has been observed in pancreatic [26], prostate [27], small cell lung [28], head, neck [29], breast cancers [22], lymphoma [29, 30], myxofibrosarcomas [31], melanoma [32], and glioblastoma [22, 33].

This dissertation elucidates a macromolecule nanoparticle platform that has a potential of being a commercial product that resolves some of the issues that are faced by the current standard drug formulation for macromolecules. The enzyme, arginine deiminase (ADI), is encapsulated using an emulsion process that suspends the enzyme in the hollow core of a liposome, where it remains active while being protected through the secondary layer of silica. Chapter 2 discusses the characteristics of the native ADI enzyme and its purification process. Chapter 3 explains the PEGylation of ADI and how this increases its serum half-life. Chapter 4 outlines the synthesis of synthetic hollow enzyme encapsulated (SHELS) and its potential as a useful platform for enzyme drug delivery. This platform was terminated because the synthesis process was not robust enough for reproducibility. Then, Chapter 5 discusses a different approach to deliver enzymes by using liposomes for encapsulation. Lastly, Chapter 6 summarizes the *in vitro* and *in vivo* study of the different ADI formulations.

The dissertation concludes by exploring the future potential applications of the silica coated liposome encapsulated enzymes for macromolecule delivery with a focus on arginine deiminase.

Chapter 2: Native Arginine Deiminase

2.1 Arginine Deiminase

Arginine is a semi-essential amino acid in humans with diverse roles in normal and malignant cells. The downregulation of the biosynthetic enzyme, argininosuccinate synthetase or ASS, is determined to be the rate limiting step in arginine synthesis. This causes the tumor cells to be dependent on the extracellular arginine due to its inability to produce arginine for growth. This dependency is known as arginine auxotrophy. It is beneficial to understand the importance of arginine in tumorigenesis from the biological perspective [34]. Several discoveries in the last century have identified arginine as a precursor for many metabolic pathways [35]. These include the production of nitric oxide (NO), polyamines (putrescine, spermine, and spermidine), urea, creatine, nucleotides, proline, glutamate, and agmatine, in addition to other protein synthesis [34]. Arginine and many of its downstream molecules have been suggested to play roles in tumor development, shown in Figure 2.1, with animal studies confirming a modulatory effect of arginine on tumorigenesis [36, 37]. When mice with transplantable tumors are fed arginine, they exhibited enhanced tumor growth [38]. On the other hand, depleting dietary arginine inhibited the development of liver metastases [39].

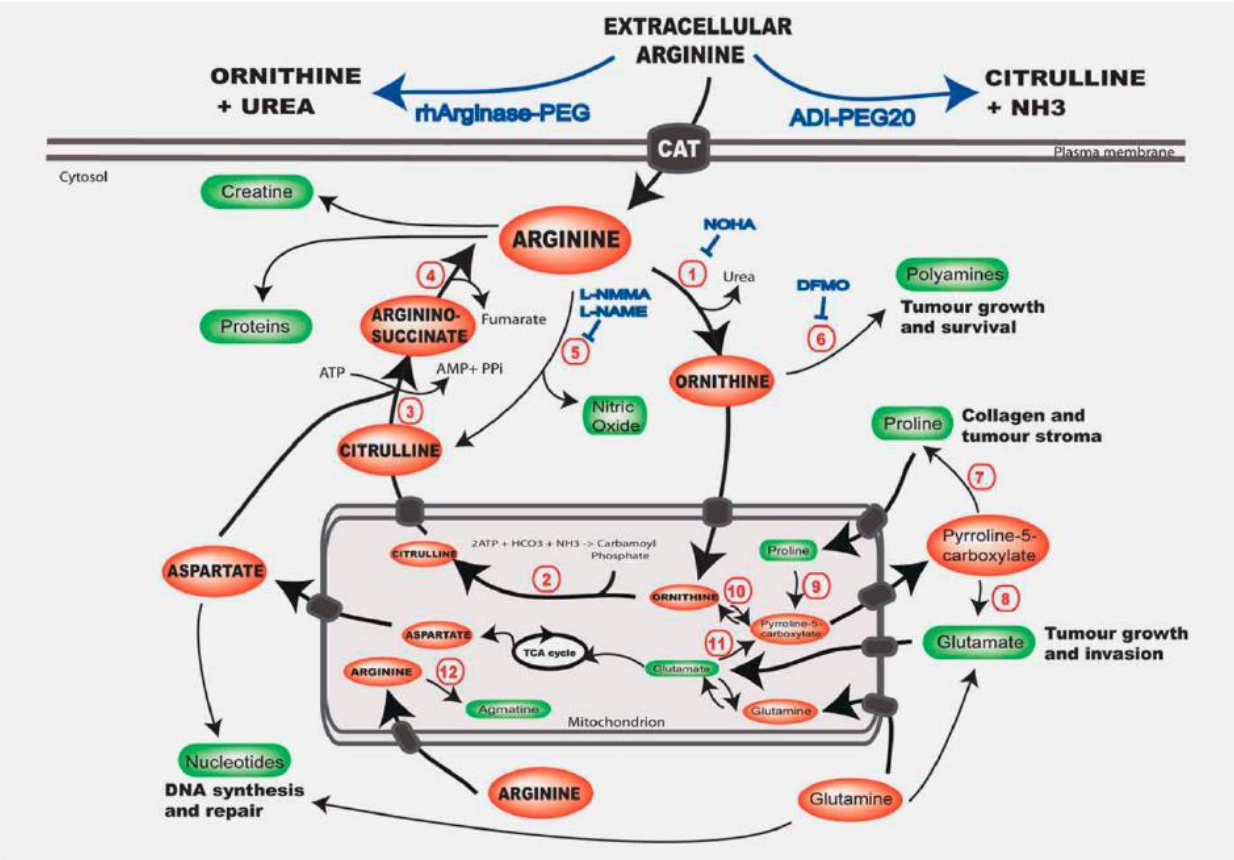

Figure 2.1: This schematic shows how arginine is utilized in cancer. The key enzymes are shown and enumerated in the Figure as follow: (1) arginase 1; (2) ornithine transcarbamylase (OTC); (3) argininosuccinate synthetase (ASS1); (4) argininosuccinate lyase; (5) nitric oxide synthase; (6) ornithine decarboxylase; (7) pyrroline-5-carboxylate reductase; (8) pyrroline-5-carboxylate dehydrogenase; (9) proline oxidase (dehydrogenase); (10) ornithine aminotransferase; (11) pyrroline-5-carboxylate synthase; (12) arginine decarboxylase. Several drugs affecting arginine bioavailability and metabolism are highlighted in blue: ADI-PEG 20, pegylated arginine deiminase; rhuArg-PEG, pegylated human arginase; DFMO, difluoromethylornithine; LNAME, N omega-nitro-L-Arginine methyl ester; L-NMMA, N-monomethyl-L-arginine; NOHA, N hydroxy-L-arginine [1].

Delage *et al*. suggests that downregulation of tumoral ASS expression is poorly understood, but the resulting arginine auxotrophy has been exploited in recent years with the use of arginine catabolizing enzymes as anticancer agents [40]. A comparable enzyme-based therapy, PEG-asparaginase, has already been approved in the management of childhood acute lymphoblastic leukemia (ALL), which is auxotrophic for asparagine due to the lack of

biosynthetic enzyme, asparagine synthetase (ASNS) [41]. Similarly, the mycoplasma derived enzyme, arginine deiminase, degrades arginine resulting in tumor cell death [24].

Arginine deiminase or ADI is found among prokaryotic organisms and some anaerobic eukaryotes, but has never been discovered in humans or other higher eukaryotes [1]. ADIs catalyze the hydrolysis of L-arginine to L-citrulline and ammonia [42]. ADIs have been isolated, purified, and characterized from bacteria, archaea, and a few eukaryotes [23]. Several recombinant ADIs have been characterized in terms of enzyme activity, functional expression level, optimal temperature, optimal pH, substrate affinity, and half-life in human plasma [23, 43]. Several crystal structures of recombinant ADIs have also been solved and used for better understanding of ADI structure function relationships. Arginine depletion is a target-specific therapy for arginine auxotrophic tumors deficient in the urea cycle enzyme argininosuccinate synthase (ASS), and therefore sensitive to arginine deprivation [23]. Thus, ADI based antitumor therapies have successfully passed phase II clinical trials in the treatment of hepatocellular carcinomas (HCCs) and melanomas [44, 45]. Additional therapeutic uses for ADI beyond its antitumor activity have been discovered, specifically its antiangiogenic activity via the suppression of nitric oxide generation [46, 47, 48]. The cooperative antiproliferative and antiangiogenic activities of ADI are believed to be the key assets that turn ADI into an effective therapeutic molecule in the treatment of several tumors and diseases [1].

Several ADIs have been structurally and pharmacologically characterized from various bacteria, but the most studied ADI is the one derived from *Mycoplasma arginini* because of its therapeutic potentials [49]. *M. arginini* ADI is composed of 410 amino acids and two identical subunits with a total molecular weight of 90 kDa with an isoelectric point (pI) of 4.7. The value of V_{max} is defined as the maximum rate that the enzyme achieves when the given substrate

saturates, and K_m or Michaelis constant is defined as the concentration of substrate at half of its maximum rate. The V_{max} and K_m for *M. arginini* ADI values for substrate arginine is estimated to be about 50 international unit per mg of protein (IU/mg) and 0.2 mM, respectively. This enzyme is most active at 50°C under pH 6.0 – 7.5 condition [50]. *Mycoplasma hominis* arginine deiminase, which will be the main focus of this dissertation, because its PEGylated formulation is currently being tested in clinical trials. *M. hominis* ADI is made up of 409 amino acids and two identical subunits with each subunit having a molecular weight of 46.3 kDa. The stable dimer, shown in Figure 2.2, has a total molecular weight of 92.6 kDa and an isoelectric point of 5.37. Its estimated enzyme activity is about 18 IU/mg and a K_m of less than 10 μM. *M. hominis* has one cysteine active site per monomer where the conversion of arginine into citrulline happens.

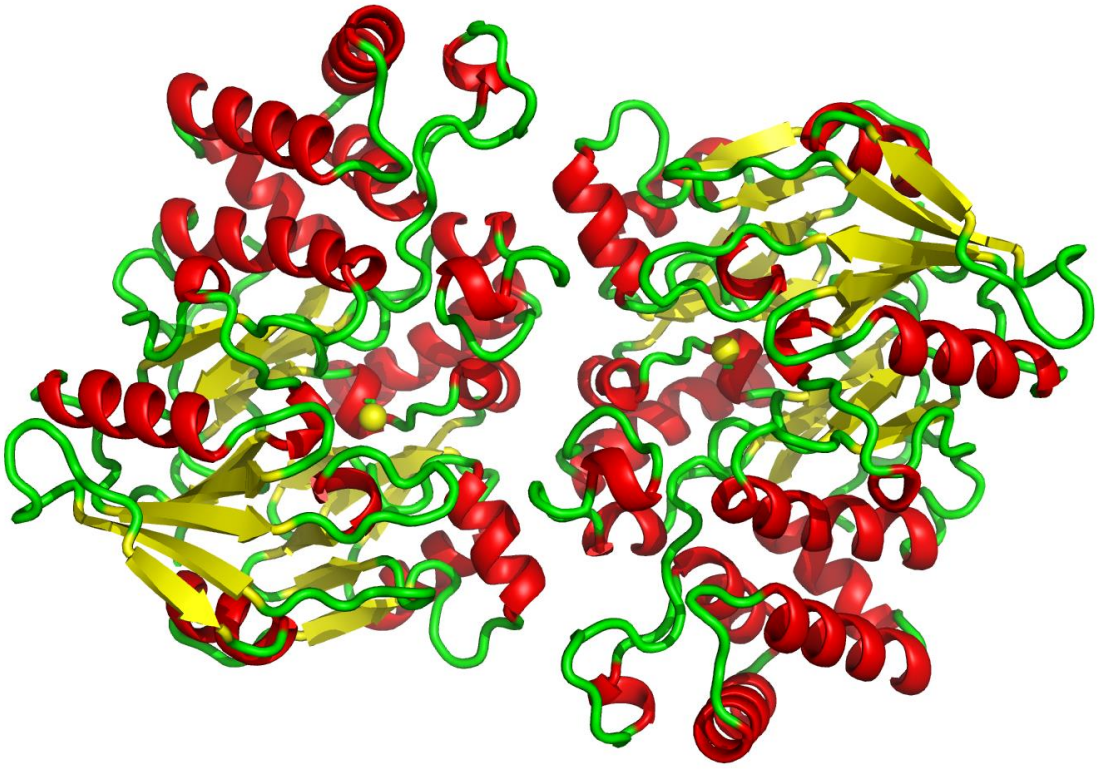

Figure 2.2: Protein structure of *Mycoplasma hominis* arginine deiminase. The yellow sphere in the middle of each monomer shows the active site, cysteine, of the enzyme.

In summary, arginine is a precursor for a variety of molecules influencing tumor growth, proliferation, invasion, immunity, metastasis, and angiogenesis [34]. Depleting arginine in the body potentially helps limit cancer cell survival. In this case, arginine deiminase has been chosen over human arginase because of the better physicochemical properties of the molecule that allow better efficacy in hepatocellular carcinoma and melanoma patients [44, 45]. Additionally, *M. hominis* ADI has been chosen because it is the same species as the current clinically used drug.

2.2 Materials

The gene sequence of *M. hominis* ADI was synthesized by Invitrogen, Carlsbad, California. pET-21a(+) DNA vector was purchased from Novagen, Inc., Madison, Wisconsin. One Shot Mach1-T1 Chemically Competent *E. coli* and One Shot BL21(DE3) Chemically Competent *E. coli* cells were purchased from Invitrogen, Carlsbad, California. Restriction enzymes NdeI and XhoI and Quick Ligation Kit were purchased from New England Biolabs, Ipswich, Massachusetts. QIAprep Spin Miniprep Kit and QIAquick Gel Extraction Kit were purchased from Qiagen, Hilden, Germany. LB agar plates with 100 μg/mL carbenicillin were purchased from Teknova, Hollister, California. Benzonase Nuclease was purchased from Sigma Aldrich, St. Louis, Missouri. E-Gel EX SYBR Gold II 1% agarose gels, E-Gel 1 kb Plus DNA ladder, NuPAGE® 4-12% Bis-Tris Protein Gels, 1.0 mm, 10- and 12-well, NuPAGE® MES SDS Running Buffer (20×), NuPAGE® LDS Sample Buffer (4×), NuPAGE® Sample Reducing Agent (10×), Mark12 Unstained Protein Standard, and XCell SureLock Mini-Cell gel tank were purchased from Thermo Fisher Scientific, Waltham, Massachusetts. Q Sepharose Fast Flow resin, Phenyl Sepharose High Performance resin, Superdex 200 Prep Grade resin, and ÄKTA protein purification system were all purchased from GE Healthcare Life Sciences, Marlborough, Massachusetts. All chemicals were used as received and purchased from Sigma Aldrich, St. Louis, Missouri.

2.3 Methods

2.3.1 Molecular Cloning of Arginine Deiminase

The 1212 bp synthesized gene sequence of *Mycoplasma hominis* ADI was received in pMA-T vector. 100 μL of water was used to reconstitute 50 μg of lyophilized DNA. 0.1 μL of

the plasmid DNA was used to transform into 25 μL of the One Shot Mach1-T1 Chemically Competent *E. coli* cells. The transformed cells were grown in 1 mL of LB media at 37°C for 1 hour. 10 μL of the transformed cells in LB media was diluted with 90 μL of LB media and spread with sterile glass beads on LB agar plates with 100 μg/μL of carbenicillin. The plate was incubated at 37°C overnight for the cell colonies to grow. Two single colonies were picked and grown in 5 mL LB media with ampicillin at 37°C overnight. To purify the plasmid DNA from the cell culture, the Qiagen QIAprep spin miniprep kit was used. Using a NanoDrop Lite Spectrophotometer, the concentration of the DNA samples were measured in ng/μL.

The purified plasmid which is the *M. hominis* ADI gene in pMA-T vector and purchased empty pET-21a vector plasmid were digested with NdeI and XhoI restriction enzymes for 30 – 60 minutes at 37°C to obtain an insert with the *M. hominis* gene of interest and linearized pET-21a vector, respectively. Once both DNAs were digested, the samples were loaded into E-Gel EX SYBR Gold II 1% agarose gel at a constant voltage of 50 V for 80 minutes to separate the digested plasmids. Using a clean razor blade, DNA bands of interest were excised from the gel. The Qiagen QIAquick gel extraction kit was used to purify the digested DNA in the gel. The *M. hominis* gene was cut from the original pMA-T vector then ligated into the linearized pET-21a vector. To perform DNA ligation, a molar ratio of 1 vector DNA to 3 insert DNA was used. Quick Ligation Buffer and Quick T4 DNA Ligase were mixed with the vector and insert DNA and incubated at room temperature for 10 minutes.

Next, 2 μL of ligated DNA containing the *M. hominis* ADI gene in pET-21a vector was mixed with 25 μL of Mach1-T1 competent cells. The mixture was incubated on ice for 30 minutes, heat shocked in a 42°C water bath for 30 seconds, and placed back on ice for 2.5 minutes. Then, 500 μL of LB media was added to the transformed cells and the cells were then

shaken at 37°C for 1 hour. The cells were then spread onto LB agar plates with carbenicillin. Two volumes of cells were plated, 10 μL and 100 μL. The 10 μL sample was diluted with 90 μL of LB media prior to plating. The agar plates were then incubated at 37°C overnight.

To verify that the transformed DNA was correct, 3 – 5 single colonies were picked from the plates and grown in 5 mL of LB media with ampicillin overnight at 37°C. The bacteria cells were pelleted the next day for DNA extraction using the QIAprep spin miniprep kit. Purified DNA was screened in-house with NdeI and XhoI restriction enzyme digestion followed by running on an agarose gel to check DNA size. Positive samples were sent out to Retrogen, Inc., San Diego, California, for DNA sequencing.

Sequence verified DNA was then used to transform into BL21(DE3) chemically competent cells, which were selected for their higher efficiency of protein expression. 25 ng of DNA was mixed with 12 μL of BL21(DE3) cells. After letting the mixture sit on ice for 30 minutes, samples were heat shocked in a 42°C water bath for 30 seconds and placed back on ice for 2.5 minutes. Next, 500 μL of LB media was added to the transformed cells and the samples were then shaken at 37°C for 1 hour. 25 μL of cells were diluted into 75 uL of LB media and spread on LB agar plates with carbenicillin. The plates were incubated at 37°C overnight to allow the cells to grow. Two single colonies were picked to make 15% glycerol bacteria stock and stored at -80°C.

2.3.2 Protein Expression and Renaturing of Arginine Deiminase

The bacteria stocks were used to grow a 5 mL bacteria culture that was used to inoculate 1 mL of cells into 1 L of sterile terrific broth (TB) media with the following autoinduction supplements: 20 mL of 50× M-Salts containing 1.25 M Na_2HPO_4, 1.25 M KH_2PO_4, 2.5 M

NH_4Cl, and 0.25 M Na_2SO_4, 20 mL of 50× 5052 containing 25% Glycerol, 2.5% D-Glucose, and 10% α-Lactose monohydrate [51], 1 mL of 1 M Magnesium sulfate, and 1 mL of 100 mg/mL of ampicillin. The culture was shaken at 250 rpm for 18 – 22 hours at 37°C. Cell density was checked by measuring OD_{600}, and the culture was then pelleted at 10,000 rpm for 15 minutes at 4°C to obtain a cell paste.

The bacteria cell pellet was resuspended in 10 mM $NaPO_4$ pH 7.0 buffer using a handheld homogenizer. The bacteria sample was then passed through a microfluidizer system twice to lyse the cells. Lysed cells were centrifuged at 10,000 rpm for 30 minutes. The supernatant was discarded and the pellet, also known as an inclusion body (IB), was resuspended with 10 mM $NaPO_4$ pH 7.0 buffer. This suspension was centrifuged at 10,000 rpm for 30 minutes and the supernatant was discarded. This IB wash process was repeated twice, or until the supernatant was clear, completing the IB extraction process.

To refold the inclusion body, the pellet was resuspended in 10 mM $NaPO_4$ pH 7.0 buffer with 2 mM Dithiothreitol (DTT) and 2% N-lauryl Sarcosine (NLS) with a ratio of 50 mg of IB per mL of buffer. The enzyme benzonase was added to the IB solution at a ratio of 1 g of IB per 1 μL of benzonase. The IB solution was gently stirring at room temperature for about 1 hour to solubilize the ADI protein. Insoluble material from the IB solution was removed through centrifugation at 25,000 rpm for 30 minutes, and the supernatant containing ADI protein was collected. The supernatant was diluted 10 fold into 20 mM hydroxypropyl β-cyclodextrin to start the refolding process for 16 – 20 hours. The buffer of the refolding buffer was then adjusted to 20 mM $NaPO_4$ pH 8.5 by adding concentrated 0.5 M $NaPO_4$ pH 8.5, which completed the ADI protein renaturing process.

2.3.3 Protein Purification of Arginine Deiminase

Using an ÄKTA purification system, the renatured arginine deiminase (ADI) was loaded onto a Q-Sepharose Fast Flow column. Flow through and column wash fractions were saved. Using the UNICORN software, the column run program was programmed to run a gradient of 0 to 1 M NaCl with a base buffer of 20 mM $NaPO_4$ pH 8.5. Fractions were collected and pooled after analysis for further purification. Pooled sample fractions were adjusted to 1 M ammonium sulfate, $(NH_4)_2SO_4$, by adding 144 mg of $(NH_4)_2SO_4$ per 1 mL of sample and stirred at 4°C for 30 minutes. The sample was then loaded onto a Phenyl High Performance column, and the software was programmed to run a gradient of 1 to 0 M $(NH_4)_2SO_4$ with a base buffer of 20 mM $NaPO_4$ pH 8.5. Collected fractions were pooled after analysis for the final purification step. The pooled fractions were concentrated to a volume of 5 – 10 mL and run on a SuperDex 200 column using 10 mM HEPES pH 7.5 + 150 mM NaCl buffer. Collected fractions of the desired protein were pooled and stored at -80°C prior to future experiments and characterization.

2.3.4 Characterization of Arginine Deiminase

To analyze fractions from each step of the purification process, samples were run on sodium dodecyl sulfate polyacrylamide gel electrophoresis (SDS-PAGE) gels, specifically NuPAGE® 4-12% Bis-Tris gels, to qualitatively determine the purity of proteins in each fraction. 5 µL of each fraction was mixed with 5 µL of running dye and loaded on an SDS-PAGE gel in 1× MES (2-(N-morpholino)ethanesulfonic acid) running buffer at a constant voltage of 200 V for 40 minutes. Coomassie blue stain was used to stain the proteins in SDS-PAGE gels overnight. Gels were then de-stained to an acceptable level using water and analyzed. Protein

concentration of fractions collected from each purification column was also measured to track the amount of protein throughout the purification process.

The final purified protein sample was also analyzed for enzymatic activity using a modified blood urea nitrogen (BUN) assay, which will also be referred to as the arginine citrulline colorimetric assay. The protein was diluted to roughly 1 mg/mL and re-measured using a NanoDrop Lite Spectrophotometer. From there, the protein sample was diluted to 500 nM in assay buffer containing 50 mM HEPES pH 7.35, 160 mM NaCl, and 0.1% BSA. Next, 10 µL of the 500 nM enzyme sample was mixed with 80 µL of assay buffer. The sample was incubated in a thermocycler at 37°C for 5 minutes prior to start of reaction. The ADI enzyme reaction was started by adding 10 µL of 50 mM arginine at 37°C. The reaction was stopped after two minutes with the addition of 75 µL color development reaction acid (CDR acid). The sample was immediately placed on ice after reaction termination. 25 µL of color development reagent (CDR) was added into the sample and mixed well with a pipette. The sample was heated at 95°C for 10 minutes then removed from the thermocycler. Subsequently, the sample was cooled down at 20°C for 10 minutes. 100 µL of sample was transferred to a clear, flat-bottom reading plate. The absorbance was measured at 530 nm using a SpectraMax Plus microplate spectrometer. In order to quantify the results, a citrulline standard curve was run with the enzymatic reaction.

2.4 Results

The 1212 bp *Mycoplasma hominis* ADI gene and the transformation of this gene into BL21(DE3) *E. coli* bacteria was sequence confirmed. ADI protein was successfully expressed by BL21(DE3) *E. coli* bacteria in 1 L of TB media at 37°C. The ADI protein formed inclusion

bodies inside the cells, which required denaturing and renaturing to restructure the enzyme into its correct quaternary structure and gain proper enzymatic function.

To isolate the active enzyme from the pool of expressed proteins, three purification columns were used to obtain pure ADI protein. First, the ion exchange column, Q-Sepharose Fast Flow, was used after the renaturing of the ADI protein. The chromatogram shown in Figure 2.3 shows the first purification run of ADI, where 0 to 1 M NaCl was run over 0 to 100% gradient over 10 column volumes. There are two main peaks that the protein eluted from the column, with the first peak eluted at about 300 mM NaCl and the second peak eluted around 460 mM NaCl. After running an SDS-PAGE gel on the different elution fractions shown in Figure 2.4, fractions 10 – 15 were pooled with a total of 120 mL of protein sample to proceed onto the next purification step. Other protein fractions were discarded due to protein contaminates.

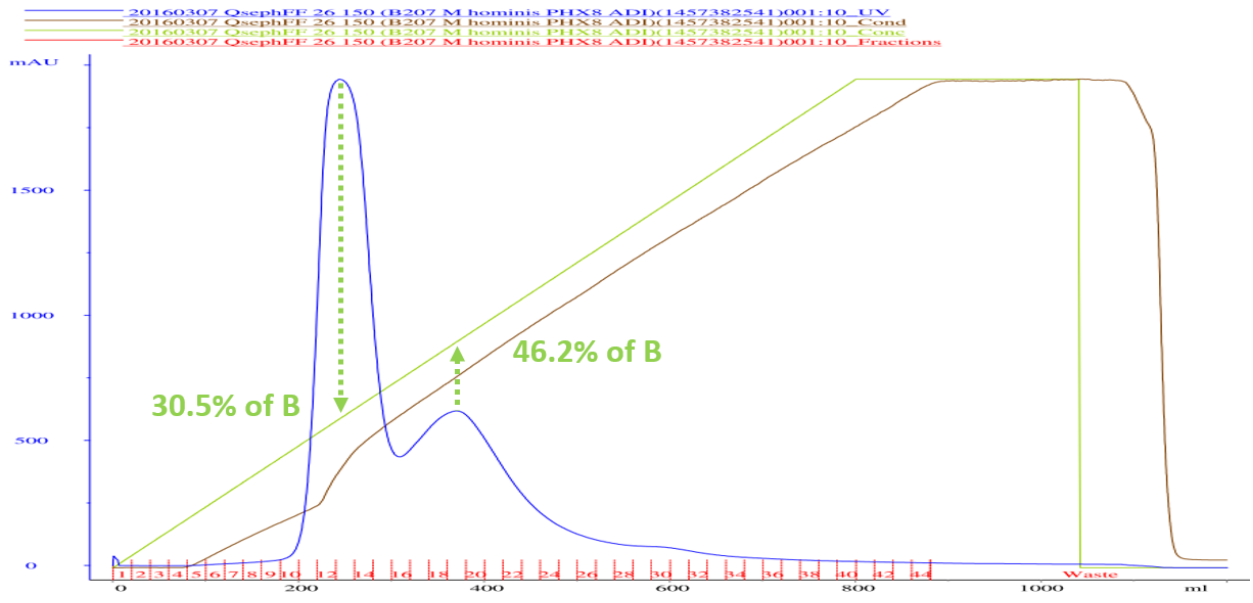

Figure 2.3: Q Sepharose Fast Flow ADI Purification Chromatogram

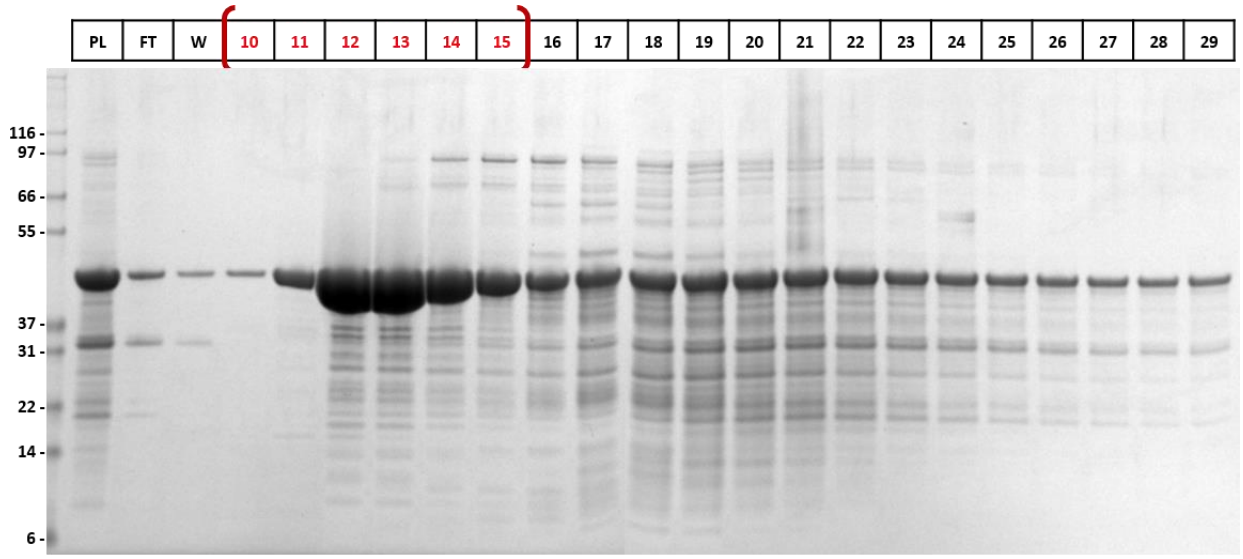

Figure 2.4: Q-Sepharose Fast Flow purified fractions: Coomassie Blue Stained Protein Gel, 4-12% NuPAGE gel ran for constant 200 V for 45 minutes

Pooled fractions were loaded onto a hydrophobic interaction column following the addition of 1 M ammonium sulfate salt. Figure 2.5 shows the chromatogram of the Phenyl Sepharose High Performance column run where the gradient was also run over 10 column volumes. The protein eluted off the column when the ammonium sulfate ($(NH_4)_2SO_4$) concentration was reduced down to approximately 530 mM. Eluted fractions were analyzed on an SDS-PAGE gel to determine which fractions to pool. From the results in Figure 2.6, fractions 15 – 28 were pooled with a total volume of 280 mL for the next purification step.

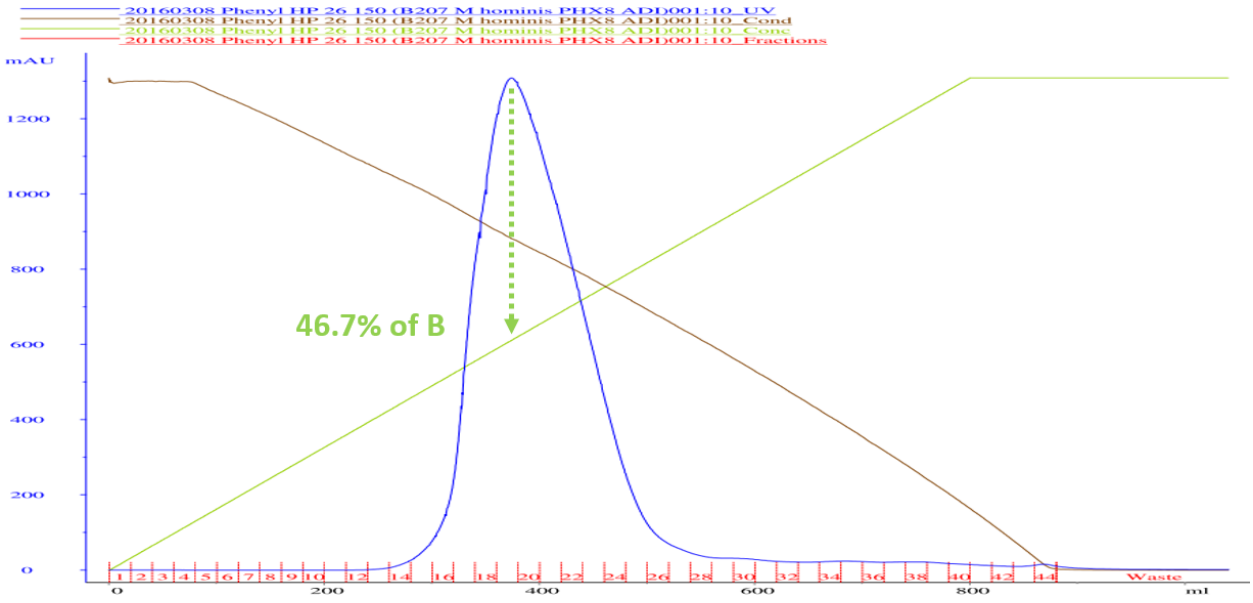

Figure 2.5: Phenyl Sepharose High Performance ADI Purification Chromatogram

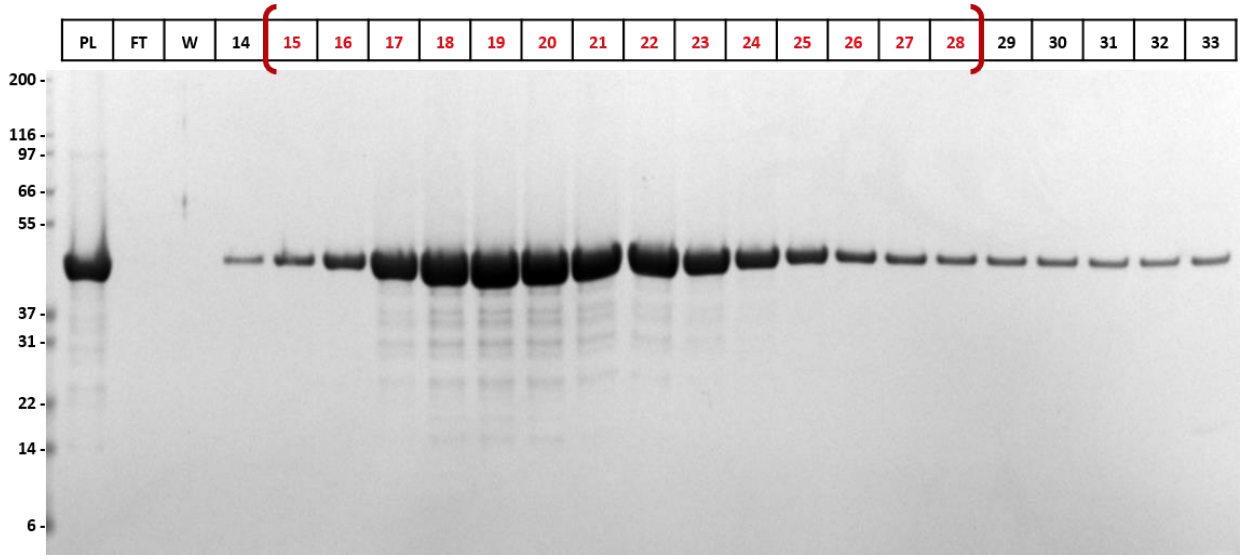

Figure 2.6: Phenyl Sepharose High Performance purified fractions: Coomassie Blue Stained Protein Gel, 4-12% NuPAGE gel ran for constant 200 V for 45 minutes

The pooled samples were concentrated from 280 mL to 20 mL using an Amicon Stirred Cell with an Ultracel 10 kDa cutoff membrane. The concentrated sample was then loaded onto a 600 mL Superdex 200 Prep Grade column, and the protein was eluted at around 303 mL

retention volume. Based on the standard curve in Figure 2.7, the calculated molecular weight is about 93.3 kDa, and the theoretical size of ADI is 92.6 kDa. The chromatogram, shown in Figure 2.8, shows the size exclusion run of the ADI protein. Figure 2.9 shows the SDS-PAGE gel of the fractions eluted off the column to determine fractions of interest. From the results, fractions 37 – 45 were pooled with a total of 72 mL of protein sample. The sample was concentrated down to around 20 mL for storage purposes. The final protein concentration was 12.8 mg/mL, with a final yield of approximately 256 mg of ADI protein after the 3 steps of purification.

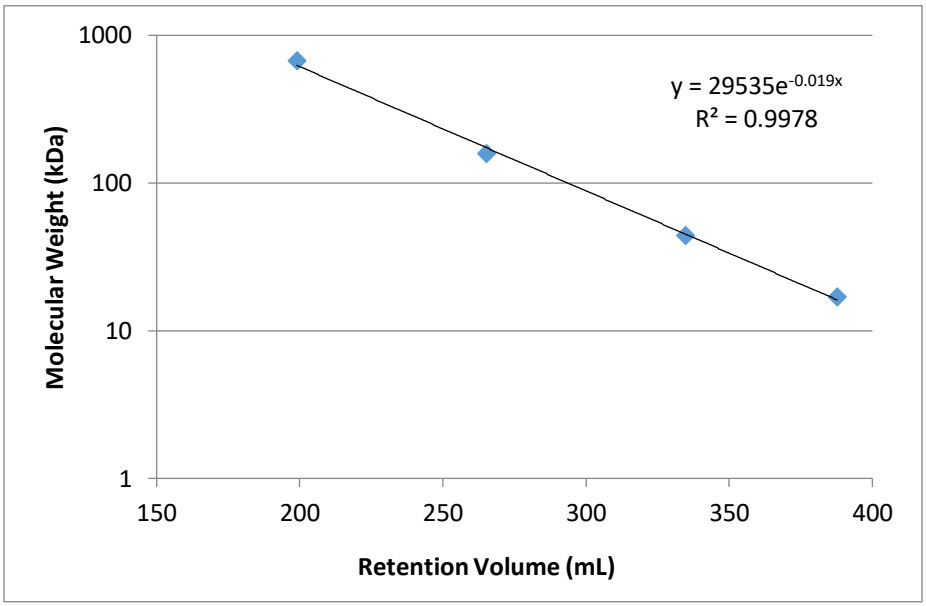

Figure 2.7: Superdex 200 Prep Grade of Known Size Molecular Weight Standards: Thyroglobulin (198.93 mL, 670 kDa), Gamma globulin (265.13 mL, 158 kDa), Ovalbumin (334.73 mL, 44 kDa), and Myoglobin (387.67 mL, 17 kDa).

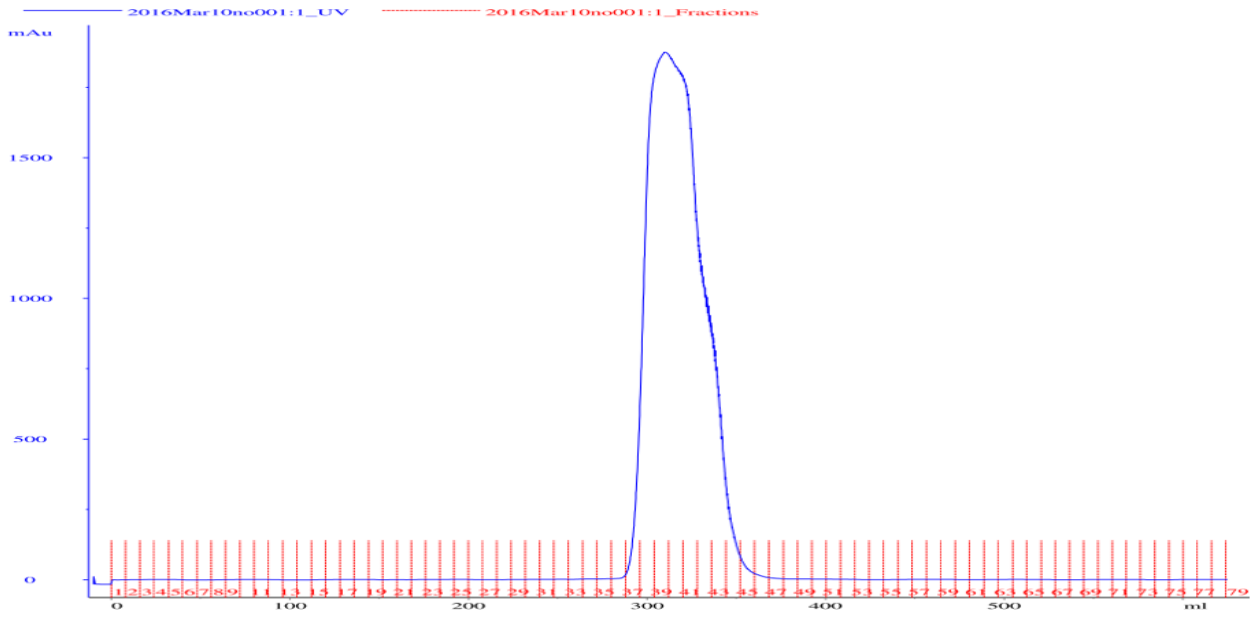

Figure 2.8: Superdex 200 Prep Grade ADI Purification Chromatogram

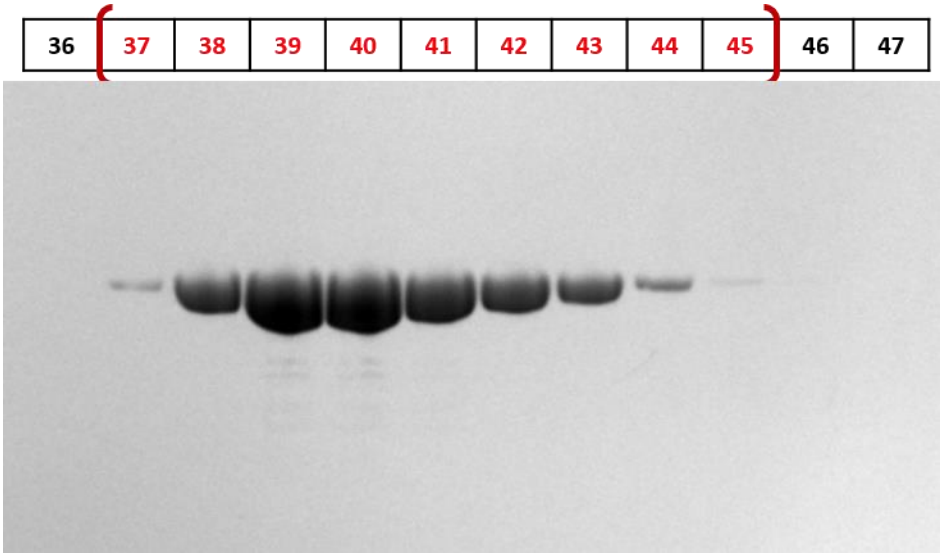

Figure 2.9: Superdex 200 Prep Grade purified fractions: Coomassie Blue Stained Protein Gel, 4-12% NuPAGE gel ran for constant 200 V for 45 minutes

The enzyme activity of the purified ADI protein was tested using the arginine citrulline colorimetric assay. The final sample absorbed at 530 nm was read to be 0.3549. Using the

equation from the citrulline standard curve, this value was calculated to be 42.5 μM of citrulline converted per minute of reaction per 50 nM of ADI enzyme, or having a specific activity of 18.4 IU/mg. In other words, 1 mg of ADI enzyme converted 18.4 μmol of product per minute during this reaction.

2.5 Discussion

The gene of interest, arginine deiminase from *Mycoplasma hominis*, was designed and synthesized. Subcloning of the gene was done into the desired pET-21a vector, allowing the plasmid to be used in a T7 promotor system in the chemically competent *E. coli* BL21(DE3) cell. This overexpression system resulted in a high yield of recombinant ADI protein. 1 L of *E. coli* cells produced approximately 3.7 g of inclusion bodies, which were refolded and purified to yield about 256 mg of active ADI enzyme. Different protein refolding methods and conditions were attempted. Traditional methods of renaturing are to use either guanidine hydrochloride or urea to completely linearize the protein, then slowly renature by reducing the salt concentration. This method did not result in high protein yield as compared to N-lauryl sarcosine denaturing and refolding with hydroxypropyl β-cyclodextrin. Therefore, N-lauryl sarcosine along with hydroxypropyl β-cyclodextrin were chosen to use for denaturing and renaturing the ADI protein.

Ion exchange chromatography allows separation of different net surface charge molecules. Molecules varying considerably in their surface charge properties will exhibit different degrees of interaction with the charged chromatography media, according to differences in the overall charge, charge density, and surface charge distribution. *M. hominis* ADI has a net negative surface charge in pH 8.5 buffer because the pI of the molecule is less than the pH of the running buffer. Thus, Q-Sepharose Fast Flow column was picked because the negatively charged

protein binds to the cation column. The increase in sodium chloride salt increases the ionic strength within the running buffer in which the salt competes with the protein to interact with the cationic resin. Once the salt concentration is high enough, it outcompetes the protein to resin interaction. As a result, the protein elutes off the column because the salt has disrupted the interaction. Typically, the eluted protein of interest is correctly folded since the improperly folded proteins become stuck to the column. This does not mean all eluted proteins are considered the protein of interest. This column discriminates different proteins with different surface properties. As shown in Figure 2.3, it is clear that there are two different protein populations based on its surface charge and properties.

In contrast, the hydrophobic interaction column works differently than the ion exchange column. Typically, the three-dimensional structure of a protein is a result of intramolecular interactions, as well as interactions with the surrounding solvents. In the case of soluble proteins, the solvent is water and the hydrophobic side chains are usually hidden in the interior of the protein. To allow the protein to bind to the hydrophobic resins, the addition of ammonium sulfate salt was added. Under high salt concentration, hydrophobic patches of the protein are exposed on its surface. Ultimately, this allows the proteins to bind to the hydrophobic resins of the column. To disrupt the interaction between the protein and the resin, decreasing the hydrophobicity of the protein allows it to have a weaker protein to resin interaction. Therefore, the protein elutes from the column. Proteins will typically deform or aggregate under high levels of ammonium sulfate salt because the hydrophobic residues will become overexposed, causing protein aggregation or sticking to the column. This often occurs when the protein is not completely folded correctly. This column is especially good to purify out any inactive ADI proteins.

Finally, the size exclusion, or gel filtration column was used. This column consists of a porous matrix of spherical particles with chemical and physical stability and inertness, which it lacks reactivity and adsorptive properties. Generally, high molecular weight molecules will move through the column matrix much faster than low molecular weight molecules because the high molecular weight molecules will have partial access to the pores of the matrix. Small molecules such as salts will have full access to the pores moving down from the column, but do not separate from each other. Therefore, size exclusion column is used to separate any large molecules or aggregates from the protein of interest, which after the previous two columns, the protein should be relatively pure. This column can also be used to buffer exchange the protein sample since there are no real interactions between the protein and column resin. Lastly, Figure 2.9 shows that there are no aggregations of the final purified ADI protein because of its single peak.

Mycoplasma hominis ADI was briefly characterized by testing the activity of the purified native enzyme using the modified blood urea nitrogen or BUN assay. It is a discontinuous assay used to determine the specific activity of an enzyme, in this case the ADI enzyme. Figure 2.10 depicts the chemical reaction of urea condensing with diacetyl to form diazine that occurs in the Fearon procedure for serum urea quantification in the BUN assay [52]. Since the molecule diacetyl is unstable, diacetyl monoxime is substituted and generates the required diacetyl in the same reaction mixture [53]. In addition, thiosemicarbazide and ferric ions are added to enhance and stabilize the product [54]. While urea in solution is transparent to all visible and UV wavelengths, the new product, diazine, has a strong absorption at 530 nm and its concentration is directly related to the concentration of urea [55]. The assay was modified to utilize the side chain of the citrulline molecule, shown in Figure 2.11, which is very similar to the urea molecule. The

enzyme ADI catalyzes the catabolism of arginine to citrulline and ammonia through the enzyme's active site comprised of two cysteines. The modified BUN assay can be used to detect citrulline produced by ADI. The assay has two parts, the enzymatic reaction of the ADI and the detection of the product citrulline. This assay was able to show that the enzyme activity of *M. hominis* is comparable to the activity reported in the literature by Holtsberg *et al*.

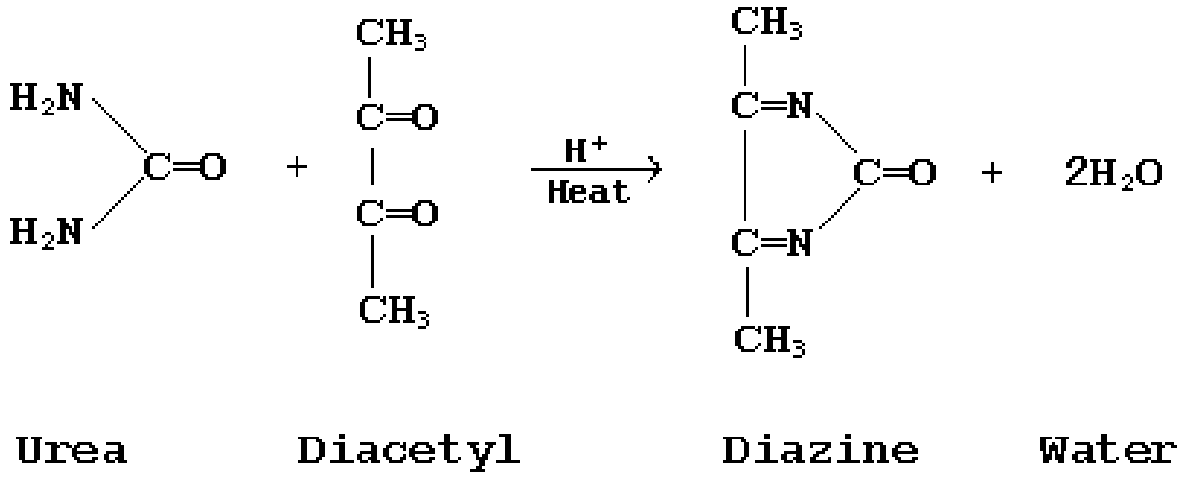

Figure 2.10: Fearon Colorimetric Assay Reaction [52]

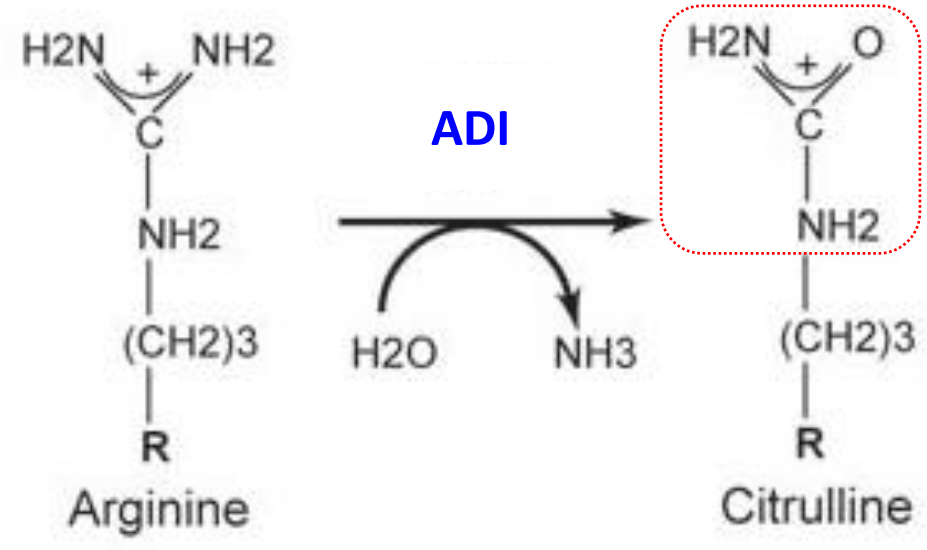

Figure 2.11: Chemical reaction of arginine deiminase converting arginine to citrulline.

2.6 Conclusion

In this chapter, we have demonstrated that recombinant protein arginine deiminase from *Mycoplasma hominis* was expressed, purified, and its basic characterization and confirmation completed. In short, the gene for *M. hominis* was cloned and transformed into a chemically competent *E. coli* cell for protein expression. The inclusion body purified from the supernatant was successfully renatured and further purified using ion exchange, hydrophobic interaction, and size exclusion columns to achieve the highest purity protein possible. Then, the purified enzyme was tested for its activity under an environment that mimics the human blood using the modified BUN assay.

In the next chapter, we will look at a way to potentially address problems related to the enzyme's short circulation half-life in blood and its triggering of the immune response. To solve these issues, polyethylene glycols (PEGs) can be attached to the enzyme can increase circulation half-life of ADI in the bloodstream and to delay the immune response.

2.7 Acknowledgments

This chapter and its methods were developed and owned by Polaris Pharmaceuticals, Inc., San Diego, California. Collaborators for this development: Jason (Li-Chang) Chen, Richard Showalter, Wei-Jong Shia, Wes Sisson, Derek Lee, Bob Alamassy, and Jim Thomson. The dissertation author was the primary investigator and author of this material.

Chapter 3: PEGylated Arginine Deiminase

3.1 PEGylation

The most commonly used polymer for protein conjugation is poly(ethylene glycol) due to its biocompatibility, low immunogenicity, ease of conjugation, and high degree of hydration to create a water solvation layer around the conjugates which masks the protein from the removal processes in the body [56]. The conjugation of proteins with polyethylene glycol (PEG), or PEGylation, has become a common method of improving a protein's half-life in serum. The increase in circulation half-life is through the reduction of urinary excretion of the molecule [57], and also the reduction in enzyme degradation due to the increased steric bulk [58]. The addition of the PEG moiety can increase the immunological profile of a molecule by reducing the ability of the molecule to raise antibodies in humans [59].

PEG is an inert, biodegradable polymer made of long-chain amphiphilic molecules linked together by identical ethylene glycol units [60]. PEGs usually have a descriptor associated with them that represents the mean molecular weight of the molecule [61]. As an example, PEG500 has a mean molecular weight of 500 with a 5-10% variance, so in the PEG mixture it contains PEG molecular weight of 450 to 550. PEG can be produced in different configurations, including linear or branched structures [62], and in different molecular weights [60]. The structures of these PEGs are detailed in Figure 3.1. In some instances, higher molecular weight PEGs can have some degree of branching. An example is 4-armed PEG20k, which means the PEG20k is split into four 5,000 molecular weight PEGs. Most PEGs that are used to conjugate biological molecules are polydispersed in nature, which can lead to a range of drug molecules with subtly

different biological properties [63]. The impact of polydispersity must be considered when dealing with these conjugated biological molecules [58].

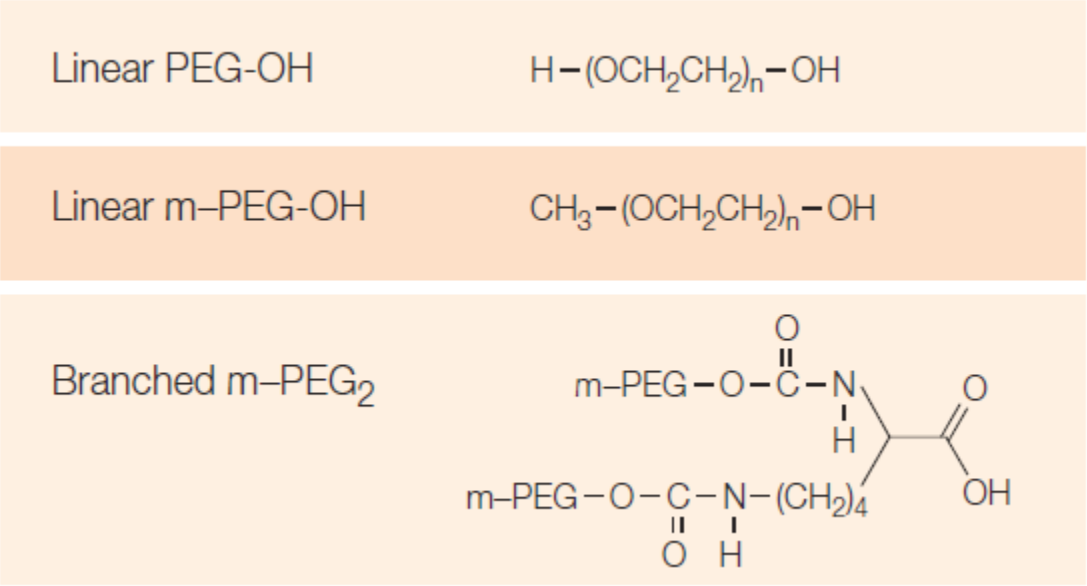

Figure 3.1: Structural formula of polyethylene glycol (PEG) molecules [62]

Therapeutic proteins are rapidly cleared from the blood by the liver, kidneys, and other organs through a number of mechanisms, which include the reticuloendothelial system, specific cell-protein interactions, renal filtration, or by proteolytic enzymes [60]. Protein clearance will vary depending on the molecule ionic charge, molecular weight, and the presence of cellular receptors [64]. Formulation changes have been investigated to modify the molecular and biochemical characteristics of proteins [65, 66, 67].

PEGylation was first developed by Davis, Abuchowski, and colleagues in the 1970s [68]. Their goal was to enhance the delivery of therapeutic molecules. More importantly, PEGylation has been shown to change the pharmacokinetics (PK) and pharmacodynamics (PD) of the therapeutic molecule [65, 69]. The pharmacokinetic modifications produced in PEGylated

proteins compared to their unmodified proteins have led to the investigation of this technology for a number of therapeutic applications. According to Harris *et al.*, there are a variety of molecules that can be conjugated to PEG, such as small molecule drugs, affinity ligands and cofactors, peptides, proteins, saccharides, oligonucleotides, lipids, liposomes and particulates, and biomaterials [60]. The advantage of using PEG for nonprotein molecules is primarily related to increased water solubility, reduced renal clearance, and decreased toxicity [69]. The focus of this dissertation thesis chapter will be testing PEG conjugation on proteins, specifically on enzymes.

3.2 Materials

Methoxy Succinimidyl Succinate PEG MW 20k was purchased from JenKem Technology USA, Plano, Texas. NuPAGE® 4-12% Bis-Tris Protein Gels, 1.0 mm, 10- and 12-well, NuPAGE® MES SDS Running Buffer (20×), NuPAGE® LDS Sample Buffer (4×), NuPAGE® Sample Reducing Agent (10×), Mark12 Unstained Protein Standard, XCell SureLock Mini-Cell gel tank, and MAbPac RP LC column were all purchased from Thermo Fisher Scientific, Waltham, Massachusetts. Trifluoroacetic acid and lyophilized bovine serum albumin (BSA) powder were all purchased from Sigma Aldrich, St. Louis, Missouri. Acetonitrile was purchased from Honeywell Burdick & Jackson (B&J), Muskegon, Michigan. All chemicals were used as received and purchased from Sigma Aldrich, St. Louis, Missouri.

3.3 Methods

3.3.1 PEGylation of Arginine Deiminase

To create PEGylated arginine deiminase (ADI), one needs to conjugate PEG onto native arginine deiminase. In this case, methoxy succinimidyl succinate 20,000 Da poly(ethylene glycol), to be referred as M-SS PEG20k, was used to produce PEGylated ADI. M-SS PEG20k was stored at -20°C as a lyophilized powder. First, the ADI concentration was held constant at 0.8 mg/mL and the PEG to ADI mole to mole ratio was varied from 20:1 PEG:ADI to 50:1 PEG:ADI in 5 molar increments. The appropriate amount of lyophilized M-SS PEG20k was weighed out for a 50 μL PEGylation reaction. Based on the actual weight of the PEG, the amount of native ADI needed and final volume of the PEGylation reaction in 100 mM $NaPO_4$ pH 8.5 was calculated. ADI and 100 mM $NaPO_4$ pH 8.5 were premixed in a separate tube using the calculated volumes. This mixture was then added to the lyophilized PEG as quickly as possible because the reaction half-life of PEG20k in solution is approximately 8 minutes. The tube with the ADI solution mixture was inverted several times to check that the PEG was fully dissolved. The PEGylation reaction was left at room temperature for 1 hour. The completed PEGylation reaction was then ready to be characterized.

3.3.2 Characterization of PEGylated Arginine Deiminase

The PEGylation reaction was first checked by a sodium dodecyl sulfate polyacrylamide gel electrophoresis (SDS-PAGE) gel. Based on the various PEGylation reactions, 500 ng of protein sample was loaded on a NuPAGE® 4-12% Bis-Tris SDS-PAGE gel and run using 1× MES (2-(N-morpholino)ethanesulfonic acid) running buffer at a constant voltage of 200 V for 60

minutes. Coomassie blue stain was used to stain the proteins in the SDS-PAGE gels overnight. The gels were then de-stained with water to an acceptable background for analysis.

Taking the same PEGylation reaction samples that were used for the protein gel, the arginine citrulline assay was run to determine the enzyme activity of the PEGylated proteins. PEGylated sample was diluted to 500 nM in assay buffer containing 50 mM HEPES pH 7.35, 160 mM NaCl, and 0.1% BSA. Next, 10 μL of the 500 nM PEGylated sample was then mixed with 80 μL of assay buffer. The sample was incubated in a thermocycler at 37°C for 5 minutes prior to the start of reaction. The ADI enzyme reaction was initiated by adding 10 μL of 50 mM arginine at 37°C, and the reaction was allowed to proceed for 2 minutes at 37°C. The reaction was stopped with the addition of 75 μL color development reaction acid (CDR acid). The sample was immediately placed on ice after reaction termination. 25 μL of color development reagent (CDR) was added into the sample and mixed well with a pipette. The sample was next heated at 95°C for 10 minutes, removed from the thermocycler, and cool downed at 20°C for 10 minutes. Lastly, 100 μL of sample was transferred to a clear, flat-bottom reading plate. The absorbance was measured at 530 nm using a SpectraMax Plus microplate spectrometer. In order to quantify the results, a citrulline standard curve was run with the enzymatic reaction.

Reversed phase high performance liquid chromatography (RP-HPLC) utilizing an ultraviolet (UV) detector was used to analyze the PEGylated arginine deiminase and to better quantify the number of PEGs on the ADI. The PEGylated sample was diluted to 2 mg/mL in 0.4 mg/mL bovine serum albumin (BSA) in water. After dilution, 10 μL of the 2 mg/mL sample was immediately injected into the MAbPac reversed phase liquid chromatography column. The chromatography program was programmed to run a gradient from 55% to 25% Mobile Phase A, with Mobile Phase A containing 0.1% trifluoroacetic acid (TFA) in water and Mobile Phase B

containing 0.1% TFA in 90% acetonitrile and 9.9% water. The entire reversed phase run was performed at 80°C.

3.4 Results

A PEGylation time course was done at a 20 to 1 mole of PEG to mole of ADI ratio. The results pictured in the SDS-PAGE gel in Figure 3.2 show that after 1 hour of PEGylation reaction, the PEGylation state stayed relatively constant. Following the time course, various PEG to ADI mole to mole ratios were tested. Figure 3.3 shows the ADI PEGylation reaction result on an SDS-PAGE gel that was run for the different PEG to ADI mole to mole ratios of 20, 25, 30, 35, 40, 45, and 50 to 1 respectively. From the gel, it is clear that the PEGylation state increased with an increase in PEG to ADI ratio by holding the reaction time constant. The results suggest that the most comparable final compound to ADI-PEG20, the drug used in current clinical trials, is the 45 to 1 PEG to ADI mole to mole ratio.

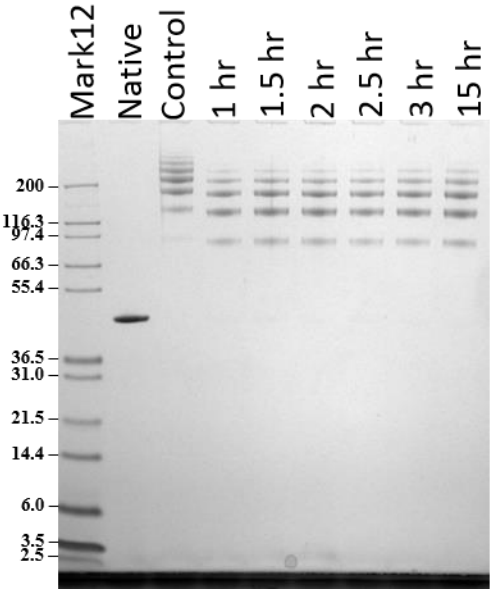

Figure 3.2: Time course of *M. hominis* PEGylation with reaction time of 1, 1.5, 2, 2.5, 3, and 15 hours. ADI-PEG20 is the control.

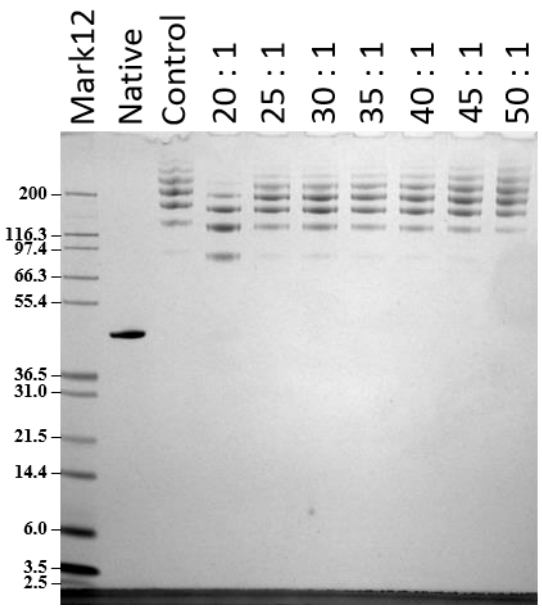

Figure 3.3: *M. hominis* PEGylation gel with different PEG to ADI mole to mole ratio from 20, 25, 30, 35, 40, 45, and 50 to 1. ADI-PEG20 is the control.

Further characterization was done on the 45 to 1 PEG to ADI ratio PEGylated sample. Enzyme activity was tested to see the effect of PEG on the enzyme. The activity of native ADI is about 18.6 IU/mg and PEGylated ADI is 5.7 IU/mg. Once the enzyme was PEGylated, there was an approximately 70% reduction in its activity with an average of 5 to 6 PEGs attached to each monomer.

The number of PEGs attached to each monomer was further quantified and verified by reversed phase high performance liquid chromatography. Figure 3.4 shows the chromatogram depicting different peaks, with distinct peaks representing different number of PEGs attached to each monomer. From the pictured distribution, the calculated average PEG number per monomer is 5.3 PEGs per monomer, with 65% of the enzymes having 4 to 6 PEGs attached and 90% of the enzymes having 3 to 7 PEGs attached.

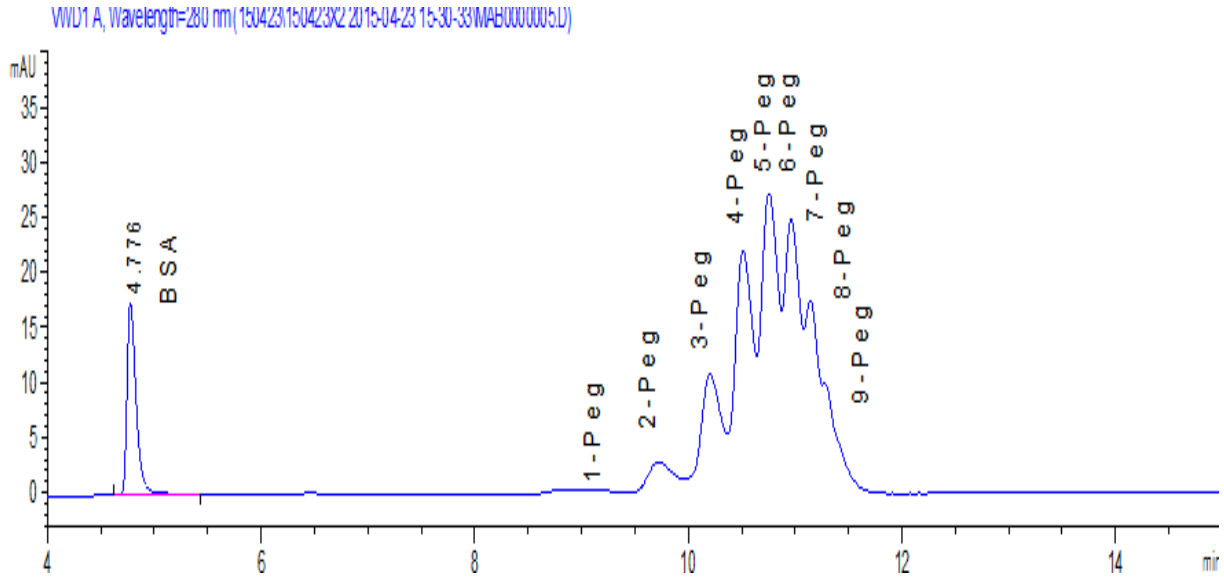

Figure 3.4: Reversed Phase Chromatography of PEGylated Arginine Deiminase

3.5 Discussion

Based on the experiments done by Holtsberg *et al.*, the methoxy succinimidyl succinate conjugated 20 kDa PEG [70], whose chemical structure is shown in Figure 3.5, was decided for all future experiments in this dissertation thesis. A further justification is that this PEG formulation is the same as ADI-PEG20, a drug already tested in previous and current clinical trials for treating hepatocellular carcinoma [72]. The methoxy succinimidyl succinate PEG covalently binds to the surface lysines on the protein as shown in the chemistry in Figure 3.6. Even though it is a stable bond, the succinimidyl succinate (SS) linker between the PEG and the lysine contains an ester group, which has limited stability *in vivo* at neutral pH and is subject to hydrolysis by endogenous esterases [73]. This mPEG-SS protein conjugate ester hydrolysis can result in a "tag" that still bound to the lysines on the protein [74, 75, 76, 77]. Therefore, over time, the protein will get cleared out by the system since no PEG protection will remain once the PEG detaches from the ester linkage.

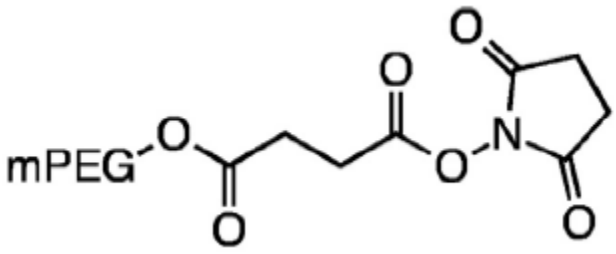

Figure 3.5: Chemical structure of methoxy succinimydl succinate PEG [71]

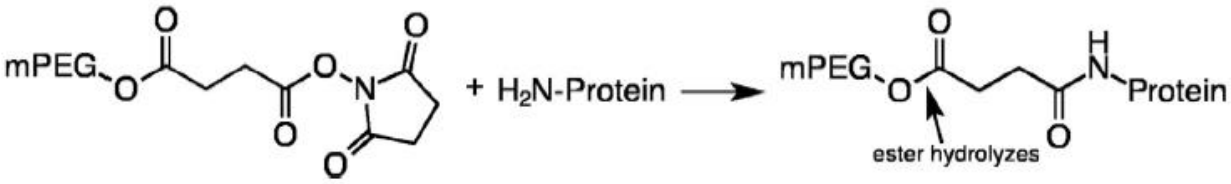

Figure 3.6: Conjugation of PEG to a protein by a SS linker. Ester hydrolysis may result in removal of PEG at the position indicated by the arrow [71]

According to Holtsberg *et al*., as the number of PEG increases per monomer, there is a decrease in enzymatic activity [70]. As shown in Figure 3.7, increasing in PEG number resulted in a linear decrease in ADI enzyme activity. Decreasing in enzyme activity with increasing PEGylation could potentially be due to hindrance by the PEGs on the enzyme movement or losses of ADI stability once PEGylated. It is also possible that some of the PEGs were attached on to the more sensitive lysines, which explains the 70% decrease in activity between the *M. hominis* native ADI versus the 20 kDa PEGylated ADI synthesized for 1 hours at 45 to 1 mole of PEG to mole of ADI ratio. In other words, the enzyme is less efficient in converting its substrate, arginine, into citrulline on a per minute per mg of enzyme basis. This trend of enzymes losing activity when PEGylated has also been shown in other ADI enzymes such as that of *M. arginini*,

as well as ADI dimers from other species that have been tested by other researchers and during the course of this dissertation research.

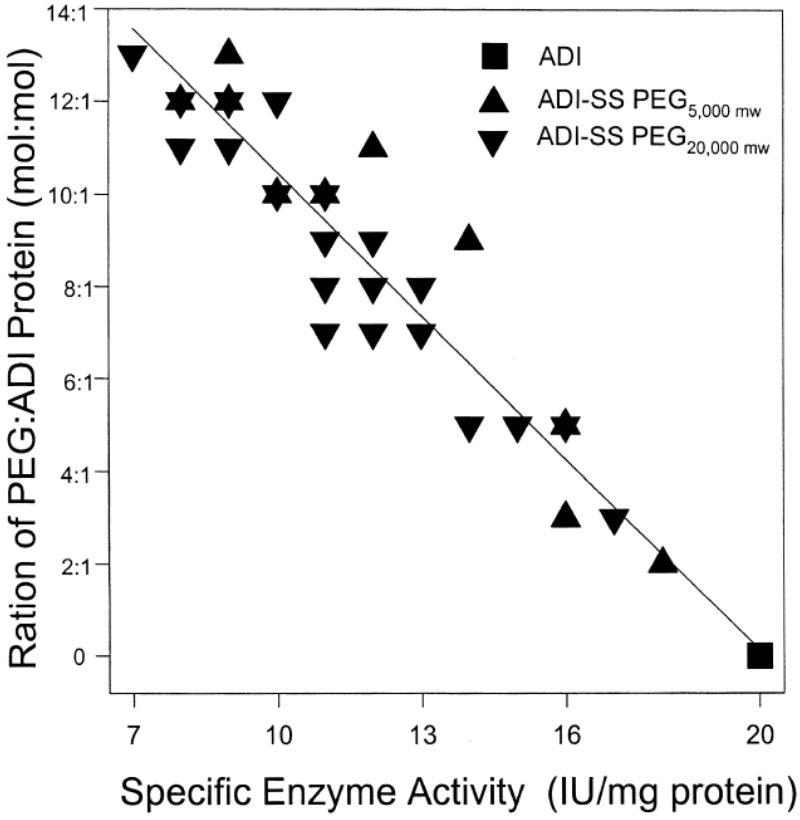

Figure 3.7: The effect of various ratios of PEG attached to ADI protein on the enzyme activity [70]

The reversed phase high performance chromatography demonstrated good separation of monomeric PEGylated ADI with distinct peaks for mono-PEG ADI, di-PEG ADI, tri-PEG ADI, all the way up to 9 or more-PEG ADI, which are the results shown in Figure 3.4. Additionally, de-PEGylated or native ADI co-eluted with similar retention times, or similar elutions. Bovine serum albumin (BSA) was used as an internal standard to prevent errors in defining 1-PEG, 2 PEG, etc. The purity of PEGylated ADI is defined as a percentage of total PEGylated ADI peak

areas divided by the number of peaks that are detected. The ability to quantify each PEG number peak can help calculate the average PEG number per monomer, since the entire chromatography run is under denatured conditions at 80°C with organic solvents as mobile phases. Therefore, the dimers are denatured into linearized monomers.

3.6 Conclusion

The experiments in this chapter were used to help develop a PEGylated version of ADI that is identical to the current standard drug, ADI-PEG20, which has been used in previous and current clinical trials. Many of the characterizations were done to verify the developed PEGylated molecule to have similar characteristics as the standard drug. First, similar PEGylation patterns to the standard drug were obtained by testing different PEG to ADI mole to mole ratios, as confirmed by SDS-PAGE gel. The time course on the PEGylation reaction was then run to verify the short half-life of the methoxy succinimidyl succinate linker on the PEG. Then various ratios of PEG to ADI were tested to find the best ratio to achieve similar PEG patterns as the standard drug.

Further characterization of the drug points to the possibility that once the enzyme is PEGylated, the PEG hinders enzyme movement and some sensitive surface lysines were PEGylated, which contributed to the lower activity. Lastly, the qualitative method of determining the number of PEGs on the enzyme by gel was compared to the quantitative method of calculating the average PEG number per monomer of enzyme by running the sample through a reversed phase chromatography column. Both the data from qualitative and quantitative data agreed with each other. In short, a comparable PEGylated ADI was developed successfully compared to the standard drug of ADI-PEG20 being used in clinical studies.

3.7 Acknowledgements

This chapter and its methods were developed and owned by Polaris Pharmaceuticals, Inc., San Diego, California. Collaborators for this development: Jason (Li-Chang) Chen, Richard Showalter, Wei-Jong Shia, Wes Sisson, Derek Lee, Bob Alamassy, and Jim Thomson. The dissertation author was the primary investigator and author of this material.

Chapter 4: SHELS Arginine Deiminase

4.1 Synthetic Hollow Enzyme Loaded Nanospheres (SHELS)

As discussed in Chapter 3, PEGylating arginine deiminase has provided benefits of increasing serum circulating half-life and decreasing the sensitivity of the immune response to ADI. However, its efficacy can still be improved. These challenges may be addressed with the design of a nanoparticle-based enzyme delivery system. Delivery systems in the form of enzyme encapsulated nanoparticles have been developed because of persistent immunogenicity and loss of activity of therapeutic enzymes after PEGylation. The strategies for enzyme encapsulation usually involve loading enzymes into nanoparticle carriers. The potential advantages of using nanoparticles as enzyme carriers may include improved enzyme stability, reduced immunogenicity, and reduced toxicity [78]. In addition, varying the material size, shape, and surface functional groups of the nanoparticles may further extend the circulation half-life of the nanoparticles and the encapsulated enzymes [79]. These strategies assume that the enzyme is stable throughout the circulation of the nanoparticle.

The most common types of nanoparticles studied for therapeutic enzyme delivery are liposomes, polymeric nanoparticles, and silica nanoparticles [78]. Although there is potential for success in applying these nanoparticles to therapeutic enzyme delivery, none of these enzyme encapsulated nanoparticles have not yet been tested in clinical trials. Currently, the only nanoparticles, including liposomes and polymeric nanoparticles, tested in clinical trials or approved as drugs have been involved in the delivery of small molecules [79, 80] rather than macromolecules such as enzymes.

Another approach that promises lower cost and more generality is a platform where enzymes are encapsulated in a protecting structure, which either releases the enzyme at the target [81, 82, 83, 84] or allows substrate to access the enzyme [85, 86, 87, 88, 89]. The approaches that depend on the release of the enzymes often suffer from nonspecific release as well as inefficient synthesis and loading [81, 82, 83, 85]. Therefore, the encapsulation of enzymes in nanoporous and mesoporous matrices made of materials such as silica [86, 90], polyelectrolyte [88], or polymer [85], and inorganic hollow nanoparticles such as gold [89] have been studied extensively. However, these approaches also suffer from limitations such as low encapsulation efficiencies, reduced enzyme activity, stability of the enzyme and nanoparticles, and nanoparticle toxicity [87, 88].

Synthetic hollow enzyme loaded nanospheres (SHELS) are a versatile class of nanoparticles developed by Ortac *et al*. group with a robust manufacturing process that can lead to a universal delivery system for nonhuman enzymes. This platform exhibits some important features for delivery of a bacterial enzyme such as ADI, including exquisite control in synthesis, above average enzyme entrapment, protection from neutralizing antibodies and proteases access, no loss in enzyme activity, and decent circulation half-life and stability [91]. Ortac *et al*. have shown some promising results with L-asparaginase encapsulation in this platform, demonstrating the ability of the substrate asparagine to enter the SHELS particle, but to prevent macromolecule movement in or out.

To summarize the design of nanoparticles as carriers for therapeutic enzyme delivery for systemic amino acid depletion, there are some important considerations. First, the material for the nanoparticles must be biocompatible to avoid any toxicity to the body and must be biodegradable to avoid accumulation that leads to long-term toxicity. Second, the synthesis of

these enzyme encapsulated nanoparticles must not affect the activity of the enzyme. Third, these nanoparticles must protect the enzymes from proteases and mask the immunogenic epitopes on the surface of the enzyme from immune cells. Lastly, the nanoparticles must have long circulating half-life in the serum in order to maintain therapeutic efficacy of the enzyme.

The SHELS developed by Ortac *et al*. have shown most of the important characteristics for therapeutic enzyme delivery. The question remains as to whether a modified version of the platform described by Ortac *et al.* can be utilized with arginine deiminase to achieve similar results. This chapter discusses a potential approach and the limitations of amino acid depletion therapy for cancer treatment that drive the design of a silica based nanoparticle for the delivery of a therapeutic enzyme, arginine deiminase, as an amino acid depletion therapy for the treatment of cancer patients.

4.2 Materials

Nanobead NIST traceable particle size standard 200 nm was purchased from Polysciences, Inc., Warrington, Pennsylvania. Carboxyl latex 4% w/v 0.06 μm was purchased from Life Technologies, Inc., Carlsbad, California. 1× Phosphate Buffer Saline without calcium and magnesium was purchased from Corning, Inc., Corning, New York. Ethanol, hydrochloric acid, 97% (3-Aminopropyl)trimethoxysilane, 99% Tetramethyl orthosilicate, Poly-L-Lysine hydrobromide MW 300,000 lyophilized powder gamma-irradiated BioXtra were purchased from Sigma Aldrich, St. Louis, Missouri. Recombinant Proteinase K, PCR grade was purchased from Thermo Fisher Scientific, Waltham, Massachusetts. Fisherbrand borosilicate, squared cover glass, 22 mm × 22 mm was purchased from Fisher Scientific, Hampton, New Hampshire.

VWR hot plate was purchased from VWR International, Radnor, Pennsylvania. Q125 Sonicator was purchased from QSonica, LLC, Newtown, Connecticut. All chemicals were used as received and purchased from Sigma Aldrich, St. Louis, Missouri.

4.3 Methods

4.3.1 Synthetic Hollow Mesoporous Nanospheres Synthesis

To synthesize 1× of synthetic hollow mesoporous nanospheres (SHMS), 50 μL of template, 200 nm amine group functionalized polystyrenes on the surface, was added drop by drop into 40 μL of mask, 60 nm carboxyl group functionalized polystyrenes, while slowly vortexing the mixture. The final mixture was vortexed and then shaken at room temperature for 30 minutes. This created the core structure of the nanosphere. Then, 1 mL of ethanol containing 1 μL tetramethyl orthosilicate (TMOS) and 0.5 μL (3-Aminopropyl)trimethoxysilane (APTMS), were mixed to make the silica mixture. Next, the polystyrene core structure mixture was then added into the silica mixture with a final volume of about 1091.5 μL. The mixture was shaken at room temperature for 12 – 21 hours. After this incubation, the mixture was vortexed to ensure the silica and polystyrene were well re-suspended. The mixture was then centrifuged at 14,000 rpm (18,000 rcf) at 4°C or room temperature for 5 – 10 minutes. The supernatant was discarded as toxic waste because it contained TMOS, and 1 mL of ethanol was added to fully re-suspend the pellet. The washing of the silica pellet was repeated 3 times and the final volume was adjusted to 50 μL of ethanol after the wash. The final volume was the volume of the initially used template, but if the silica coated polystyrene was too viscous, additional ethanol was added to a maximum of twice the starting volume.

The final silica coated polystyrene mixture was re-suspended, vortexed, and bath sonicated. Using a pipette, every 200 μL of sample mixture was slowly dripped onto the center of a 22 mm by 22 mm borosilicate glass slide with a thickness of about 0.16 to 0.19 mm. The sample was dried on the glass slide inside a chemical hood with a clean environment where no particulates can contaminate the sample. Once the samples were dried, the glass slides were placed on a hot plate covered under a foil-covered glass beaker heating at 450°C for 12 hours. This process is referred to as calcination.

After the calcination process, the glass slides were carefully removed from the hot plate. The samples appeared white, dried, and opaque on the glass slides. Using a pipette tip containing ethanol, the synthetic hollow mesoporous nanospheres (SHMS) were gently scraped off the glass slide into a 1.7 mL Eppendorf tube until most of the SHMS (white, opaque color) were off the glass slide. The scraped off SHMS sample was centrifuged at 14,000 rpm (18,000 rcf) at 4°C or room temperature for 5 – 10 mins. The supernatant containing TMOS was disposed as toxic waste and 1 mL of 1× PBS was added to fully re-suspend the pellet. The washing of the SHMS was repeated 3 times and the final volume was adjusted with 1× PBS to 50 μL. A probe sonicator was then used to fully disperse the SHMS on ice with 40% amplitude for 10 seconds total with a 1 second pulse on and 1 second pulse off. A final vortex and quick centrifugation after probe sonication completed the synthesis of SHMS.

4.3.2 Characterization of Synthetic Hollow Mesoporous Nanospheres

To characterize the synthetic hollow mesoporous nanospheres (SHMS) and check that they were properly synthesized, the samples were imaged using a scanning electron microscope (SEM). To prepare the samples, 1 μL of SHMS sample was diluted into 499 μL of ddH_2O. Then,

1 μL from the 500 μL diluted sample was pipetted onto a silicon chip. After the sample dried overnight, iridium was sputter coated onto the sample for imaging.

4.3.3 Loading Arginine Deiminase into Synthetic Hollow Mesoporous Nanospheres

To load the arginine deiminase (ADI) enzyme into synthetic hollow mesoporous nanospheres (SHMS), 10 μL of 100 mg/mL ADI was added into 49 μL of SHMS in 1× PBS. This sample mixture was shaken at 4°C overnight. To make 1% Poly-L-Lysine hydrobromide (PLL), 500 μL of dH_2O was added into 5 mg of lyophilized PLL powder. To start the sealing of the enzyme inside the SHMS, 5 μL of 1% PLL and 1 mL of 1× PBS were added into this mixture and left in a 4°C shaker temporarily. In the meantime, silicic acid, $Si(OH)_4$, stock was prepared by adding 75 μL of TMOS into 500 μL of 1 mM HCl. $Si(OH)_4$ stock was prepared fresh and used immediately due to precipitation within an hour. The $Si(OH)_4$ was vortexed well, and 25 μL of $Si(OH)_4$ was then added into the sample mixture in the 4°C shaker. This sample mixture remained for 2 – 4 hours in the 4°C shaker. This completed the loading and sealing of the ADI inside the SHMS.

The sol-gel coated SHMS, also known as synthetic hollow enzyme loaded nanospheres (SHELS), were then centrifuged at 14,000 rpm (18,000 rcf) at 4°C for 10 minutes. Once again, the supernatant was discarded as toxic waste and 1 mL of 1× PBS was added to fully re-suspend the pellet. The washing of the SHELS was repeated 3 times, and the final volume was adjusted to 200 μL with 1× PBS. Bath sonication of the 200 μL of SHELS was continued for 10 minutes at 4°C. The 200 μL sample was aliquoted into 2 tubes of 100 μL of SHELS each, where one sample was then treated with proteinase K and the other was left untreated. 1 μL of 20 mg/mL proteinase K was added into the first 100 μL SHELS sample to achieve a final proteinase K concentration

of 0.2 mg/mL. Both samples, with and without proteinase K treatment, were then shaken at 37°C for overnight.

4.3.4 Characterization of SHELS Arginine Deiminase

The modified BUN assay was run on the proteinase K treated samples to check protein loading and enzyme activity. The SHELS arginine deiminase sample was diluted with different dilution factors for the enzymatic assay using the assay buffer containing 50 mM HEPES pH 7.35, 160 mM NaCl, and 0.1% BSA. Next, 10 µL of the diluted sample was mixed with 80 µL of assay buffer. The sample was incubated in a thermocycler at 37°C for 5 minutes prior to the start of reaction. The ADI enzyme reaction was started by adding 10 µL of 50 mM arginine at 37°C and the reaction was run for 2 minutes at 37°C. The reaction was stopped with the addition of 75 µL color development reaction acid (CDR acid). The sample was immediately placed on ice after reaction termination. Then, 25 µL of color development reagent (CDR) was added into the sample and mixed well with a pipette. The sample was heated at 95°C on the thermocycler for 10 minutes followed by a 20°C cool down for 10 minutes. It is critical to remove the sample from the thermocycler between temperature adjustments. 100 µL of sample was transferred to a clear, flat-bottom reading plate and the absorbance at 530 nm was measured by a SpectraMax Plus microplate spectrometer.

4.4 Results

To make synthetic hollow enzyme loaded nanospheres (SHELS) with arginine deiminase, high concentrations (100 – 150 mg/mL) of recombinant *M. hominis, M. brale-arg,* and *M. gal-ine* arginine deiminase were made and purified in a similar way as *M. hominis*. The synthetic

hollow mesoporous nanospheres (SHMS) were then synthesized. Many iterations of SHMS synthesis were done to optimize the synthesis conditions and combinations to arrive at the final synthesis protocol. The variables that were optimized were the 200 nm NIST polystyrene particles (template), 60 nm carboxyl conjugated polystyrene particles (mask), tetramethyl orthosilicate (TMOS), (3-Aminopropyl)trimethoxysilane (APTMS), and silica reaction time.

To begin, different template to mask ratios were attempted, from 50 µL to 125 µL of template and from 40 µL to 60 µL of mask. Using Malvern's Zetasizer Nano, the template has a zeta potential of about -36 mV, while the mask has a zeta potential of about -38 mV. Figure 4.1 shows the scanning electron microscopy (SEM) images of the initial template to mask ratio being held constant with varying TMOS, APTMS, and silica reaction time. Out of the 12 conditions tested, some were better than others, but none of the conditions produced good SHMS for arginine deiminase loading. Further optimizations were tested until the synthesis of SHMS was acceptable, meaning there were holes on the surface in this hollow silica nanospheres, which are needed to allow the enzymes to be loaded into the hollow spheres. The structure of these optimal nanospheres is comparable to wiffle balls.

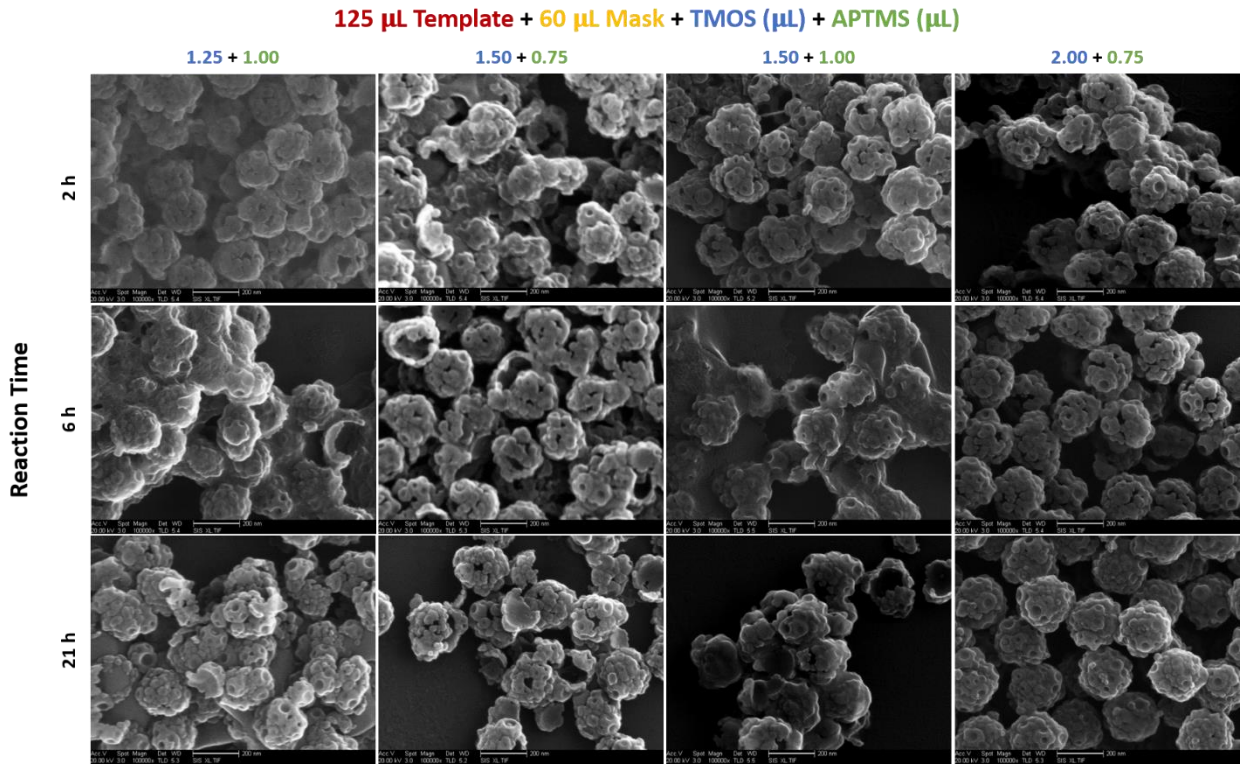

Figure 4.1: Scanning electron microscopy (SEM) images of optimization of SHMS

After many iterations of trial and error, a final condition was found where the SEM images of these silica hollow particles showed enough holes on their surfaces. The finalized condition is described in Figure 4.2, where 80 µL of template was mixed with 60 µL of mask. The silica reaction consisted of an 18 hour reaction with 1.5 µL of TMOS and 1 µL of APTMS. This combination created is so called "1× Particles", which was estimated to be 2 billion nanospheres quantified by Malvern's NanoSight in conjunction with its built-in function nanoparticle tracking analysis (NTA). This NTA can track particle sizes from 10 – 2000 nm in solution. The SEM images in Figure 4.2 roughly estimated these SHELS ADI particles to be around 215 nm to 240 nm in diameter. Additional 1× SHMS batches were made in order to load ADI and seal the hollow particles to create SHELS by using PLL and silicic acid, a form of silica, to close off the holes on the SHMS. After proteinase K (PK) treatment, the enzyme

activity of these SHELS ADI were tested. The results shown in Figure 4.3 describe the native *M. brale-arg* and *M. gal-ine* were assay controls where PK destroyed *M. brale-arg* enzyme but PK did not destroy *M. gal-ine*. Nanoparticle encapsulated *M. brale-arg* had an encapsulation efficiency of approximately 40%, while nanoparticle encapsulated *M. gal-ine* did not showed any difference in activity. These results make sense, especially for *M. gal-ine* nanoparticles because the native enzyme itself can stay functional even after incubating with PK.

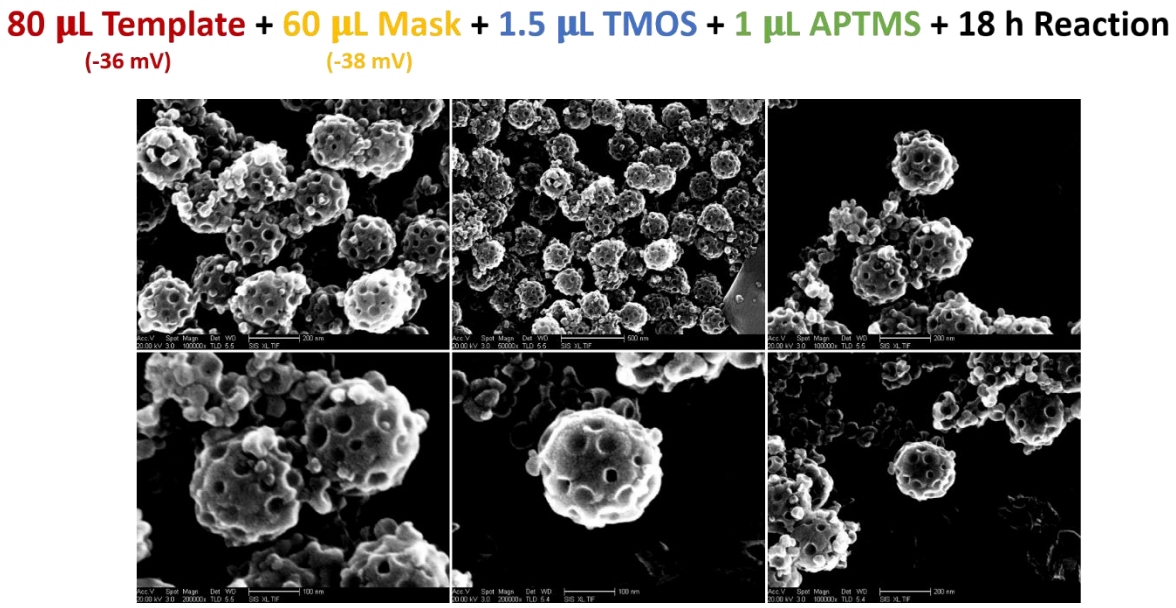

Figure 4.2: Scanning electron microscopy (SEM) images of finalized synthesis condition for SHMS

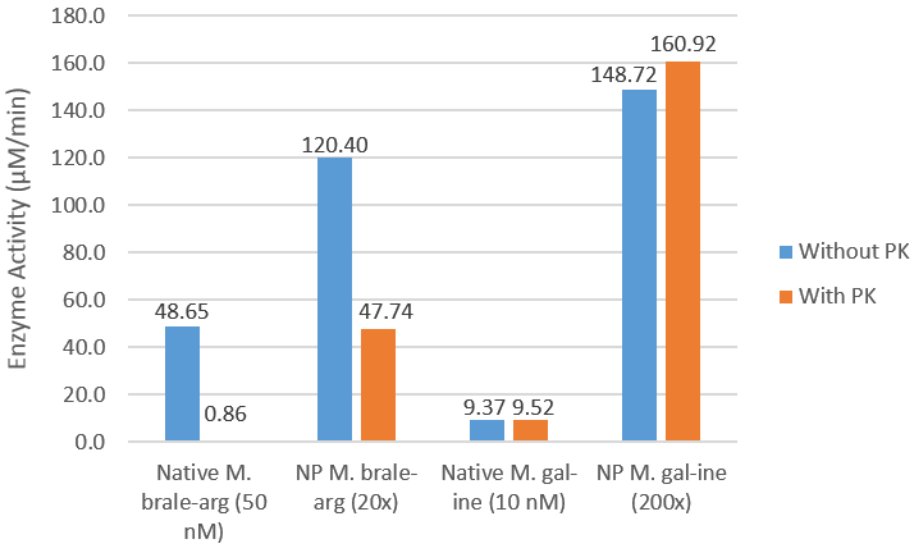

Figure 4.3: Nanoparticle encapsulated ADI enzyme, *M. brale-arg* and *M. gal-ine*, comparing enzyme activity before and after PK treatment.

Since there were potentially promising results, the next planned step was to scale up and produce ten batches of 1× particles for ADI loading, but unfortunately, the production process was not robust enough to repeat the synthesis of these SHMS after a couple months of idle production. As a result, troubleshooting involved the replacement of all materials and reagents, purchase of new and different polystyrene particles, and adjustment of synthesis conditions. Over these months of optimization, synthesis of SHMS with surface holes on the hollow particles was unsuccessful. Only divots were formed, rather than holes on the surface of these SHMS. Despite numerous attempts over several months, SHMS was not reproducible. Ultimately, further synthesis and optimization attempts were terminated.

4.5 Discussion

The synthesis of SHELS is based on the synthesis of SHMS, depicted in Figure 4.4. The 200 nm template and 60 nm mask interacts electrostatically through differences in the surface

charges of the polystyrene nanoparticles. Both the template and mask are negatively charged, but the mask is more negatively charged relative to the template. Therefore, the slight difference in zeta potential creates an electrostatic interaction between the two different polystyrene particles. Figure 4.5 shows the silica formation chemistry, during which silica deposits between the masks and onto the template. The melting temperature for silica is 1,710°C [93], while for polystyrene is 249°C [94]. Therefore, at 400°C, the polystyrenes that helped form the core structure of these hollow silica nanospheres will be calcinated while the coated silica will not melt. The holes formed on the nanospheres we produced were measuring between 2 nm to 6 nm in diameter, which is large enough for an enzyme to pass through. The process of loading the enzyme into the SHMS occurs when the enzyme reaches equilibrium between the inside and outside of the SHMS. The poly L-lysine (PLL) polymer is a positively charged polymer that coats over the SHMS particle to reduce the size of the holes. Lastly, a final silica based silicic acid coating coats over the positive PLL layer to further reduce the pores to smaller sizes so that only small molecules can pass through. The entire process is shown in Figure 4.6.

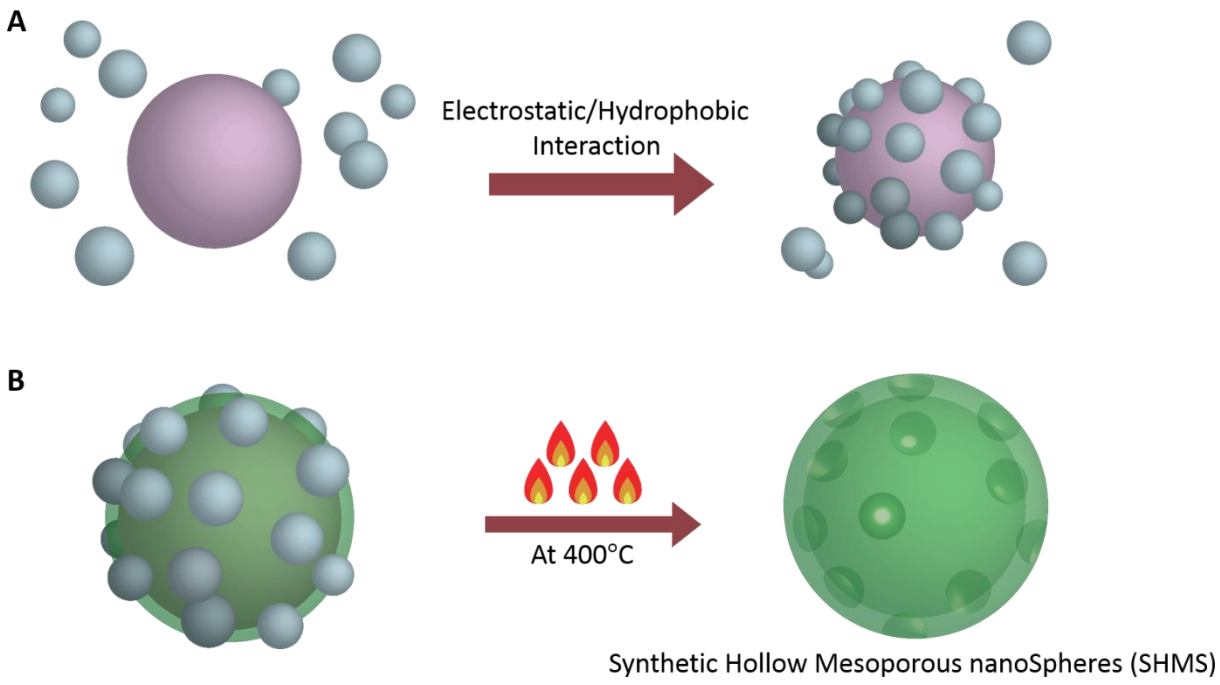

Figure 4.4: SHMS Synthesis Process: (A) The formation of the SHMS core structure through electrostatic and hydrophobic interaction of the polystyrene particles, (B) Silica coating on core structure followed by calcination process to create SHMS

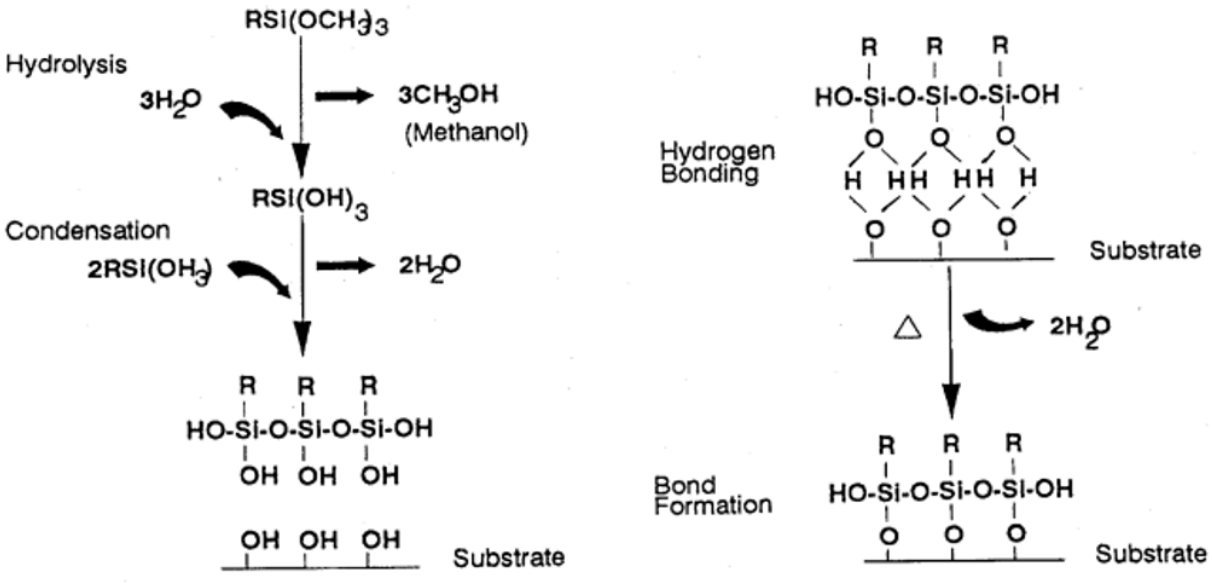

Figure 4.5: The chemistry of alkoxy silanes to depict how silica is formed on the surface of the nanoparticles [92]

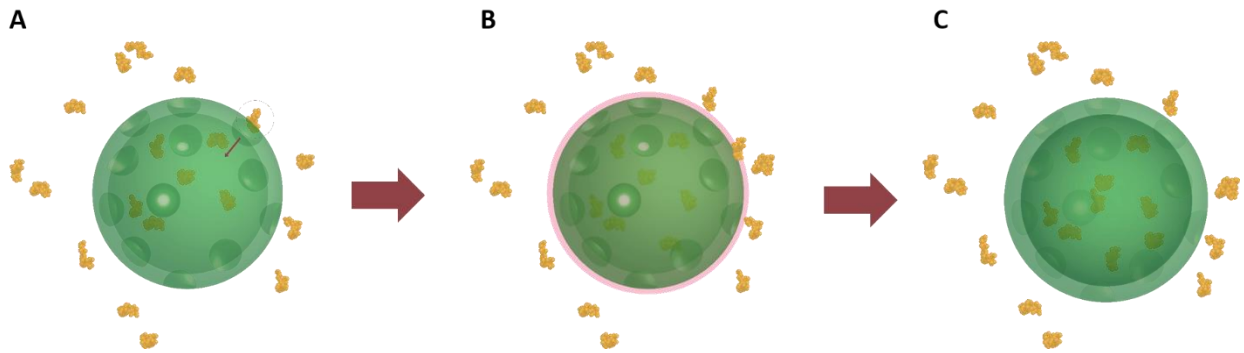

Figure 4.6: Enzyme loading and silica coating. (A) Enzyme diffusion through mesopores (B) Cationic polymer coating (C) Sol-gel reaction

These SHMS were created and two different sizes of arginine deiminase enzymes were loaded into the nanospheres. One of the loaded ADI was a dimer named *M. brale-arg* with a molecular weight of about 93 kDa. The other ADI loaded was a hexamer named *M. gal-ine* with a molecular weight of about 278 kDa. Both ADIs were successfully loaded into SHMS to form the final SHELS ADI. Proteinase K (PK) was used to get rid of any ADIs that were on the exterior of the SHELS particle, but the activity of native *M. gal-ine* did not change from before to after the PK treatment [95]. PK was shown to be a serine protease with a specificity as an enzyme for any peptide bonds adjacent to the carboxylic group of aliphatic and aromatic amino acids [96]. Therefore, it is safe to say that the enzyme activity tested in these SHELS particle is coming from the encapsulated enzymes within the silica.

Many of the issues faced during the synthesis of SHMS involved creating the silica coating on the core structure of the polystyrene particles. One of the issues encountered was that formation of silica is rapid in solution, so if too much precursor were used, both TMOS and APTMS, the silica would not form on the surface of the polystyrenes. The APTMS silica was used because it has amine groups attached to the silicon, which carries a positive charge to help TMOS, which is negatively charged, form on the surface of the polystyrenes, which are also

negatively charged. The second issue is the weakness of the electrostatic interaction between the template and mask. When the silica forms on the polystyrene particles, it often started to form in between the template and mask. As a result, after calcination of the sol-gel nanospheres, divots were formed instead of holes. It is suspected that the silica formation and interaction is greater than the interaction between the template and mask, which caused the silica to deposit between the two.

Different types of template were explored to potentially solve the issue of weak interactions between the template and mask. For instance, amine conjugated polystyrenes were tried because amine groups carry positive charge and they complement well with carboxyl groups, which is what the masks are conjugated with. The results of that optimization did not solve the weak electrostatic interactions between the template and mask. Further testing involved adding smaller amounts of TMOS and APTMS but increasing reaction time with hope that the silica would deposit better on the polystyrene particles. That did not solve the issue of forming holes. Reducing the temperature of the silica formation from room temperature to 4°C also did not resolve the issue. A number of additional conditions were also tested, but did not solve the issue of divots forming instead of holes.

4.6 Conclusion

After many iterations of optimizing SHMS synthesis, a final condition of 80 μL of template was mixed with 60 μL of mask with an 18 hour silica reaction consisting of 1.5 μL of TMOS and 1 μL of APTMS was able to produce a batch of good SHMS. To seal the enzymes within the hollow nanospheres after loading, positively charged PLL and silicic acid were used to create a fine mesh. It was shown through an *in vitro* modified BUN assay that for these

SHELS, the dimeric ADI was encapsulated successfully. On the other hand, the encapsulation of the hexameric ADI cannot be concluded since the addition of PK was not able to destroy the hexameric enzyme activity.

Additional batches of SHMS particles were planned to be synthesized for the making of SHELS ADI for further characterization and analysis before testing in an animal study. Issues arose during this production. The SHMS were not reproducible with the same conditions as optimized, and attempts at resolving the issues with hole formation were not successful. Unfortunately, this SHELS particle had to be terminated because of the extensive time and efforts being invested without producing a resolution to the synthesis production issues.

4.7 Acknowledgements

This chapter and its methods are developed and owned by Ortac and Esener *et al*. from the University of California San Diego, La Jolla, California with a co-development with Polaris Pharmaceuticals, Inc., San Diego, California. Collaborators for this development: Jason (Li-Chang) Chen, Ya-San Yeh, Negin Mokhtari, Jim Thomson, and Sadik Esener. The dissertation author was the primary investigator and author of this material.

Chapter 5: Silica Coated Arginine Deiminase Liposome

5.1 Liposome

In 1961, British hematologist Alec D. Bangham first described liposomes at the Babraham Institute in Cambridge, United Kingdom [97, 98, 99]. Bangham described how molecules such as phospholipids interact with aqueous solutions to form a unique, closed, bilayer structure, which are now designated as liposomes [100]. The word liposome derives from two Greek words: *lipo* meaning fat and *soma* meaning body. Today, liposomes are established as a useful model membrane system, and they have demonstrated potential as a drug delivery system. A wide variety of amphipathic molecules have been used to form liposomes, and the method of preparation can be tailored to control their size and morphology. The medicinal material can either be encapsulated in the aqueous space or intercalated into the lipid bilayer. The exact location of a drug in the liposome depends on its physicochemical characteristics and the composition of the lipids.

Liposomes are artificially made biological, spherical vesicles that are composed of natural, synthetic, or a mixture of derived phospholipid layers surrounding aqueous layers [101]. Liposomes are formed by a stable bilayer of phospholipids, where the hydrophobic lipid tail of the amphiphiles forms the interior of the bilayer, and the hydrophilic lipid head is exposed to aqueous solutions [102]. There are several other components to create a stable liposome. Phospholipids such as phosphatidylcholines provide the backbone and structure to lipids, cholesterol changes the mechanical properties of the lipid bilayers [103] and the anionic dicetylphosphate (3-dihexadecylphosphate) or the cationic stearylamine or DOTAP (1,2-dioleoyl-3-trimethylammonium-propane) prevents vesicular fusion [104]. To prevent rapid

clearance from the bloodstream, the lipid polymer derivative of polyethylene glycol (PEG) is used to synthesize liposomes [105]. The interior of the vesicle is an aqueous core which has the same chemical composition of the protein or drug being encapsulated. Furthermore, it can also contain hydrophobic payloads, shown in Figure 5.1, and it protects the encapsulated payload from metabolic processes and immune clearance [107, 108].

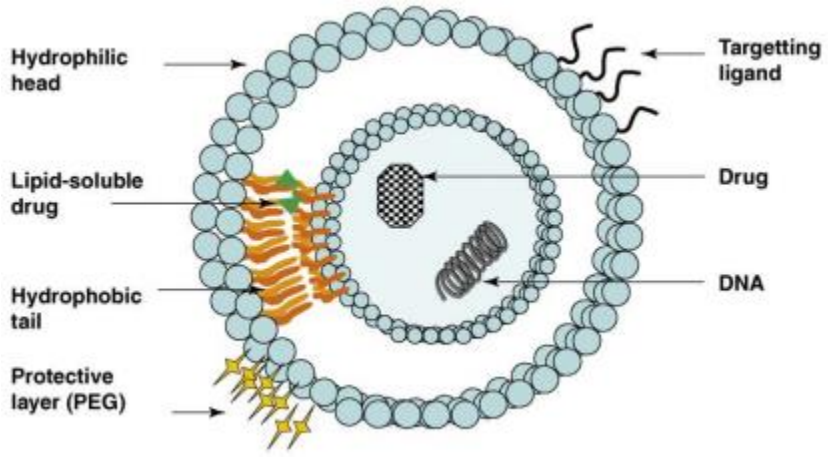

Figure 5.1: Structure of a liposome showing its ability to capture different properties of payloads [106]

Liposomes are available in many different sizes and shapes for different applications. They are classified according to the number of phospholipid bilayers and the size of the vesicle. Liposomes can be multilamellar, oligolamellar, or unilamellar. Multilamellar liposomes contain multiple lipid layers separated by aqueous layers and have diameter greater than 500 nm. Oligolamellar vesicles contain two to three lipid bilayers with a diameter of 100 nm to 1000 nm. Unilamellar vesicles contain only one lipid bilayers and their size range varies depending on their classification as small (20 – 100 nm) or large (greater than 100 nm) unilamellar vesicles. Lastly, giant vesicles are multilamellar vesicles by definition because their diameters are larger

than 10 μm [109, 110]. The size of liposomes varies from 20 nm to 10 μm in diameter, which serves as a convenient delivery platform.

There are several materials that have been encapsulated into liposomes because of their biocompatibility, biodegradability, low toxicity, and multifunctionality to encapsulate both hydrophilic and hydrophobic materials. These include anticancer agents such as doxorubicin [111, 112, 113], vaccines such as cytokines [114, 115], antifungal agents such as amphotericin B [116, 117], antibiotics such as vancomycin [118, 119], and proteins such as insulin [120]. Some critical factors for successful liposomal formulation are the colloidal and chemical stability of the phospholipid bilayer. These tiny lipid vesicles have a tendency to accumulate within the organs of the reticuloendothelial system (RES) and also at the disease sites, which includes tumors [121, 122, 123, 124]. As a result, liposomes have the potential to modify the pharmacokinetics and pharmacodynamics of the entrapped drugs.

Given liposomes' biocompatibility, low toxicity, and ability to encapsulate payloads, the development of a silica coated liposome encapsulated arginine deiminase (ADI) is an appealing alternative drug delivery system for the enzyme. Extensive research on delivering a foreign enzyme in the human body is being carried out. The current standard formulation of an enzyme for delivery *in vivo* is PEGylation, which was discussed in Chapter 3, but there are still many issues associated with this formulation. The rationale behind adding a chemically assembled silica layer on the external surface of the liposomes has been shown to have potential because it allows the retention of the fundamental properties of the free liposomes [125]. These silica coated liposomes act as nonporous particles for large molecules such as proteins and are extremely permeable for small molecules like glucose, amino acids, and vitamins [126]. Silica nanoparticles can be synthesized from different processes, such as self-assembly of bioinspired

synthesis [127], noncovalently and covalently bonded organic substrates [128], precipitation and condensation reactions [129], and sol-gel polymerization [91].

This chapter discusses an alternative enzyme delivery platform that is more robust in manufacturing and has all the essential features of a delivery platform compared to the synthetic hollow enzyme loaded nanospheres (SHELS) described in Chapter 4. Instead of creating synthetic hollow mesoporous nanospheres (SHMS) to capture the enzyme, liposomes will be used to encapsulate the ADI enzymes. The final outermost layer coating will be a silicic acid coating similar to the one used to coat SHMS particles.

5.2 Materials

Chicken egg PC, ovine cholesterol, 18:1 TAP (DOTAP), 14:0 PEG5000 PE (PEG lipid), extruder device, 1 mL glass syringes, and 10 mm filter supports were all purchased from Avanti Polar Lipids, Inc. Alabaster, Alabama. Nuclepore track-etched polycarbonate, 19 mm, membranes with pore sizes 0.2, 0.4, and 0.8 μm were purchased from Whatman plc, Maidstone, United Kingdom. Recombinant Proteinase K, PCR grade was purchased from Thermo Fisher Scientific, Waltham, Massachusetts. Diethyl ether, chloroform, hydrochloric acid, 97% (3-Aminopropyl)trimethoxysilane, and 99% Tetramethyl orthosilicate were purchased from Sigma Aldrich, St. Louis, Missouri. Float-A-Lyzer G2 dialysis device with 100 kDa MWCO was purchased from Spectrum Laboratories, Inc., Rancho Dominguez, California. All chemicals were used as received and purchased from Sigma Aldrich, St. Louis, Missouri.

5.3 Methods

5.3.1 Synthesis of Arginine Deiminase Liposome

Liposome synthesis was performed with four different lipids: Egg PC (L-α-phosphatidylcholine) from chicken, cholesterol from ovine, 18:1 TAP (DOTAP) (1,2-dioleoyl-3-trimethylammonium-propane, chloride salt), and 14:0 PEG5000 PE (1,2-dimyristoyl-sn-glycero-3-phosphoethanolamine-N-[methoxy(polyethylene glycol)-5000], ammonium salt). Their chemical structures are presented in Figure 5.2. Prior to synthesis, the three main lipids were mixed in three separate glass vials as the following: 295 µL of 25 mg/mL Egg PC, 50 µL of 50 mg/mL cholesterol, and 120 µL of 10 mg/mL DOTAP were added to a glass vial labeled "A". In glass vial "B", 50 µL of 50 mg/mL cholesterol, 120 µL of 10 mg/mL DOTAP, and 60 µL of 50 mg/mL PEG lipid were added. Lastly, 60 µL of 50 mg/mL PEG lipid was added to vial "C". Solvent chloroform ($CHCl_3$) in all 3 vials were evaporated with a small stream of nitrogen gas along with vortex mixing.

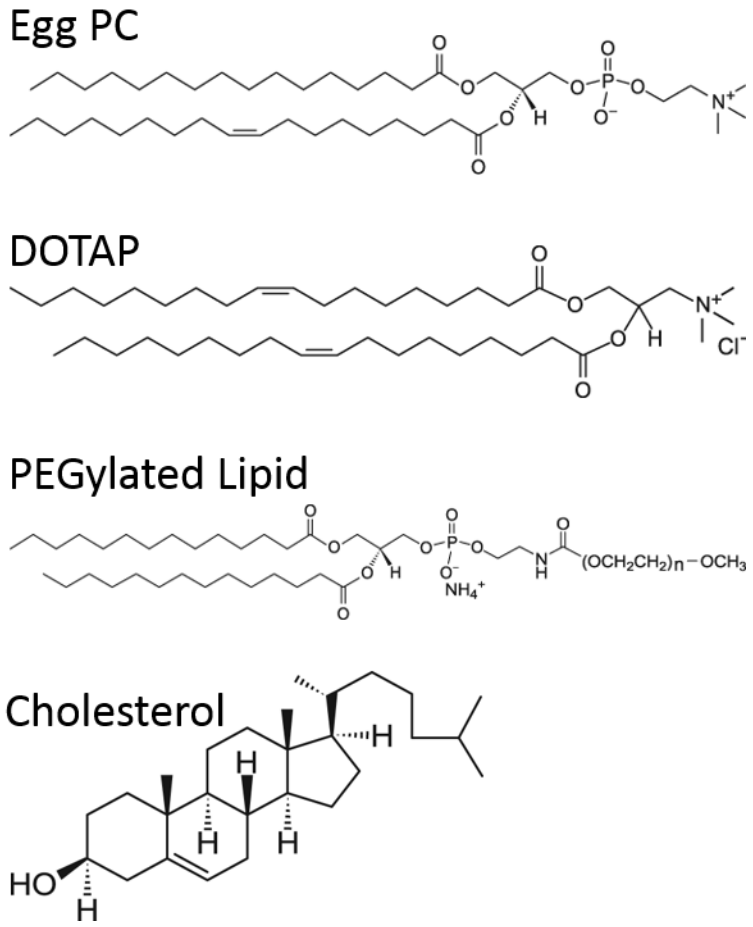

Figure 5.2: Chemical structures of lipids used for the synthesis of liposome

To reconstitute vial A, 1 mL of diethyl ether (Et_2O) was added. Next, 100 µL of 157 mg/mL arginine deiminase (ADI) was added in to vial B. Lastly, 1 mL of 1× PBS was added in to vial C. To help dissolve the vial B mixture, 100 µL of vial A mixture was added to vial B. Mixture B was then slowly added, dropwise with vortexing into vial A. Vial A and B mixture was vortexed vigorously and mixed with a homogenizer for 30 seconds. Solvent diethyl ether was evaporated with a small stream of nitrogen gas and vortexed until the mixture was in a gel form. Mixture C was slowly transferred into the vial A and B mixture and this final mixture was placed in a vacuum desiccator for at least an hour to ensure all residual solvents were evaporated.

To narrow down the size unity of the liposomes, the extrusion process was performed with three different membrane sizes. Starting from the biggest membrane filter of 800 nm, the liposome encapsulated ADI was pushed through the membrane back and forth three times. This extrusion process was repeated with 400 nm and 200 nm membrane filters respectively. The extruder device is depicted in Figure 5.3 below. The extruded liposomes, referred to as the non-dialyzed sample, were transferred into a Float-A-Lyzer dialysis device with a 100 kDa MWCO (molecular weight cutoff). The dialysis device was placed in a beaker containing 1 L of 1× PBS on a stir plate and left at 4°C overnight for dialysis.

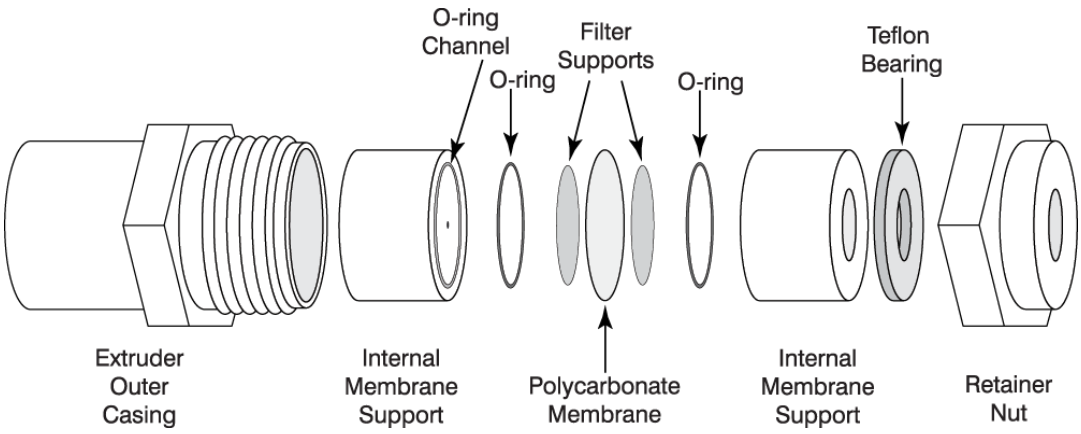

Figure 5.3: Mini extruder device from Avanti Polar Lipids Inc.

5.3.2 Characterization of Arginine Deiminase Liposome

To characterize the liposome encapsulation of arginine deiminase, enzymatic activity and protein gel quantification were performed. Both the dialyzed and non-dialyzed samples were diluted 250×, 500×, and 750× respectively using assay buffer containing 50 mM HEPES pH 7.35, 160 mM NaCl, and 0.1% BSA. The enzymatic assay was performed as described in detail under Section 5.3.4. As for protein quantification using gel, sodium dodecyl sulfate

polyacrylamide gel electrophoresis (SDS-PAGE) gels, specifically NuPAGE® 4-12% Bis-Tris gels were run. Bovine serum albumin (BSA) protein standard was run along with native ADI, dialyzed ADI liposomes, and non-dialyzed ADI liposomes. The BSA protein standard curve was made up of 0.5, 1, 2, 3, and 4 μg of BSA. For native ADI, 1 μg was run, while non-dialyzed versus dialyzed sample was run with 1:2 volume to volume ratio. To ensure that the liposome were fully disrupted, 1 μL of Triton X-100 [130] was added to the samples during the sample denaturing process. The SDS-PAGE gel was run in 1× MES running buffer at a constant voltage of 100 V for 90 minutes. Coomassie blue stain was used to stain the proteins in SDS-PAGE gels overnight. The protein gel was de-stained in water to an acceptable background level for analysis. Lastly, each protein sample amount on the gel was quantified using Image Lab software from Bio-Rad.

5.3.3 Synthesis of Silica Coated Arginine Deiminase Liposome

To synthesize these silica coated liposome encapsulated ADI, a couple of silica precursors were used. To coat, 2 μL of APTMS was added into 200 μL of liposome sample followed by the dropwise addition of a premixed mixture of 25 μL of TMOS in 50 μL of 1 mM HCl. After silica coating, the 200 μL of sample was split into two aliquots of 100 μL. Subsequently, 2.5 μL of 20 mg/mL proteinase K (PK) was added to one of the 100 μL silica coated liposome. Both PK treated and untreated samples were incubated at 37°C for 2 hours. The PK treatment reaction was stopped by placing both samples on ice before an enzymatic activity assay is performed. This completed the coating of silica onto the arginine deiminase liposomes.

5.3.4 Characterization of Silica Coated Arginine Deiminase Liposome

The silica coated arginine deiminase liposome sample was diluted with different dilution factors for the enzymatic assay using the assay buffer containing 50 mM HEPES pH 7.35, 160 mM NaCl, and 0.1% BSA. Next, 10 μL of the diluted sample was mixed with 80 μL of assay buffer. The sample was incubated in a thermocycler at 37°C for 5 minutes prior to the start of reaction. The ADI enzyme reaction was initiated by adding 10 μL of 50 mM arginine at 37°C, and the reaction proceeded for 2 minutes at 37°C. The reaction was then halted with the addition of 75 μL of color development reaction acid (CDR acid). The sample was immediately placed on ice after reaction termination. 25 μL of color development reagent (CDR) was added into the sample and mixed well with a pipette. The sample was heated at 95°C on the thermocycler for 10 minutes followed by a 20°C cool down for 10 minutes. The sample was taken out of the thermocycler while changing the temperature from 95°C to 20°C. 100 μL of sample was transferred to a clear, flat-bottom reading plate and the absorbance at 530 nm was measured by a SpectraMax Plus microplate spectrometer.

5.4 Results

To synthesize liposome encapsulated arginine deiminase, high concentration of approximately 150 mg/mL of *M. hominis* ADI was used. Erwinase enzyme was also encapsulated in liposomes to show that this platform can be utilized with different enzymes. To synthesize 1 mL of liposomes, a total of 7.375 mg of Egg PC, 5 mg of cholesterol, 2.4 mg of DOTAP, and 6 mg of PEG lipid were used. These amounts of lipids were used instead of the original protocol used for β-lactamase (BLA) enzyme, which still produced similar results. Extrusion was performed to make as many of the liposomes as possible into unilamellar

liposomes. From the initial results in Figure 5.4, the non-dialyzed sample of liposome encapsulated ADI shows an enzyme activity of 58.6 μM/min, which is higher in activity compared to the activity of the dialyzed liposomes at 39.1 μM/min. This suggests that following dialysis, the enzymes that were not encapsulated inside the liposome structure were dialyzed out. The calculated encapsulation percentage of ADI was about 66.8% using the ratio of the enzyme activity of dialyzed to non-dialyzed liposome. Moreover, many batches of liposome encapsulated ADI were synthesized, and they all showed consistent appearances with very similar activity enzyme results.

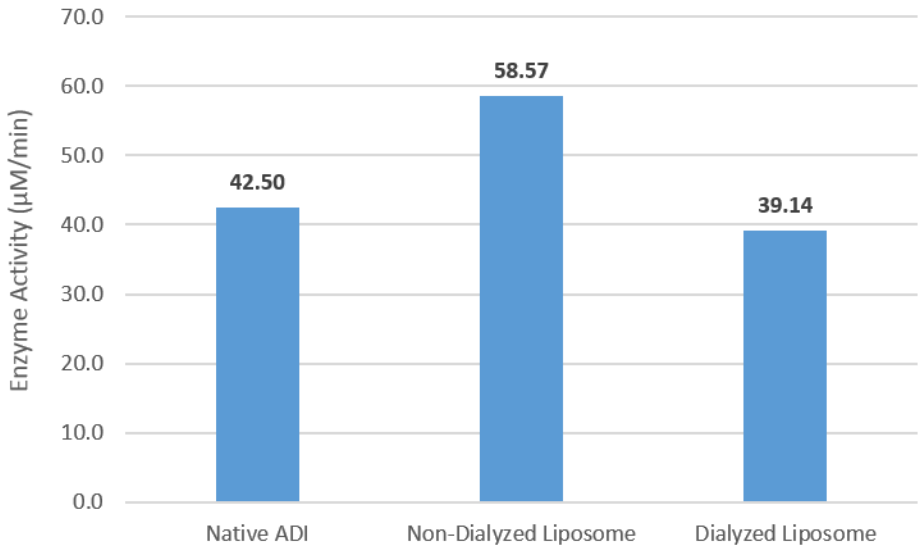

Figure 5.4: Enzyme activity of native ADI, non-dialyzed liposome encapsulated ADI, and dialyzed liposome encapsulated ADI

To confirm the liposome encapsulation efficiency of ADI, the liposome samples were denatured and run on an SDS-PAGE gel. Utilizing a known concentration of BSA, a standard curve of BSA was formed based on the protein band intensity on the same gel. Figure 5.5 shows the gel, and Figure 5.6 graphs the calculated protein concentration for both dialyzed and non-

dialyzed liposome samples. The protein concentration of the non-dialyzed liposome is calculated to be 0.8259 mg/mL, while the protein concentration of the dialyzed liposome is calculated to be 0.5310 mg/mL. The protein encapsulation efficiency of the liposome was calculated to be 64.3% based on the protein band quantification.

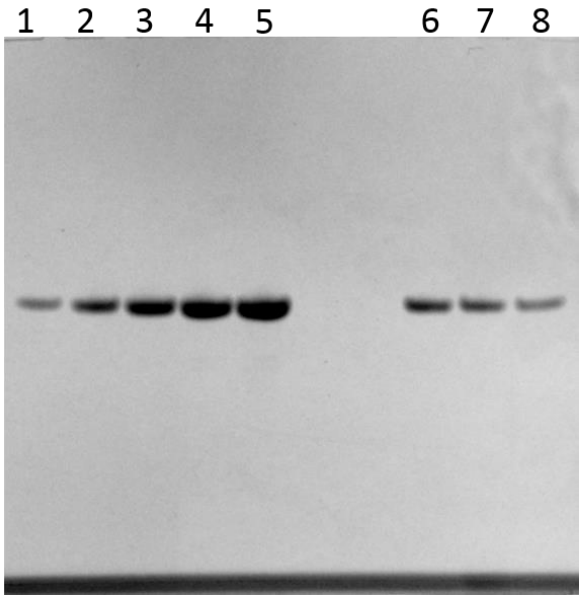

Figure 5.5: Coomassie blue stained protein gel: (1) – (5) BSA standard curve of 0.5, 1, 2, 3, 4 µg of BSA protein; (6) Native ADI; (7) Non-dialyzed liposome encapsulated ADI; (8) Dialyzed liposome encapsulated ADI

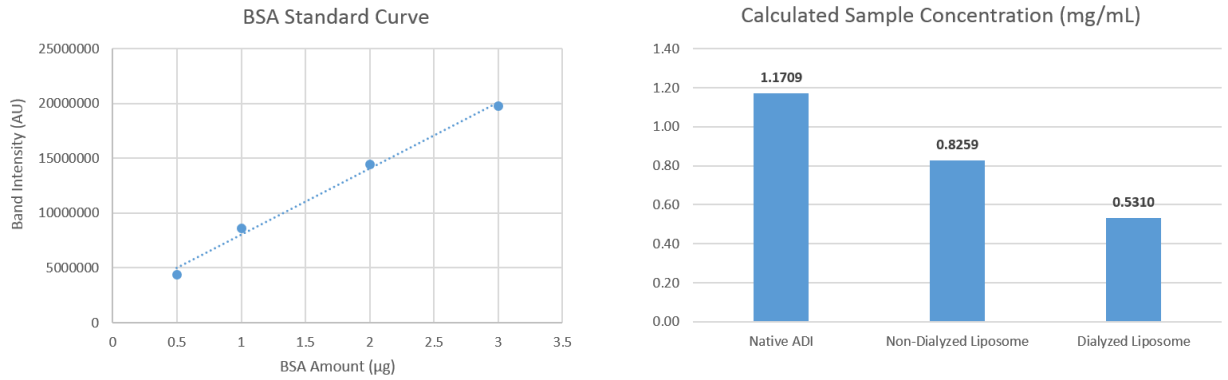

Figure 5.6: Calculated protein concentration based on the BSA standard curve for native ADI, non-dialyzed liposome encapsulated ADI, dialyzed liposome encapsulated ADI

After verification of enzymes remaining active through the liposome formation process, the majority of the time was spent optimizing coating the liposome encapsulated ADIs. Different coating materials were attempted, such as sol-gel silica, silicic acid, and calcium phosphate. Based on a quick test of the different coating materials, silicic acid coating was determined as the best of the 3, since the other materials did not coat on the surface of the liposomes as easily as the silicic acid. Therefore, further optimization of coating was done with silicic acid by altering the parameters such as amounts of tetramethyl orthosilicate (TMOS) and (3-Aminopropyl)trimethoxysilane (APTMS), the silicic acid reaction time and temperature. The finalized silicic acid coating consisted of 25 μL of TMOS in 50 μL of 1 mM HCl with 2 μL of APTMS added into the liposomes first before the addition of silicic acid.

A couple different methods were used to test the silica coating on the liposome nanoparticles. First, proteinase K was added to treat any ADIs not encapsulated inside the liposome; second, the Si coated liposome were sonicated. The combination of these two methods was then tested for its ADI activity and the result is graphed in Figure 5.7. From the results, it is seen that if no silica coating is on the surface of the liposomes, PK kills all of the enzyme inside the liposome. Additionally, the slight decrease in enzyme activity from PK treatment is as expected. Silica coated liposomes without PK produced an enzyme activity of 8.90 μM/min, and with PK treatment yielded an activity of 7.32 μM/min. It was promising to see that the silica coated liposomes did not lose their enzyme activity after sonication of the sample. In fact, there was a slight activity increase from 8.90 to 13.64 μM/min for sonication and no PK treatment. For silica coated liposomes with sonication and PK treatment, the activity is 12.16 μM/min. Therefore, it looks very promising that the silica coating on the liposome encapsulated ADI was coated well enough to create a rigid shell because sonication did not fracture the silica layer.

Figure 5.8 shows a few examples of scanning electron microscopy (SEM) images of the stealth Si coated liposomes.

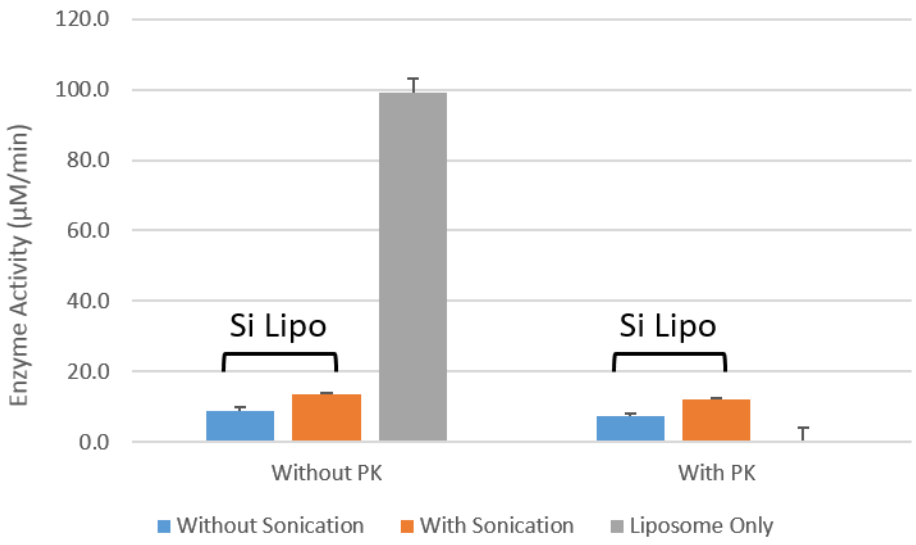

Figure 5.7: Effect of enzyme activity on Si coated liposome encapsulated ADI after different combinations of sonication and proteinase K (PK) treatment

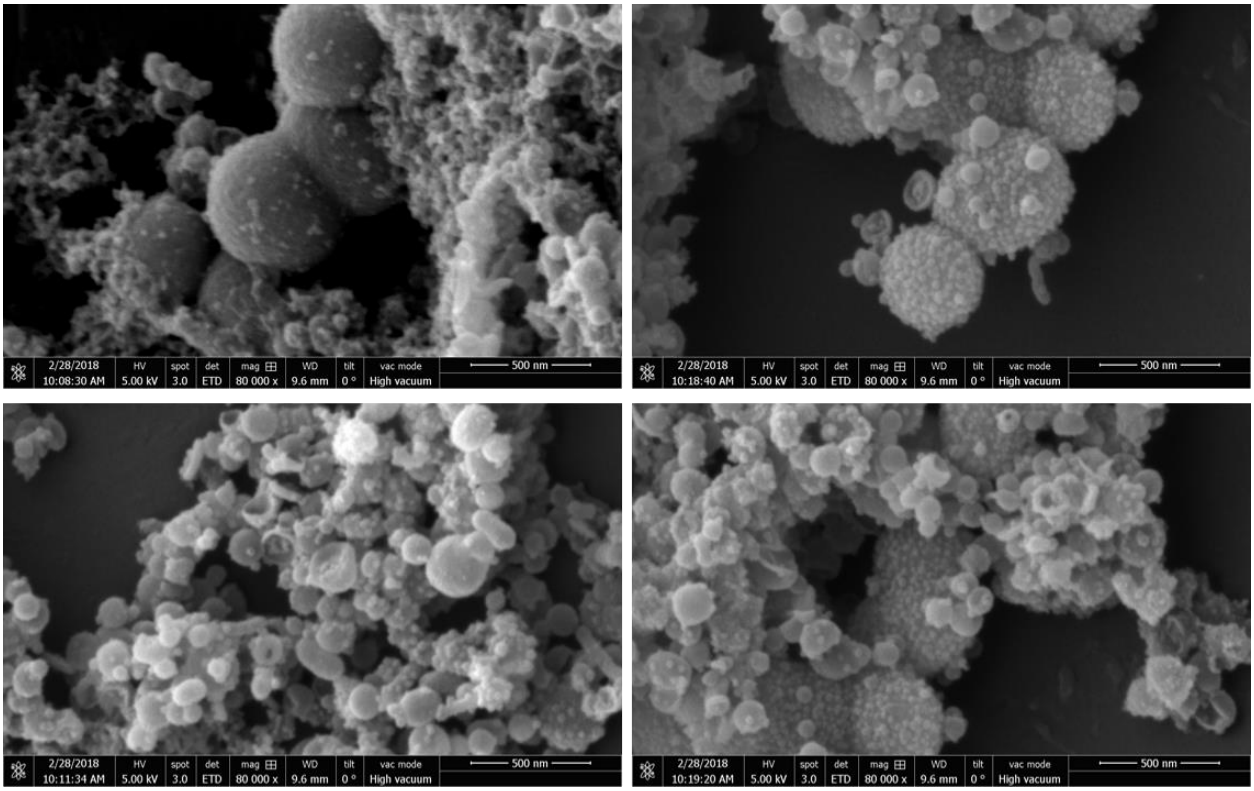

Figure 5.8: SEM images of silica coated liposome encapsulated ADI

5.5 Discussion

The synthesis of liposome encapsulated ADI was modified based on its encapsulation with another enzyme, β-lactamase (BLA). The different surface properties of each enzyme mean that each requires some optimization of the lipid type and combination to create a solid liposome. Various conditions were tested including different lipid ratios, different lipid concentrations, and slight adjustments to the process, such as the rate at which Vial B was added into Vial A, or the level of dryness of the organic solvents, etc., before the finalized 4 lipid ratios were determined. Once the liposome encapsulated ADI was synthesized, multiple different characterization tests were done, such as PK treatment and tests of its enzyme activity. With currently available technology, it is almost impossible to determine the exact concentration of the enzyme inside the nanoparticle. Therefore, multiple methods were used to help quantify the amount of enzyme

inside the liposome to calculate the enzyme encapsulation percentage as accurately as possible. Running the liposome samples on an SDS-PAGE gel to quantify its band intensity by correlating it to a standard curve gave an accurate enzyme concentration inside the liposomes. Taking the enzyme concentration ratio between the non-dialyzed and dialyzed sample resulted in an enzyme encapsulation percentage. This number was compared to the ratio that was obtained from testing the activity of the non-dialyzed and dialyzed liposomes, which gave identical results. Therefore, the SDS-gel method confirmed that the activity assay method is accurate, and that the arginine citrulline activity assay is sufficient in the future to determine the enzyme encapsulation percentage.

The hydrophilic nature of the ADI enzyme contributes to its high encapsulation percentage of about 66%. It is very likely that the enzyme is captured inside the aqueous core of the phospholipid bilayer of the liposome. The strong stability of the ADI enzyme also contributed to the high encapsulation percentage because the synthesis process can be harsh for some other enzymes, and damaged enzymes would decrease enzyme activity, which would ultimately decrease the encapsulation percentage. The extrusion process of using 800 nm, 400 nm, and 200 nm membranes helps to reduce the aggregation of liposomes or restructure multilamellar liposomes into unilamellar liposomes. However, the sheer force of the extrusion process might damage the enzyme slightly, which could affect the encapsulation percentage. Ultimately, the liposome encapsulation of ADI process seemed well tolerated by the ADI enzyme. The next step following encapsulation was to optimize the silica coating of the liposome.

Initially, sol-gel silica, silicic acid, and calcium phosphate were tested to find the best coating for liposome encapsulated ADIs. The results showed that silicic acid had the best

potential of coating the liposomes well because it has the highest liposome coating ability and the coated silica provided great protection to the ADI enzymes inside the particle. Moreover, the silica coating was also very rigid and did not break during sonication. Therefore, further optimization was done with silicic acid coating such as changing the amounts of TMOS added into HCl to form silicic acid and the addition of APTMS. It was found that adding APTMS straight onto the liposomes and then adding the silicic acid mixture into the APTMS liposome mixture resulted in the best protective coating. The APTMS creates a slight positive layer on the liposome for the negatively charged silicic acid to coat onto. The silicic acid reaction time and temperature were also optimized. The final condition chosen was adding 25 μL of TMOS into 50 μL of 1 mM HCl with 2 μL of APTMS added into the liposomes prior to addition of silicic acid.

To verify that the coating securely protected the ADI enzyme, proteinase K (PK) was used to treat the nanoparticles to prevent background activity from leftover ADI outside of the coating. In combination with PK treatment, sonication of the Si coated liposomes was also performed. The results suggest that the Si coating was well synthesized because sonication did not break the Si coating. If it was broken, the combination of sonication and PK treatment would have destroyed the ADI enzymes inside the nanoparticle, resulting in little to no enzyme activity detectable by assay. In fact, the sonication actually helped the enzyme activity increase slightly even with the presence of PK. The reason behind this increase may be that some of the enzymes were immobilized during the liposome encapsulation process, and the subsequent step of sonication broke the lipid bilayer of the liposome to potentially mobilize the ADI enzymes inside.

5.6 Conclusion

To conclude, the robust manufacturing of the Si coated liposome encapsulated ADI showed promising results compared to the inconsistent synthesis of the synthetic hollow enzyme loaded nanospheres from the previous chapter. With the initial characterization of the Si coated liposome particle in combination with PK treatment plus sonication, the coating was shown to protect the payload inside and allow the diffusion of the substrate arginine to enter into the nanoparticle and the product citrulline to escape out. This Si coated liposome encapsulated ADI will be further characterized along with native and PEGylated ADI in the next chapter. These characterization results will dictate further directions for cell assay studies and animal studies. So far, this robust method of synthesizing Si coated liposome encapsulated ADI has not shown many issues.

5.7 Acknowledgements

This chapter and its methods are developed and owned by Vaidyanathan and Esener *et al*. from the University of California San Diego, La Jolla, California with a co-development with Polaris Pharmaceuticals, Inc., San Diego, California. Collaborators for this development: Jason (Li-Chang) Chen, Grace (Ting-Yu) Chang, Mukanth Vaidyanathan, Ya-San Yeh, Negin Mokhtari, Jim Thomson, and Sadik Esener. The dissertation author was the primary investigator and author of this material.

Chapter 6: *In vitro*/*In vivo* Study of Different Formulations of Arginine Deiminase

6.1 Comparison of Different Formulated Arginine Deiminase

In the previous chapters, it was shown that recombinant native arginine deiminase from *Mycoplasma hominis* was successfully purified. Taking the purified native ADI, the PEGylation process was developed and also successfully synthesized PEGylated arginine deiminase. The next formulation of native ADI was to encapsulate it into synthetic hollow enzyme loaded nanospheres (SHELS). Unfortunately, synthesis of SHELS ADI was not a robust enough process. Ultimately, silica coated liposome ADI were developed and synthesized for their more robust manufacturing process.

Following the successful development of a silica coated liposome ADI, the next step in characterizing this formulation was to compare it to native, untreated ADI and PEGylated ADI, the standard formulation for enzyme therapy. In theory, ADI should kill cancer cells which are deficient in ASS enzymes. In *in vitro* testing on cancer cells, this allows the isolation of cells of interest and control all outside variables other than effects from the drug of interest. Additionally, it is important to understand how a drug behaves in an *in vivo* setting to ensure that any risks that cannot be detected or occurred in *in vitro* are addressed in producing the final drug formulation. Furthermore, these enzyme macromolecules can function completely differently *in vivo* once all of the variables in a living environment is present.

Prior to testing new drug formulations *in vivo*, it is important to eliminate outside risks to animal health. In this case, one major concern is endotoxin contamination. Endotoxins are complex lipopolysaccharides (LPS) with a molecular weight of 3,000 to 4,000 Da derived from the cell membrane of Gram-negative bacteria [131]. In pharmaceutical industries, endotoxins can

be introduced through the production processes or contaminates the final drug product. Although endotoxins originate in the bacterial cell wall, they are continuously released into the environment. The release does not only occur during cell death, but also during cell growth. Since bacteria can grow and survive in almost any condition, endotoxins are found almost everywhere. One single *E. coli* cell contains about 2 million LPS molecules. Endotoxins elicit a wide variety of pathophysiological effects. When the body is excessively exposed to LPS or even the smallest traces of LPS is introduced into the blood stream, a systemic inflammatory reaction can occur, leading to endotoxin shock, tissue injury, or death [132, 133, 134]. Therefore, all samples being tested *in vivo* need to be endotoxin-free.

This chapter details the endotoxin removal processes to prepare samples for *in vivo* testing and then focuses on the comparison of native, PEGylated, and nanoparticle ADI *in vitro* and *in vivo* to further assess the pros and cons of the different formulations of ADI.

6.2 Materials

Allantoin, Triton X-114, bovine serum albumin (BSA), L-Arginine-HCl, and L-Citrulline were purchased from Sigma Aldrich, St. Louis, Missouri. Pooled normal human plasma with K2 EDTA anticoagulant was purchased from Innovative Research, Novi, Michigan. Pierce LAL Chromogenic Endotoxin Quantitation Kit and formic acid (HPLC Grade) were purchased from ThermoFisher Scientific, Waltham, Massachusetts. PANC-1 and DLD-1 cell lines were purchased from American Type Culture Collection (ATCC), Manassas, Virginia. Resazurin was purchased from R&D Systems, Minneapolis, Minnesota. CellTiter-Glo 2.0 Assay was purchased from Promega, Madison, Wisconsin. Acetonitrile and methanol were purchased from Honeywell Burdick & Jackson (B&J), Muskegon, Michigan. LC-MS Grade water was purchased from EMD

MilliporeSigma, Burlington, Massachusetts. $^{15}N_4$-Arginine-HCl and (5-^{13}C, 4,4,5,5-D_4)-Citrulline were purchased from Cambridge Isotope Laboratories, Inc., Tewksbury, Massachusetts. Triple Quad 4000 mass spectrometer was purchased from SCIEX, Framingham, Massachusetts. Shimadzu DGU-14A degasser and SCL-10A system controller were purchased from Shimadzu Corporation, Nakagyo-ku, Kyoto, Japan. 1100 Series Well-plate Sampler was purchased from Agilent Technologies, Santa Clara, California. Venusil ASB C_{18} HPLC column was purchased from Agela Technologies, Torrance, California. All chemicals were used as received and purchased from Sigma Aldrich, St. Louis, Missouri.

6.3 Methods

6.3.1 Endotoxin Treatment of Arginine Deiminase

To remove endotoxin in solution or weakly associated with native arginine deiminase (ADI), 300 mg of allantoin crystalline powder was added per 1 mL of ADI solution [135]. The protein sample and allantoin were mixed at room temperature for about 1 hour. The sample was then centrifuged at 3,000 rpm (8,100 rcf) for 3 minutes and filtered with a 0.45 μm filter. To minimize loss of protein, 1× PBS was used to re-suspend the allantoin pellet. The sample was centrifuged at 3,000 rpm (8,100 rcf) for 3 minutes and filtered using a 0.45 μm filter. Both filtered supernatants were combined and filtered with a 0.2 μm filter. The Pierce LAL chromogenic endotoxin quantitation kit was used to determine the level of endotoxin in the sample after treatment. The endotoxin quantitation reaction is shown in Figure 6.1.

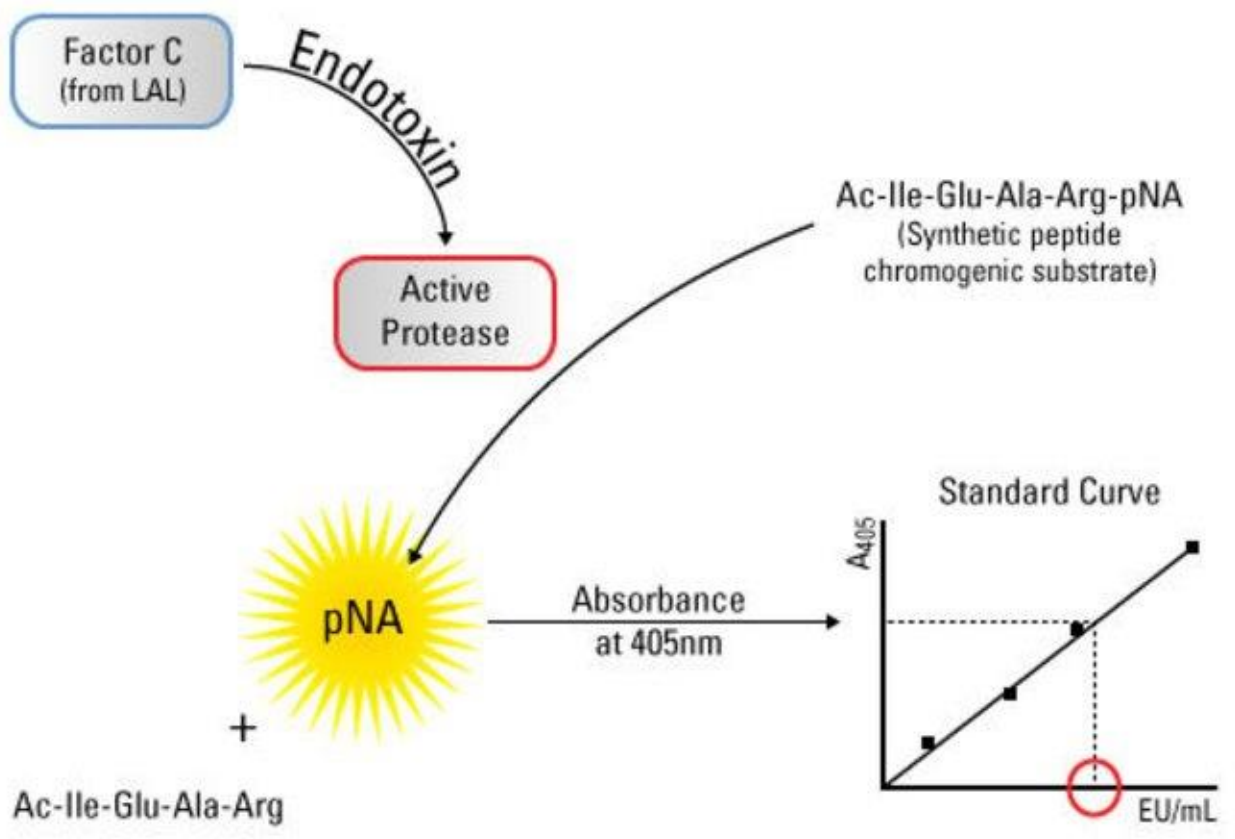

Figure 6.1: LAL Chromogenic Endotoxin Quantitation Kit reaction scheme where a small volume of the sample (10 µL) is combined with the *Limulus* Amebocyte Lysate, and endotoxins in the sample to activate the proteolytic activity of Factor C. When the chromogenic substrate is added, the activated protease catalyzes the cleavage of p-nitroalinine (pNA), resulting in yellow color that can be quantitated by measuring the absorbance at 405 nm (A405) and extrapolating against a standard curve. Taken from ThermoFisher Scientific's product overview page.

6.3.2 Endotoxin Treatment of PEGylated Arginine Deiminase

To remove endotoxin in solution or associated with PEGylated arginine deiminase (ADI), Triton X-114 was added to the protein solution to achieve final Triton X-114 concentration of 1% [136, 137, 138]. The sample mixture was mixed at 4°C for 30 minutes. Immediately, the sample mixture was then heated in a 37°C water bath for 10 minutes. Immediately following, the sample was centrifuged at 13,200 rpm (16,100 rcf) for 10 minutes. Lastly, the supernatant was

carefully removed and filtered through a 0.2 μm filter. The Pierce LAL chromogenic endotoxin quantitation kit was used to determine the level of endotoxin in the sample after treatment.

6.3.3 Endotoxin Treatment of Silica Coated Arginine Deiminase Liposome

To treat silica coated arginine deiminase liposome, the sample was exposed to UV light for 3 – 5 minutes. This process also sterilized the sample. To avoid endotoxin contamination to the silica coated arginine deiminase liposomes, endotoxin-free ADI was used in synthesizing the nanoparticles. Sterile, non-pyrogenic plastic tubes and glassware were used during synthesis to avoid introducing endotoxins to the sample. Currently, there is no effective method to remove endotoxins from contaminated silica coated arginine deiminase liposomes, but Pierce LAL chromogenic endotoxin quantitation kit was still used to determine the level of endotoxin in the sample after treatment with UV light.

6.3.4 Characterization of Different Formulations of Arginine Deiminase

Both native and PEGylated ADI were diluted to 500 nM, while nanoparticle ADI was diluted 40× for the activity assay. 10 μL of each respective diluted sample was added to 80 μL of assay buffer made with 50 mM HEPES pH 7.35, 160 mM NaCl, and 0.1% BSA. A standard curve made with 100 μL of 0, 5, 10, 20, 40, 80, 160, 320 μM of citrulline was run alongside the tested samples. The reaction plate was placed on a thermocycler at 37°C for 5 minutes prior to start of assay. The ADI enzyme reaction was started by adding 10 μL of 50 mM arginine at 37°C, and allowed the reaction to run for 2 minutes at 37°C. The reaction was stopped with the addition of 75 μL color development reaction acid (CDR acid). The sample was immediately placed on ice after reaction termination. Then, 25 μL of color development reagent (CDR) was

added into the sample and mixed well with a pipette. The sample was then heated at 95°C on the thermocycler for 10 minutes followed by 20°C cool down for 10 minutes, sample was removed while changing the temperature from 95°C to 20°C. Lastly, 100 µL of sample was transferred to a clear, flat-bottom reading plate, and the absorbance at 530 nm was measured with SpectraMax Plus microplate spectrometer.

Native, PEGylated, and nanoparticle ADI were incubated with 0, 10, 20, 40, 80, 160, 320, 640, and 1280 nM of anti-ADI (αADI) antibody for 1 hour at room temperature. The enzyme activity of each sample was tested after 1 hour of ADI antibody incubation. Furthermore, to plot the K_m curve of an enzyme, the activity of the enzyme was tested with different concentration of arginine. 10 µL of 30 nM ADI was added to 80 µL of assay buffer and incubated at 37°C for 5 minutes. To start the enzyme reaction, 10 µL of the arginine substrate was added at various concentrations to each sample with the final arginine concentration of 0, 1.5625, 3.125, 6.25, 12.5, 25, 50, and 100 µM arginine. Similar to the activity assay described above, the reaction was stopped by adding 75 µL of CDR acid followed by 25 µL of CDR. 100 µL of samples were transferred to a reading plate and the absorbance was read at 530 nm.

6.3.5 Cell Viability Assay of Different Formulations of Arginine Deiminase

Two cell lines, PANC-1 and DLD-1, were used to generate a viability curve after a 72 hour incubation with native, PEGylated, and nanoparticle ADI treatment. To split cells, a cell counter was used to approximate the concentration of cells and 10,000 cells were pipetted into each well of a 96-well plate for treatment. Ten concentrations of the native, PEGylated, and nanoparticle ADI drug were tested, and they were 0, 0.078125, 0.15625, 0.3125, 0.625, 1.25, 2.5, 5, 10, and 20 nM, which was a 2-fold serial dilution from 20 nM. CellTiter-Glo 2.0 assay reagent

from Promega was used to quantify the amount of ATP present in the cells after 72 hours of drug treatment. A luminescence reading was taken after 15 minutes of incubation with the assay reagent at room temperature on a shaker. The final viability graph was generated with values calculated based on the normalization with non-treated controls.

6.3.6 Animal Study of Different Formulations and Administration Routes of Arginine Deiminase

An animal study was carried out with 24 CD-1 male mice with body weights ranging from 35 – 45 g from Envigo. All 24 mice were purpose-bred, specific pathogen-free, and experimentally naïve at the start of study. Their body weights were measured on Day -7 and then the mice were randomized into 4 groups of 6 mice each. The pre-bleed of the mice was done on Day -7, and followed by an acclimation period from Day -7 to Day -3. All 4 groups of mice were dosed on Day 0, 7, and 14 of the study. Group 1 received 2 mg/kg of native ADI via intravenous (IV) injection, Group 2 received 2 mg/kg of PEGylated ADI via IV injection, Group 3 received 1 mg/kg of nanoparticle ADI via IV injection, and Group 4 received 1 mg/kg of nanoparticle ADI via intramuscular (IM) injection. The nanoparticle ADI dose was calculated based on native ADI enzyme activity assuming the encapsulated ADI inside the nanoparticle was fully active. Blood collections were done at Day 0 at 4 hours post dose, Day 1, 4, 7 (prior to dose), 8, 11, 14 (prior to dose), 15, 18, 21, and 28. Body weight and clinical observation were done on Day 0, 7, 14, 21, and 28. These mice were euthanized after the final blood collection on Day 28 of the study.

6.3.7 Determination of Arginine and Citrulline Levels by Liquid Chromatography Mass Spectrometry (LCMS)

A rapid, robust, and simple method is described for the quantitation of L-Arginine and L-Citrulline without prior derivatization. The method is applied to the analysis of mouse plasma that was taken after centrifugation from whole blood. Calibration standards are prepared in a surrogate matrix containing 1% bovine serum albumin in phosphate buffered saline. Quality control standards are prepared in both surrogate matrix and in pooled mouse plasma. Mouse plasma samples, calibration standards, and quality control standards are spiked with stable isotope internal standards.

On a 96-well plate, 25 µL of each unknown plasma samples, calibration standards, and quality control standards are diluted with 75 µL of 22 µM of each $^{15}N_4$-Arginine and (5-^{13}C, 4,4,5,5-D_4)-Citrulline, and then further diluted in 400 µL in LCMS grade water. 100 µL of this solution was transferred to a separate plate, then diluted with 400 µL with LCMS grade acetonitrile, shaken for 10 minutes, and centrifuged at 3,500 rpm for 15 minutes. 100 µL of supernatant was transferred to a separate plate, diluted to 250 µL with water, and injected into the LCMS system. A Shimadzu DGU-14A degasser and an Agilent 1100 Series WPALS autosampler were used. The HPLC system was controlled with a Shimadzu SCL-10A system controller and two LC-10AD pumps. The ASB C18 (4.6 mm × 100 mm) column was used with mobile phase containing 95% water, 4.9% acetonitrile, and 0.1% formic acid. An API 4000 triple quadrupole mass spectrometer was used to monitor Arginine, Citrulline, $^{15}N_4$-Arginine, and (5-^{13}C, 4,4,5,5-D_4)-Citrulline from Q1 → Q3 transitions. Data acquisition and data analysis were carried out by a collaborating analyst.

6.4 Results

6.4.1 *In vitro* Comparison between the Different Formulations

Using the Pierce LAL chromogenic endotoxin quantitation kit, native, PEGylated, and nanoparticle ADI were tested for their endotoxin level. For both native and PEGylated ADI, it was less than 0.01 EU/mg (Endotoxin Units per mg of protein), and for nanoparticle ADI, there was no secondary reaction of chromogenic substrate which resulted in no readings [139].

The activity assay was run using native, PEGylated, and nanoparticle ADI to confirm that the ADI is still active after PEGylation and nanoparticle formulation. The samples were proceeded for further characterization such as an anti-ADI (αADI) antibody neutralization assay and generation of K_m for native and PEGylated ADI. The results are shown in Figure 6.2 and Figure 6.3, respectively. Native ADI reached its maximum loss in activity when 320 nM of neutralizing antibody were incubated. At 320 nM of neutralizing antibody, PEGylated ADI loss about 50% of its activity. Lastly, nanoparticle ADI maintained majority of its activity at 320 nM of neutralizing antibody. One can conclude that the best formulation of protecting the ADI from being neutralized by αADI antibody is the nanoparticle formulation. From the Km curve, both native and PEGylated ADI have a Km value of less than 10 μM, which is the sensitivity of the BUN colorimetric assay.

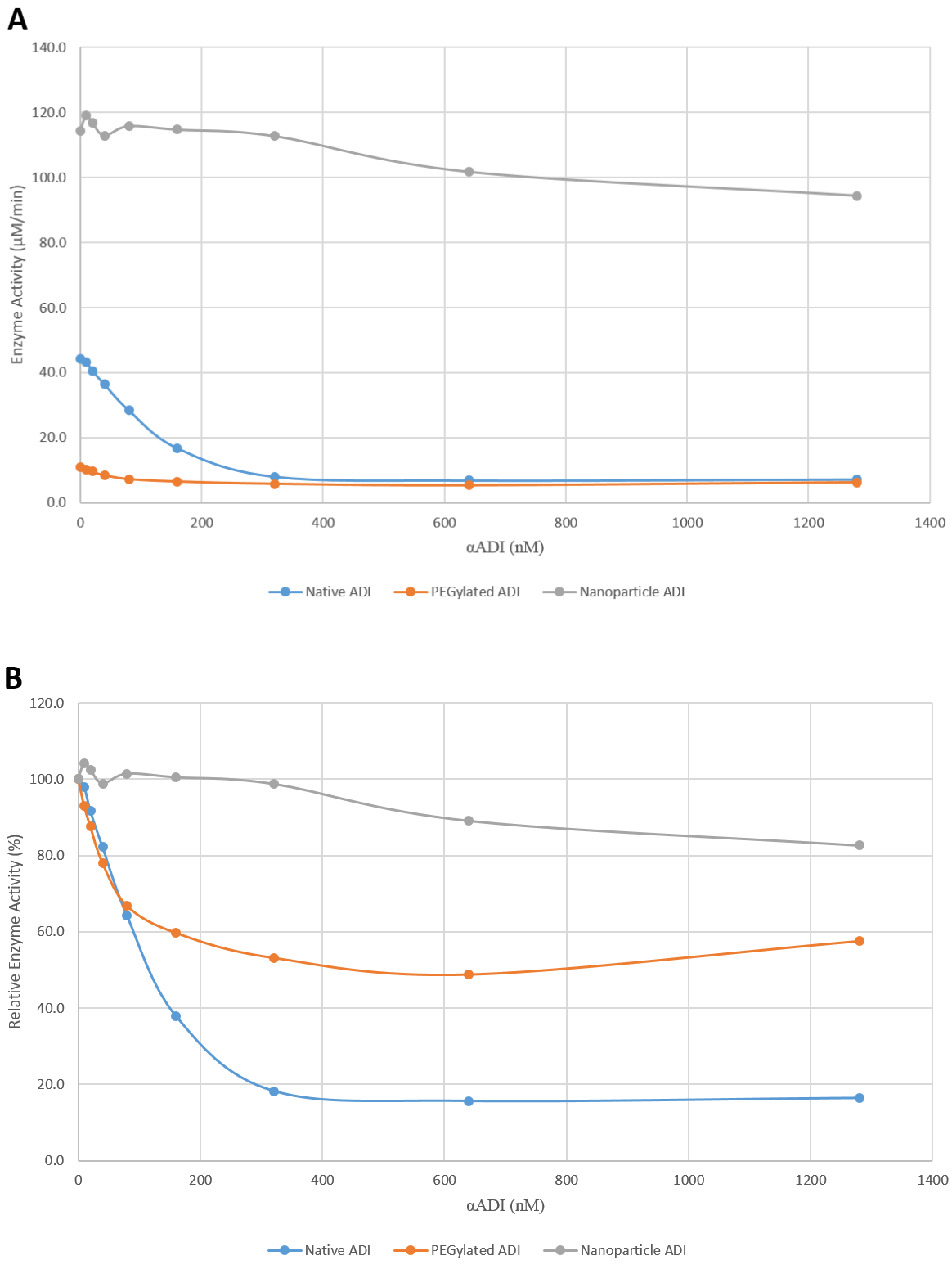

Figure 6.2: Effect of αADI antibody incubation with native, PEGylated, and nanoparticle ADI. (A) Enzyme activity in µM/min (B) Relative enzyme activity in percentage

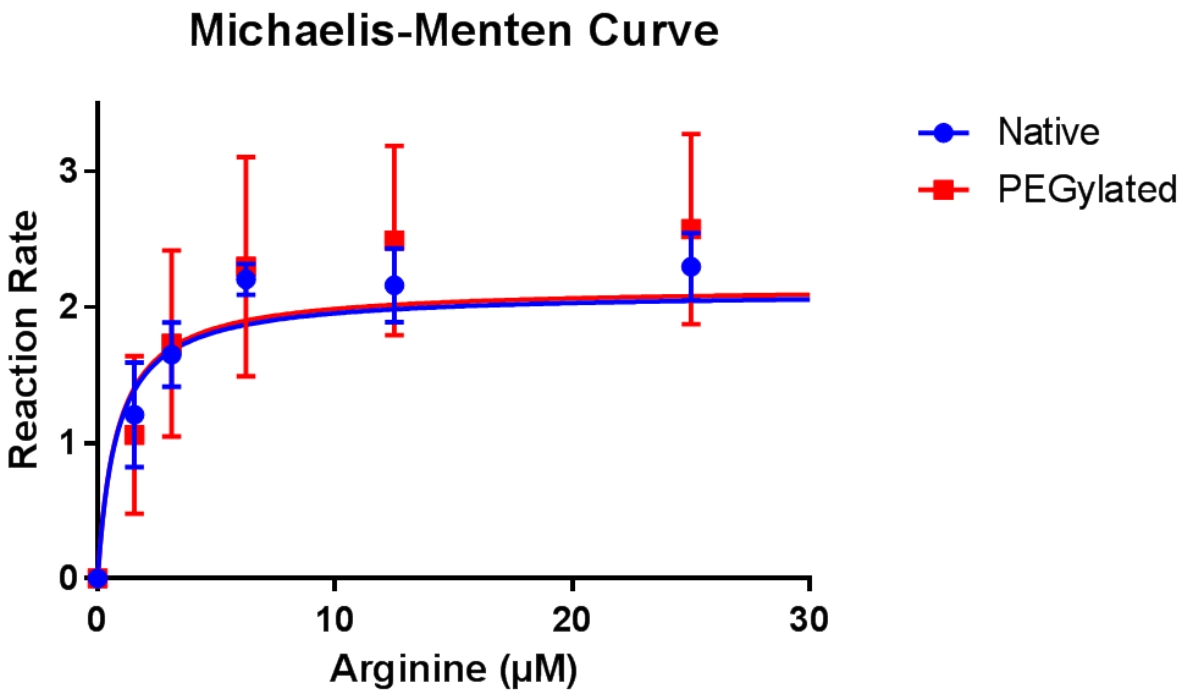

Figure 6.3: Michaelis-Menten (K_m) enzyme kinetics curve relating substrate concentration and reaction rate

The cell-based assay testing the effects of ADI on cell viability was also performed for native, PEGylated, and nanoparticle ADI in two different cell lines: PANC-1 and DLD-1. Figure 6.4 depicts the result of the 72 hour cell viability assay. The calculated PANC-1 cells IC_{50} from GraphPad Prism for native ADI is 2.04 nM, PEGylated ADI is 0.80 nM, and nanoparticle ADI is 0.52 nM.

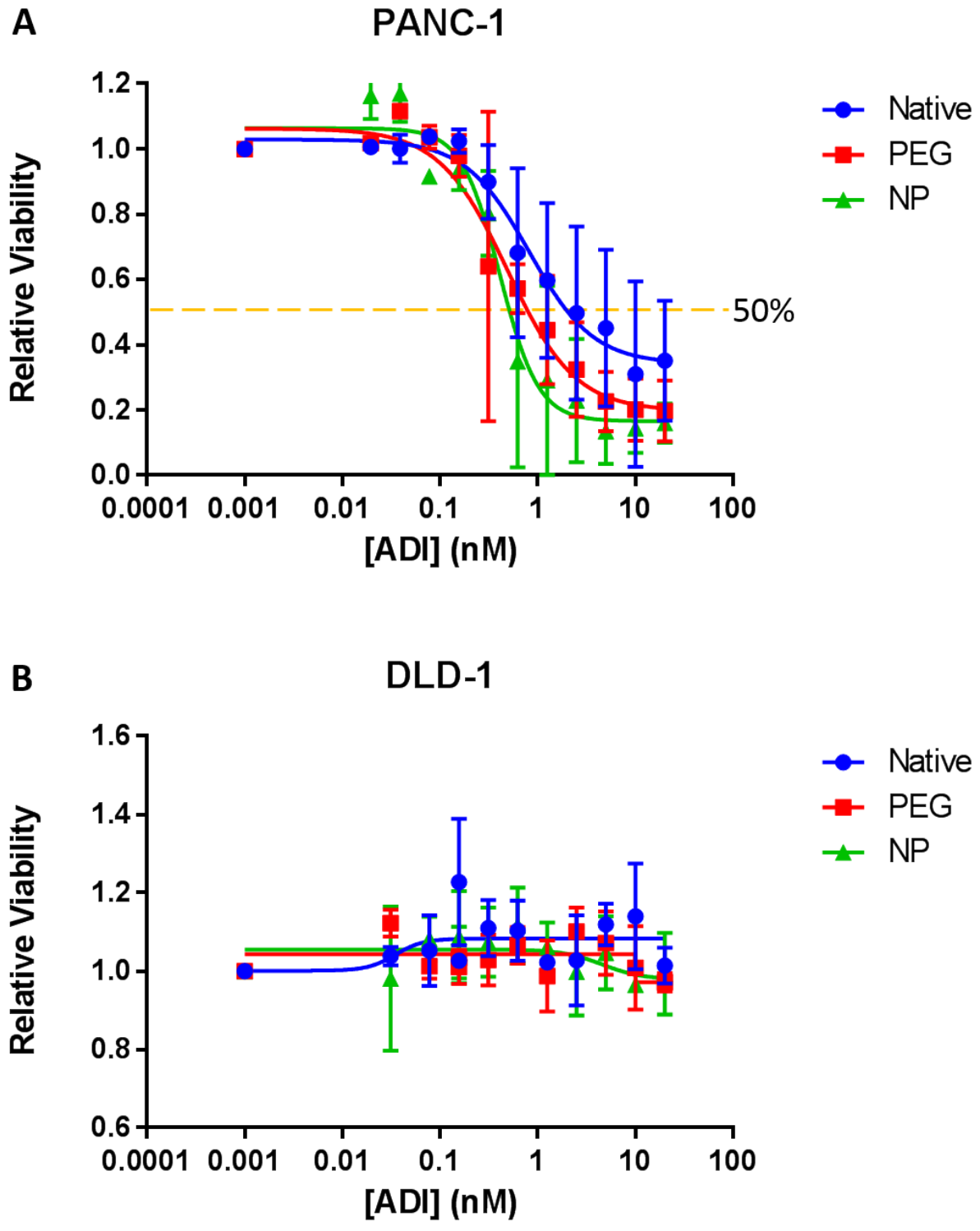

Figure 6.4: Cell Viability Assay of (A) PANC-1 and (B) DLD-1 Cell Lines

6.4.2 *In vivo* Comparison between the Different Formulations

Figure 6.5 shows the body weight of each mouse on Day 0, 7, 14, 21, and 28. There was no significant weight loss (greater than 10%) for any mice throughout the study duration. There were a few mice that dropped in weight but recovered over the course of a week. In addition, the blood arginine and citrulline concentration of the *in vivo* mice study comparing the different formulations and administration routes is shown in Figure 6.6. Both native ADI and nanoparticle ADI via IV injection were effective in decreasing arginine levels to near zero levels, but the arginine level rebounded after 1 day. Subsequent doses were not effective. For nanoparticle ADI via IM injection, arginine level dropped at 4 hours, but bounced back to baseline by Day 4. Subsequent doses had little to no effect. Lastly, PEGylated ADI was able to deplete arginine levels through Day 4, and by Day 7, the levels started to come back up. Subsequent doses were effective of depleting arginine until after Day 18, when the arginine levels slowly went back up. The citrulline levels showed a much clearer trend that PEGylated ADI was the most effective, while the other samples were not effective more than 1 day after injection, and subsequent doses did not show any effect.

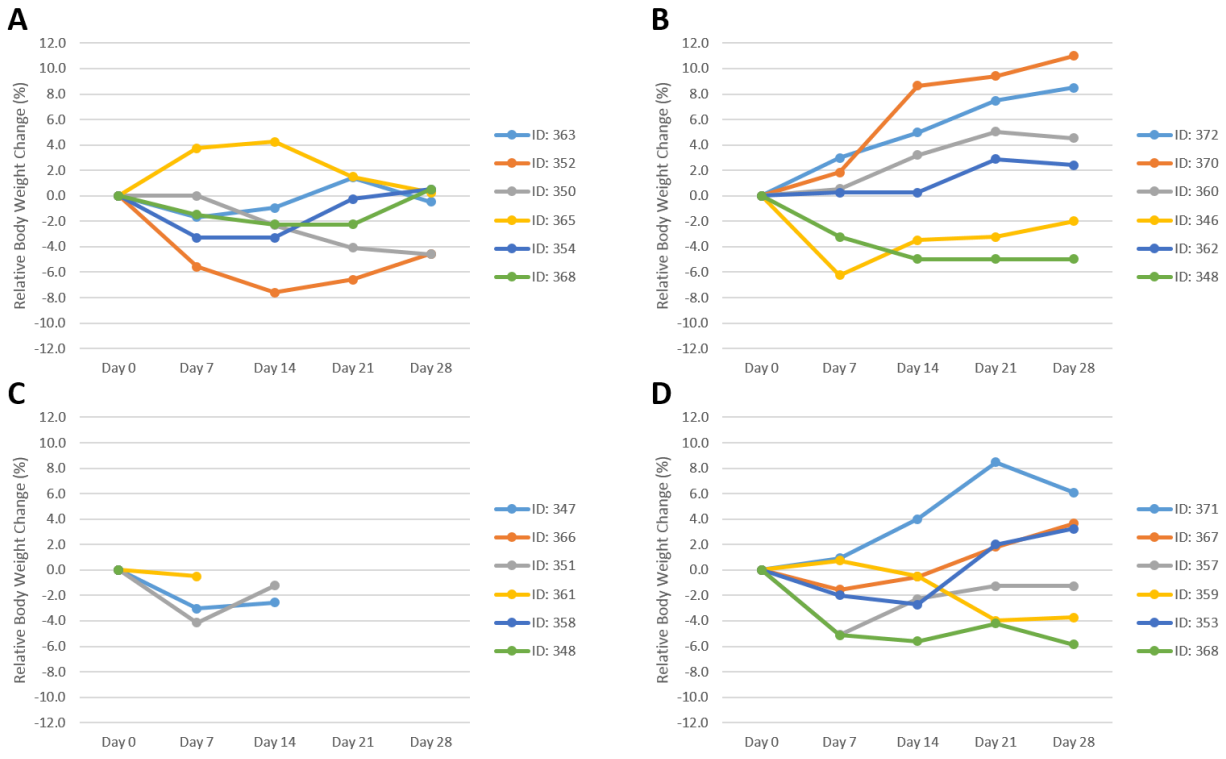

Figure 6.5: Percent change in body weight of mice throughout the one month study. (A) Group 1 Mice: Native ADI via IV; (B) Group 2 Mice: PEGylated ADI via IV; (C) Group 3 Mice: Nanoparticle ADI via IV; (D) Group 4 Mice: Nanoparticle ADI via IM

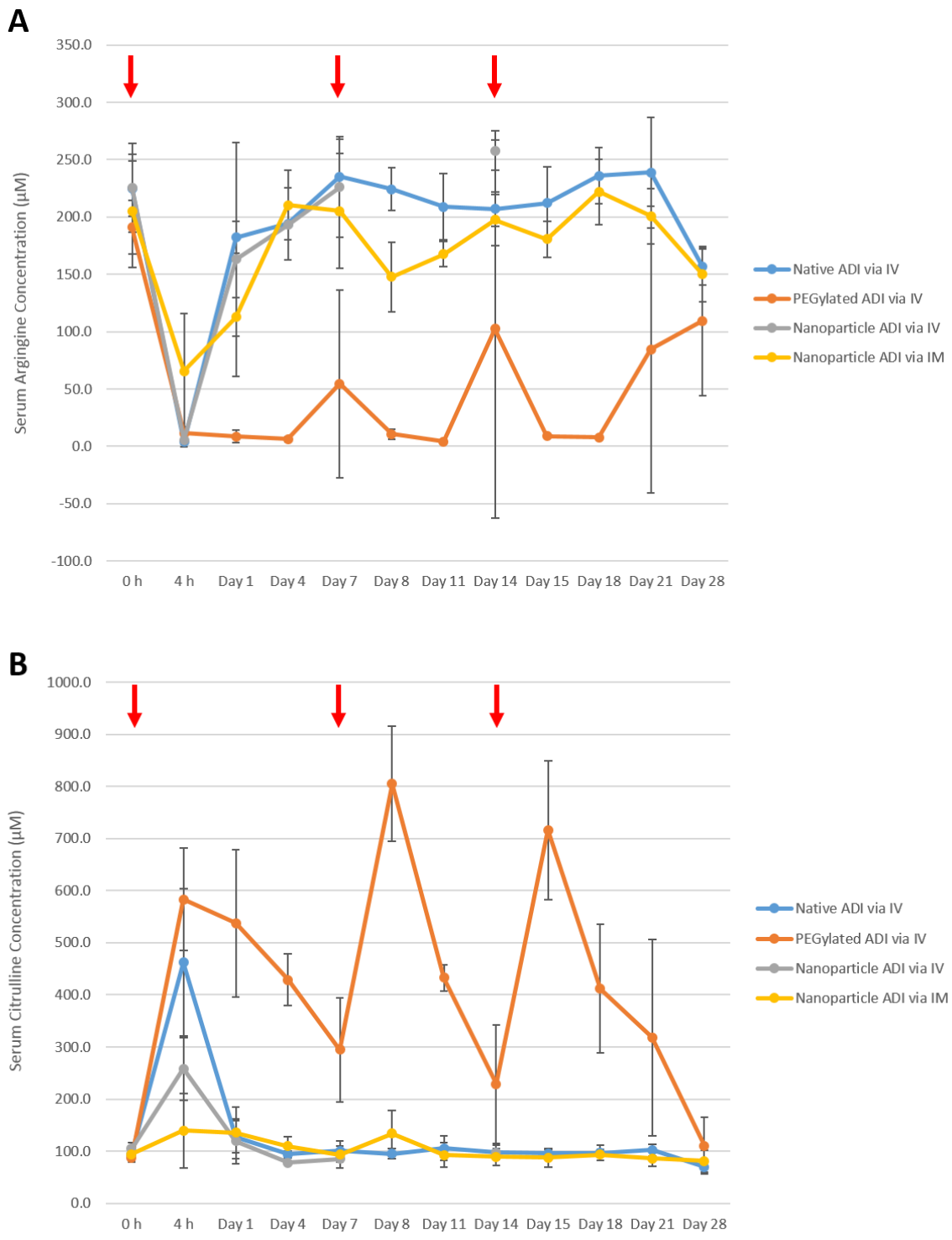

Figure 6.6: Determination of (A) Arginine and (B) Citrulline Concentration from Mass Spectrometry. Red arrows indicate drug administration: 0 h, Day 7, and Day 14. For Group 1, 2, and 4: time points 0 h and Day 28 (n = 6), 4 h, Day 1, 4, 7, 8, 11, 14, 15, 18, and 21 (n = 3). For Group 3: time points 0 h (n = 6), 4 h, Day 1, 7, and 14 (n = 2), Day 4 (n = 1), Day 8, 11, 15, 18, 21, and 28 (n = 0).

6.5 Discussion

6.5.1 *In vitro* Comparison between the Different Formulations

Before a comparison was done *in vitro*, the endotoxin levels for each sample was checked. The level of endotoxin that is safe to inject into animals is less than 1 EU/mg (Endotoxin Units per mg of protein) to avoid any endotoxin shock, issue injury, or death [132, 133, 134]. The level of endotoxin needed to be determined in order to eliminate the possibility that any unpredicted results during *in vitro* or *in vivo* experiments were caused by endotoxin contamination. In addition, it was important that the samples were endotoxin-free for all further *in vitro* and *in vivo* experiments to maintain consistency throughout any comparison experiments, in case the enzyme itself was altered during the endotoxin removal process.

As shown in Figure 6.2, the addition of 320 nM of αADI antibody to native ADI is sufficient to neutralize 80% of the native enzyme, leaving only 20% of enzyme activity. The reason being that only 80% of the enzyme are neutralized because not all αADI antibodies are neutralizing antibodies. Once the ADI is PEGylated, the αADI antibody only neutralizes 50% of the PEGylated enzyme activity, with 50% of enzyme activity remaining. When ADI is encapsulated into the silica coated liposomes, the αADI antibody did not neutralized any ADI, since greater than 95% of its activity was retained. From these results, it is clear that the nanoparticle protects the encapsulated ADI from being neutralized by the αADI antibody. At the highest concentration of αADI antibody at 1280 nM, native ADI has a relative activity compared to 0 nM αADI antibody of 16.4%, PEGylated ADI is about 57.5% relative activity, and nanoparticle ADI is about 82.6% relative activity. This supports the use of the nanoparticle encapsulation as a platform that allows the enzyme to retain its activity and also protects the

enzyme, in this case from neutralization by αADI antibodies. This is one great accomplishment of this platform.

The hyperbolic relationship between the rate of reaction and the concentration of substrate was depicted with a K_m curve. In Figure 6.3, it is shown that both native and PEGylated ADI have a very similar K_m. The K_m for both is under 10 μM, which is the limit of detection of the enzymatic assay. This potentially means that the PEGylation did not affect the concentration of the substrate that binds to the enzyme to achieve half of its maximum velocity. Since the K_m is less than limit of detection, it is difficult to draw a conclusion from the results. This also means the catalytic efficiency of ADI converting substrate arginine into product citrulline is so fast that it is undetectable with the colorimetric assay. To get the most accurate K_m value, no more than 10% of the initial substrate should be converted, but with an efficient enzyme, it is very difficult to satisfy this rule. One can reduce enzyme concentration so that the substrate does not get converted, but this can lead to problems with enzyme stability when the enzyme is very diluted in solution. The ideal case is to have an assay that measures substrate concentration compared to product concentration, which is the way that the ADI colorimetric assay is done. The K_m of nanoparticle ADI was not tested because there is no good way of quantifying the nanoparticles and enzyme concentration inside the particles.

The measured activity of native, PEGylated, and nanoparticle ADI were used to understand and model the way the different formulations might behave in the bloodstream, prior to *in vivo* studies. The last test needed before moving forward with an *in vivo* study was to test the enzyme efficacy on cells *in vitro*. For that reason, assays testing the effects of ADI dosing on cell viability were carried out with a pancreatic cancer cell line, PANC-1, which is determined to be ASS(-), and a colorectal cancer cell line, DLD-1, which is determined to be ASS(+). From

Chapter 1, it was explained that ADI as a cancer therapy drug is shown to be sensitive to ASS(-), meaning argininosuccinate synthase is absent in the cell. In ASS(+) cells, the ASS enzyme is present, rendering cells insensitive to ADI. From the results of the assay shown in Figure 6.4, it is very clear that PANC-1 cells are sensitive to ADI treatment because cell viability decreases as ADI concentration increases. Another interesting point is that the IC50 of nanoparticle ADI is lower than PEGylated ADI, which is lower than native ADI. That means that it takes less nanoparticle ADI compared to PEGylated and native ADI to get 50% cell viability. On the other hand, DLD-1 cells, showed no significant changes in viability in response to ADI addition. This was as expected, based on the fact that DLD-1 cells are ASS(+). As shown in Figure 6.4, regardless of the concentration of ADI and formulation, the DLD-1 cell viability stays close to 100%.

Cell viability was measured in this assay with Promega's CellTiter-Glo 2.0 assay reagent, which reacts with ATP to produce a signal. The mechanism of how the reagent works is explained in Figure 6.7. Living cells produce ATP, contributing to the assay signal. Mono-oxygenation of luciferin is catalyzed by the enzyme in the reagent luciferase, in the presence of magnesium, ATP, and oxygen to create light for luminescent detection. Relative cell viability was calculated based on the luminescence of ADI treated cells relative to non-ADI treated cells.

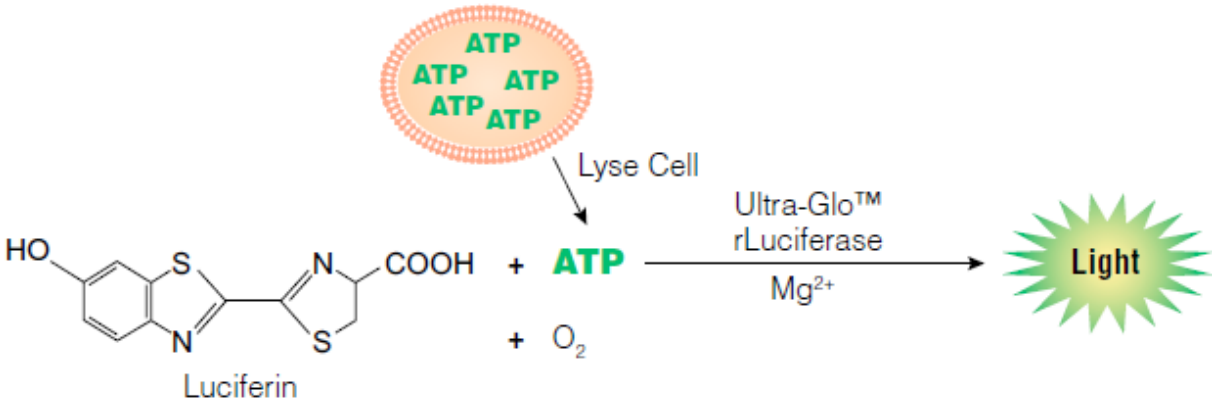

Figure 6.7: Overview of CellTiter-Glo 2.0 Assay Principle, taken from Promega CellTiter-Glo 2.0 assay protocol.

6.5.2 *In vivo* Comparison between the Different Formulations

To determine the pharmacodynamics (PD) of the *in vivo* study of comparing different formulations and routes of administration, mass spectrometry was used to precisely quantify the concentration of arginine and citrulline in the serum. First, the proteins were precipitated out of the plasma sample. Then, the serum sample was passed through a reversed phase column that binds to any polar molecules, which was then hooked up to the triple quadrupole mass spectrometry. There, the molecules of interest, arginine and citrulline, were determined and detected, respectively. The lower levels of quantitation (LLOQ) for the analytes were 0.750 µM for arginine and 1.50 µM for citrulline, respectively. In addition, the calibration standards range were: 0.750 – 600 µM for arginine and 1.50 – 1,200 µM for citrulline. The triple quadrupole mass spectrometer of Q1 → Q3 transitions for arginine was 175.09 m/z → 70.10 m/z, for citrulline was 176.15 m/z → 159.15 m/z, for $^{15}N_4$-Arginine was 179.15 m/z → 71.10 m/z, and for (5-^{13}C, 4,4,5,5-D_4)-Citrulline was 181.15 m/z → 164.00 m/z. In the Q2 transition of the triple quadrupole mass spectrometry, the parent ion collides with nitrogen gas to create fragments or

product ions. This entire process is illustrated in Figure 6.8. The final part of the measurement process is the ion particle counter detector that counts the number of ions per sample.

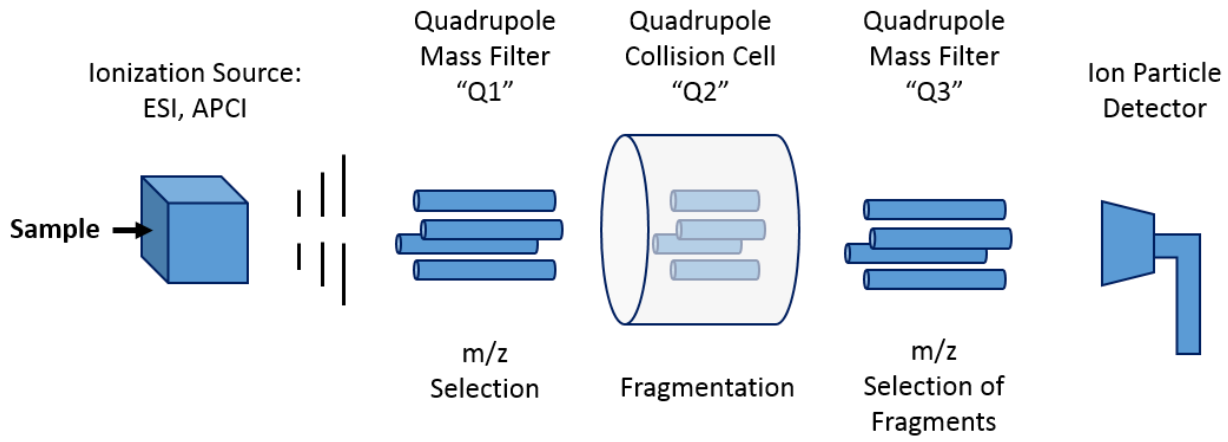

Figure 6.8: Schematic of a Triple Quadrupole Mass Spectrometry [140]

From the measured arginine levels, native ADI is only able to deplete arginine in the blood for about 24 hours before it is cleared out of the system. Multiple injections following the first dose did not deplete arginine levels, most likely due to αADI antibody being produced by the immune system. For PEGylated ADI, the arginine levels were depleted for 1 week without any αADI antibody being produced, with the exception of 1 mouse. This mouse had arginine level return to about 75% of baseline, which indicates most likely there were αADI antibodies generated in this mouse. This also showed that each body system responds differently to the drug. Subsequent doses of PEGylated ADI were able to maintain low levels of blood arginine. After the third dose on Day 14, arginine level remained low for a week, but it slowly bounced back to baseline levels after an additional week without dosing. Therefore, it looks like αADI antibody might have been slowly generated and began to neutralize the PEGylated ADI in the

bloodstream. Another possibility is that the PEGylated enzyme was removed by other body clearance mechanisms or the PEGylated enzyme was degraded.

For the nanoparticle ADI, doses of nanoparticle were reduced from the initial 2 mg/kg to 1 mg/kg because after the first injection via IV, two mice were instantly killed. Therefore, dose reduction was done as a precautionary measure to reduce silica toxicity, which was the initial assumption for the deaths. From the results, IV injection of nanoparticle ADI still saw efficacy after Day 1, but on Day 4, the arginine levels crept back to baseline. Subsequent IV injections eventually killed all the mice by Day 14. It was unlikely that the cause of death for these mice was silica toxicity, because the amount of silica injected was far less than the silica toxicity limit in animals. We suspect that the reason for the mouse deaths is that nanoparticle ADI aggregated after injection into the vein, causing the veins to clog completely. This likely occurred because the silica nanoparticles were not PEG conjugated on the surface, which can lead to particle aggregation from having biomolecules attracted on the silica surface.

A similar trend in *in vivo* was apparent in IM injection of the nanoparticle ADI, where arginine levels rose back to baseline by Day 4. As for IM injections, none of the mice died for the entire study period of 28 days. However, arginine levels did not drop to the lowest levels seen with IV injection of the drug. One possible reason why the arginine levels were not as low as compared to IV injection is that there are less blood vessels in the muscles. Since these silica nanoparticles are 200 – 300 nm and are sticky in nature, they may be trapped in the muscle and take a long time to diffuse into the bloodstream. To get an idea, average mouse capillary blood vessel ranges from 3 – 10 μm in diameter [141, 142]. Additionally, blood draw on Day 28 revealed that arginine levels in the blood were lower than baseline. This could mean that the nanoparticles are seeing the blood from the muscles or that these nanoparticles exploded or

degraded and the native ADIs encapsulated were slowly released. It is difficult to draw conclusions from these results without fluorescent tagging the nanoparticles and the ADI enzyme inside that would allow us to trace both within the body.

The citrulline level curves should theoretically be inversely proportional to the arginine level curves, as 1 arginine molecule gets converted to 1 citrulline molecule. However, as shown in the figures, this is not the case. Citrullline levels spiked up significantly compared to the depleted arginine. The hypothesis behind this is that when there are no arginine around, the body would want to make more arginine. To make arginine, the enzyme argininosuccinate synthase (ASS) needs citrulline as the substrate. As a result, citrulline is being mass produced in the gut to feed the ASS enzyme. Moreover, ASS deficient cells causes citrulline to not be able to be converted, which contributes to the high levels of citrulline. This is partly why theoretically the depletion of 1 arginine molecule should result in 1 citrulline molecule formed, but from the results, 1 arginine molecule depleted it creates 3 to 5 molecules of citrulline. At least the overall trend is consistent, where the low points on the arginine curve are where citrulline is at its highest points and vice versa.

Analyzing the arginine and citrulline levels allows us to understand and compare the pharmacodynamics (PD) of the native, PEGylated, and nanoparticle ADI. Their pharmacokinetics (PK) was not the main focus of this initial mice study. Nonetheless, from the PD data, one can get a brief idea of what data from a PK experiment would be like.

6.6 Conclusion

To sum this chapter up, a comparison of native, PEGylated, and nanoparticle ADI *in vitro* and *in vivo* was performed successfully. The endotoxin levels of these samples were well under

the safety limit of 1 EU/mg. Their enzyme activity were tested after endotoxin treatment to verify that they are still active. The αADI antibody neutralization experiment showed that at 1280 nM αADI antibody incubation, the native enzyme is almost completely neutralized with the lowest enzyme activity, followed by PEGylated ADI, and finally nanoparticle ADI, which retains the most enzyme activity. This shows that PEGylation protects ADI slightly and the nanoparticle provides the most protection. This was followed by testing of the K_m for both native and PEGylated ADI to see if PEGylation affected the kinetics of the enzyme, which the results showed were both less than 10 μM. Then, a cell viability assay was done on PANC-1 and DLD-1 cell lines to test the concept that ASS(-) cell lines are sensitive to ADI treatment, while ASS(+) cell lines are not sensitive to ADI treatment. The results supported this, with the viability of the ASS(-) cell line (PANC-1) showing a negative dose-response to ADI treatment. In this cell line, the differences between ADI formulations could be seen in the different IC50 values. Nanoparticle ADI, PEGylated ADI, and native ADI exhibited the lowest to highest IC50, respectively.

From all the different *in vitro* tests, the nanoparticle formulation showed the greatest promise. An animal study conducted in mice to compare the 2 different formulations, PEGylated versus nanoparticle, along with 2 different routes of administration, intravenous versus intramuscular. This initial study showed that the nanoparticle formulation still requires further adjustments and fine-tuning, as seen in observed toxicity and death effects and the return to baseline of arginine levels after Day 4 of administration. Given the promising results from *in vitro* testing as compared to PEGylated ADI, we believe that further development of the nanoparticle ADI platform is an avenue still worth pursuing.

6.7 Acknowledgements

This chapter and its methods were developed and owned by Polaris Pharmaceuticals Inc., San Diego, California. Collaborators for this development: Jason (Li-Chang) Chen, Grace (Ting-Yu) Chang, Richard Hickey, Ya-San Yeh, Mukanth Vaidyanathan, Jim Thomson, and Sadik Esener. The dissertation author was the primary investigator and author of this material.

Chapter 7: Conclusions and Future Directions

7.1 Conclusions

To summarize, this dissertation has described the synthesis and purification of recombinant *Mycoplasma hominis* native arginine deiminase. Taking the purified native ADI, the PEGylation process was developed and PEGylated arginine deiminase was also successfully synthesized. The next formulation was to encapsulate the native ADI into synthetic hollow enzyme loaded nanospheres (SHELS). Unfortunately, synthesis of SHELS ADI was not a robust enough process; therefore, silica coated liposome ADI was developed and synthesized instead. The comparison between the different formulations: native, PEGylated, and silica coated liposome encapsulated ADI, in *in vitro* settings showed that there are definite benefits to PEGylation and encasement of ADI in liposomes to create enzyme-loaded nanoparticles. Most noticeably, the antibody neutralization experiment demonstrated that nanoparticle ADI protects the immunogenic native ADI from being neutralized by αADI antibodies and losing its enzyme activity. The PEG surrounding the ADI creates a temporary protection layer in which slows down the neutralization process. Additionally, from a cell viability assay, it was shown that the different formulations of ADI all still had efficacy inducing cancer cell death.

The scientific contributions in this dissertation include the pharmacodynamics and pharmacokinetics comparison between native, PEGylated, and nanoparticle ADI. More specifically, the advantages of silica coated liposome encapsulated ADI found in this dissertation are that this formulation (1) protects the immunogenic ADI from being neutralized by the antibody, (2) keeps the enzyme activity from being unperturbed when encapsulated inside the nanoparticle compared to a loss of half of ADI enzyme activity after PEGylation, (3) shows

better efficacy in PANC-1 cancer cells compared to native and PEGylated forms of ADI, and (4) overall exhibits better activity compared to native and PEGylated ADI *in vitro*. As the current standard formulation for enzyme therapy is PEGylation, this formulation offers a promising direction for improvement.

7.2 Future Directions

Additional future work to be conducted includes quantifying the enzyme concentration in each silica coated liposome nanoparticle and understanding the pharmacokinetics of these silica coated liposome nanoparticles, including its biodistribution in the body, its clearance mechanism, and the stability of the nanoparticle and its encapsulated enzyme. Further animal studies will also be conducted to test tumor shrinkage in immunized mice to determine the efficacy of the drug. Targeting specific tumor types can be exploited by testing different targeting agents that can be conjugated on the surface of these silica coated liposome particles. Additionally, optimization of silica coated liposome ADI drug administration route, dose strength, and its dose frequency will need to be determined based on selected specific tumor types and to address risk factors. Depending on the results, more formulation development of the nanoparticle will be needed for ADI. Eventually, the goal is to create a finalized formulation silica coated liposome encapsulated ADI that can be robustly scaled up for mass production.

Finally, the characterization of the silica liposome nanoparticles described will need to meet the standards for pre-clinical studies by the National Cancer Institute (NCI), National Institute of Standards and Technology (NIST), and Food and Drug Administration (FDA). These three groups have established the Nanotechnology Characterization Lab (NCL) to run standardized tests that supports toxicology, pharmacology, physiochemistry, and efficacy studies

of nanoparticles in *in vitro* and *in vivo* settings [143]. These tests will assist this nanoparticle drug formulation to meet Pharmaceutical Quality and Chemistry, Manufacturing, and Controls (CMC) guidelines, which includes batch to batch consistency and reproducibility, product stability and characterization, to file for Investigational New Drug (IND) studies

References:

[1] Teixeira, C. S. S.; Fernandes, H. S.; Fernandes, P. A.; Ramos, M. J.; Cerqueira, N. M.F.S.A. Cancer Therapies Based on Enzymatic Amino Acid Depletion. *Nanostructures for Cancer Therapy*. **2017**, 623-651.

[2] Lukey, M. J.; Katt, W. P.; Cerione, R. A. Targeting amino acid metabolism for cancer therapy. *Drug Discovery Today*. **2017**, *22(5)*, 796-804.

[3] Pavlova, N. N.; Thompson, C. B. The Emerging Hallmarks of Cancer Metabolism. *Cell Metabolism*. **2016**, *23(1)*, 27-47.

[4] Warburg, O.; Wind, F.; Negelein, E. The Metabolism of Tumors in the Body. *The Journal of General Physiology*. **1927**, *8(6)*, 519-530.

[5] Eagle, H. Nutrition Needs of Mammalian Cells in Tissue Culture. *Science*. **1955**, *122(3168)*, 501-504.

[6] Jain, M.; Nilsson, R.; Sharma, S.; Madhusudhan, N.; Kitami, T.; Souza, A. L.; Kafri, R. Kirschner, M. W.; Clish, C. B.; Mootha, V. K. Metabolite Profiling Identifies a Key Role for Glycine in Rapid Cancer Cell Proliferation. *Science*. **2012**, *336(6084)*, 1040-1044.

[7] Hosios, A. M.; Hecht, V. C.; Danai, L. V.; Johnson, M. O.; Rathmell, J. C.; Steinhauser, M. L.; Manalis, S. R.; Vander Heiden, M. G. Amino Acids Rather than Glucose Account for the Majority of Cell Mass in Proliferating Mammalian Cells. *Developmental Cell*. **2016**, *36(5)*, 540-549.

[8] Cantor, J. R.; Panayiotou, V.; Agnello, G.; Georgiou, G.; Stone, E. M. Engineering Reduced-Immunogenicity Enzymes for Amino Acid Depletion Therapy in Cancer. *Methods in Enzymology*. **2012**, *502*, 291-319.

[9] Dinndorf, P. A.; Gootenberg, J.; Cohen, M. H.; Keegan, P.; Pazdur, R. FDA Drug Approval Summary: Pegaspargase (Oncaspar) for the First-Line Treatment of Children with Acute Lymphoblastic Leukemia (ALL). *The Oncologist*. **2007**, *12(8)*, 991-998.

[10] Dillon, B. J.; Prieto, V. G.; Curley, S. A.; Ensor, C. M.; Holtsberg, F. W.; Bomalaski, J. S.; Clark, M. A. Incidence and Distribution of Argininosuccinate Synthetase Deficiency in Human Cancers: A Method for Identifying Cancers Sensitive to Arginine Deprivation. *Cancer*. **2004**, *100(4)*, 826-833.

[11] Rogers, Q. R.; Visek, W. J. Metabolic Role of Urea Cycle Intermediates: Nutritional and Clinical Aspects: Introduction. *The Journal of Nutrition*. **1985**, *115(4)*, 505-508.

[12] Klein, D.; Morris, D. R. Increased arginase activity during lymphocyte mitogenesis. *Biochemical and Biophysical Research Communications*. **1978**, *81(1)*, 199-204.

[13] Haines, R. J.; Pendleton, L. C.; Eichler, D. C. Argininosuccinate synthase: at the center of arginine metabolism. *International Journal of Biochemistry and Molecular Biology*. **2011**, *2(1)*, 8-23.

[14] Castillo, L.; Chapman, T. E.; Sanchez, M.; Yu, Y. M.; Burke, J. F.; Ajami, A. M.; Vogt, J.; Young, V. R. Plasma arginine and citrulline kinetics in adults given adequate and arginine-free diets. *PNAS*. **1993**, *90(16)*, 7749-7753.

[15] Reeds, P. J. Dispensable and Indispensable Amino Acids for Humans. *The Journal of Nutrition*. **2000**, *130(7)*, 1835S-1840S.

[16] Feun, L. G.; Kuo, M. T.; Savaraj, N. Arginine deprivation in cancer therapy. *Current Opinion in Clinical Nutrition and Metabolic Care*. **2015**, *18(1)*, 78-82.

[17] Shen, L. J.; Lin, W. C.; Beloussow, K.; Shen, W. C. Resistance to the anti-proliferative activity of recombinant arginine deiminase in cell culture correlates with the endogenous enzyme, argininosuccinate synthetase. *Cancer Letters*. **2003**, *191(2)*, 165-170.

[18] Wheatley, D. N.; Campbell, E. Arginine deprivation, growth inhibition and tumour cell death: 3. Deficient utilization of citrulline by malignant cells. *British Journal of Cancer*. **2003**, *89*, 573-576.

[19] Savaraj, N.; You, M.; Wu, C.; Wangpaichitr, M.; Kuo, M. T.; Feun, L. G. Arginine Deprivation, Autophagy, Apoptosis (AAA) for the Treatment of Melanoma. *Current Molecular Medicine*. **2010**, *10(4)*, 405-412.

[20] Dillon, B. J.; Holtsberg, F. W.; Ensor, C. M.; Bomalaski, J. S.; Clark, M. A. Biochemical characterization of the arginine degrading enzymes arginase and arginine deiminase and their effect on nitric oxide production. *Medical Science Monitor*. **2002**, *8(7)*, BR248-253.

[21] Ensor, C. M.; Holtsberg, F. W.; Bomalaski, J. S.; Clark, M. A. Pegylated Arginine Deiminase (ADI-SS PEG 20,000 mw) Inhibits Human Melanomas and Hepatocellular Carcinomas *in Vitro* and *in Vivo*. *Cancer Research*. **2002**, *62(19)*, 5443-5450.

[22] Qiu, F.; Chen, Y. R.; Liu, X.; Chu, C. Y.; Shen, L. J.; Xu, J.; Gaur, S.; Forman, H. J.; Zhang, H.; Zheng, S.; Yen, Y.; Huang, J.; Kung, H. J.; Ann, D. K. Arginine Starvation Impairs Mitochondrial Respiratory Function in ASS1-Deficient Breast Cancer Cells. *Science Signaling*. **2014**, *7(319)*, 1-17.

[23] Ni, Y.; Schwaneberg, U.; Sun, Z. H. Arginine deiminase, a potential anti-tumor drug. *Cancer Letters*. **2008**, *261(1)*, 1-11.

[24] Feun, L.; Savaraj, N. Pegylated arginine deiminase: a novel anticancer enzyme agent. *Expert Opinion on Investigational Drugs*. **2006**, *15(7)*, 815-822.

[25] Feun, L.; You, M.; Wu, C. J.; Kuo, M. T.; Wangpaichitr, M.; Spector, S.; Savaraj, N. Arginine Deprivation as a Targeted Therapy for Cancer. *Current Pharmaceutical Design*. **2008**, *14(11)*, 1049-1057.

[26] Bowles, T. L.; Kim, R.; Galante, J.; Parsons, C. M.; Virudachalam, S.; Kung, H. J.; Bold, R. J. Pancreatic cancer cell lines deficient in argininosuccinate synthetase are sensitive to arginine deprivation by arginine deiminase. *International Journal of Cancer*. **2008**, *123(8)*, 1950-1955.

[27] Kim, R. H.; Coates, J. M.; Bowles, T. L.; McNerney, G. P.; Sutcliffe, J.; Jung, J. U.; Gandour-Edwards, R.; Chuang, F. Y. S.; Bold, R. J.; Kung, H. J. Arginine Deiminase as a Novel Therapy for Prostate Cancer Induces Autophagy and Caspase-Independent Apoptosis. *Cancer Research*. **2009**, *69(2)*, 700-708.

[28] Kelly, M. P.; Jungbluth, A. A.; Wu, B. W.; Bomalaski, J.; Old, L. J.; Ritter, G. Arginine deiminase PEG20 inhibits growth of small cell lung cancers lacking expression of argininosuccinate synthetase. *British Journal of Cancer*. **2012**, *106(2)*, 324-332.

[29] Huang, C. C.; Tsai, S. T.; Kuo, C. C.; Chang, J. S.; Jin, Y. T.; Chang, J. Y.; Hsiao, J. R. Arginine deprivation as a new treatment strategy for head and neck cancer. *Oral Oncology*. **2012**, *48(12)*, 1227-1235.

[30] Delage, B.; Luong, P.; Maharaj, L.; O'Riain, C.; Syed, N.; Crook, T.; Hatzimichael, E.; Papoudou-Bai, A.; Mitchell, T. J.; Whittaker, S. J.; Cerio, R.; Gribben, J.; Lemoine, N.; Bomalaski, J.; Li, C. F.; Joel, S.; Fitzgibbon, J.; Chen, L. T.; Szlosarek, P. W. Promoter methylation of argininosuccinate synthetase-1 sensitises lymphomas to arginine deiminase treatment, autophagy and caspase-dependent apoptosis. *Cell Death and Disease*. **2012**, *3*, e342, 1-9.

[31] Huang, H. Y.; Wu, W. R.; Wang, Y. H.; Wang, J. W.; Fang, F. M.; Tsai, J. W.; Li, S. H.; Hung, H. C.; Yu, S. C.; Lan, J.; Shiue, Y. L.; Hsing, C. H.; Chen, L. T.; Li, C. F. *ASS1* as a Novel Tumor Suppressor Gene in Myxofibrosarcomas: Aberrant Loss via Epigenetic DNA Methylation Confers Aggressive Phenotypes, Negative Prognostic Impact, and Therapeutic Relevance. *Human Cancer Biology*. **2013**, *19(11)*, 1-12.

[32] Feun, L. G.; Marini, A.; Walker, G.; Elgart, G.; Moffat, F.; Rodgers, S. E.; Wu, C. J.; You, M.; Wangpaichitr, M.; Kuo, M. T.; Sisson, W.; Jungbluth, A. A.; Bomalaski, J.; Savaraj, N. Negative argininosuccinate synthetase expression in melanoma tumours may predict clinical benefit from arginine-depleting therapy with pegylated arginine deiminase. *British Journal of Cancer*. **2012**, *106(9)*, 1481-1485.

[33] Syed, N.; Langer, J.; Janczar, K.; Singh, P.; Lo Nigro, C.; Lattanzio, L.; Coley, H. M.; Hatzimichael, E.; Bomalaski, J.; Szlosarek, P.; Awad, M.; O'Neil, K.; Roncaroli, F.; Crook, T. Epigenetic status of argininosuccinate synthetase and argininosuccinate lyase modulates autophagy and cell death in glioblastoma. *Cell Death and Disease*. **2013**, *4*, e458, 1-11.

[34] Delage, B.; Fennell, D. A.; Nicholson, L.; McNeish, I.; Lemoine, N. R.; Crook, T.; Szlosarek, P. W. Arginine deprivation and argininosuccinate synthetase expression in the treatment of cancer. *International Journal of Cancer*. **2010**, *126(12)*, 2762-2772.

[35] Wu, G.; Morris Jr., S. M. Arginine metabolism: nitric oxide and beyond. *Biochemical Journal*. **1998**, *336(1)*, 1-17.

[36] Yerushalmi, H. F.; Besselsen, D. G.; Ignatenko, N. A.; Blohm-Mangone, K. A.; Padilla-Torres, J. L.; Stringer, D. E.; Guillen, J. M.; Holubec, H.; Payne, C. M.; Gerner, E. W. Role of Polyamines in Arginine-Dependent Colon Carcinogenesis in *ApcMinI+* Mice. *Molecular Carcinogenesis*. **2006**, *45(10)*, 764-773.

[37] Yerushalmi, H. F.; Besselsen, D. G.; Ignatenko, N. A.; Blohm-Mangone, K. A.; Padilla-Torres, J. L.; Stringer, D. E.; Cui, H..; Holubec, H.; Payne, C. M.; Gerner, E. W. The Role of NO Synthases in Arginine-Dependent Small Intestinal and Colonic Carcinogenesis. *Molecular Carcinogenesis*. **2006**, *45(2)*, 93-105.

[38] Gilroy, E. The Influence of Arginine upon the Growth Rate of a Transplantable Tumour in the Mouse. *Biochemical Journal*. **1930**, *24(3)*, 589-595.

[39] Yeatman, T. J.; Risley, G. L.; Brunson, M. E. Depletion of Dietary Arginine Inhibits Growth of Metastatic Tumor. *Archives of Surgery*. **1991**, *126(11)*, 1376-1382.

[40] Wheatley, D. N. Controlling cancer by restricting arginine availability–arginine-catabolizing enzymes as anticancer agents. *Anti-Cancer Drugs*. **2004**, *15(9)*, 825-833.

[41] Richards, N. G. J.; Kilberg, M. S. Asparagine Synthetase Chemotherapy. *Annual Review of Biochemistry*. **2006**, *75*, 629-654.

[42] Zuniga, M.; Perez, G.; Gonzalez-Candelas, F. Evolution of arginine deiminase (ADI) pathway genes. *Molecular Phylogenetics and Evolution*. **2002**, *25(3)*, 429-444.

[43] Kim, J. E.; Jeong, D. W.; Lee, H. J. Expression, purification, and characterization of arginine deiminase from *Lactococcus lactis ssp. lactis* ATCC 7962 in *Escherichia coli* BL21. *Protein Expression and Purification*. **2007**, *53(1)*, 9-15.

[44] Glazer, E. S.; Piccirillo, M.; Albino, V.; Giacomo, R. D.; Palaia, R.; Mastro, A. A.; Beneduce, G.; Castello, G.; Rosa, V. D.; Petrillo, A.; Ascierto, P. A.; Curley, S. A.; Izzo, F. Phase II Study of Pegylated Arginine Deiminase for Nonresectable and Metastatic Hepatocellular Carcinoma. *Journal of Clinical Oncology*. **2010**, *28(13)*, 2220-2226.

[45] Ott, P. A.; Carvajal, R. D.; Pandit-Taskar, N.; Jungbluth, A. A.; Hoffman, E. W.; Wu, B. W.; Bomalaski, J. S.; Venhaus, R.; Pan, L.; Old, L. J.; Pavlick, A. C.; Wolchok, J. D. Phase I/II study of pegylated arginine deiminase (ADI-PEG 20) in patients with advanced melanoma. *Investigational New Drugs*. **2013**, *31(2)*, 425-434.

[46] Beloussow, K.; Wang, L.; Wu, J. Ann, D.; Shen, W. C. Recombinant arginine deiminase as a potential anti-angiogenic agent. *Cancer Letters*. **2002**, *183(2)*, 155-162.

[47] Park, I. S.; Kang, S. W.; Shin, Y. J.; Chae, K. Y.; Park, M. O.; Kim, M. Y.; Wheatley, D. N.; Min, B. H. Arginine deiminase: a potential inhibitor of angiogenesis and tumour growth. *British Journal of Cancer*. **2003**, *89(5)*, 907-914.

[48] Yoon, C. Y.; Shim, Y. J.; Kim, E. H.; Lee, J. H.; Won, N. H.; Kim, J. H.; Park, I. S.; Yoon, D. K.; Min, B. H. Renal cell carcinoma does not express argininosuccinate synthetase and is highly sensitive to arginine deprivation *via* arginine deiminase. *International Journal of Cancer*. **2006**, *120(4)*, 897-905.

[49] Zhang, L.; Liu, M.; Jamil, S.; Han, R.; Xu, G. Ni, Y. PEGylation and pharmacological characterization of a potential anti-tumor drug, an engineered arginine deiminase originated from *Pseudomonas plecoglossicida*. *Cancer Letters*. **2015**, *357(1)*, 346-354.

[50] Takaku, H.; Takase, M.; Abe, S. I.; Hayashi, H.; Miyazaki, K. *In vivo* anti-tumor activity of arginine deiminase purified from *Mycoplasma arginini*. *International Journal of Cancer*. **1992**, *51(2)*, 244-249.

[51] Studier, F. W. Protein production by auto-induction in high-density shaking cultures. *Protein Expression and Purification*. **2005**, *41(1)*, 207-234.

[52] Fearon, W. R. The Carbamido Diacetyl Reaction: A Test for Citrulline. *Biochemical Journal*. **1939**, *33(6)*, 902-907.

[53] Mather, A.; Roland, D. The Automated Thiosemicarbazide-Diacetyl Monoxime Method for Plasma Urea. *Clinical Chemistry*. **1969**, *15(5)*, 393-396.

[54] Boyde, T. R. C.; Rahmatullah, M. Optimization of Conditions for the Colorimetric Determination of Citrulline, Using Diacetyl Monoxime. *Analytical Biochemistry*. **1980**, *107(2)*, 424-431.

[55] Knipp, M.; Vasak, M. A Colorimetric 96-Well Microtiter Plate Assay for the Determination of Enzymatically Formed Citrulline. *Analytical Biochemistry*. **2000**, *286(2)*, 257-264.

[56] Duncan, R. Polymer conjugates as anticancer nanomedicines. *Nature Reviews Cancer*. **2006**, *6(9)*, 688-701.

[57] Yang, B. B.; Lum, P. K. Hayashi, M. M.; Roskos, L. K. Polyethylene Glycol Modification of Filgrastim Results in Decreased Renal Clearance of the Protein in Rats. *Journal of Pharmaceutical Sciences*. **2004**, *93(5)*, 1367-1373.

[58] Veronese, F. M.; Pasut, G. PEGylation, successful approach to drug delivery. *Drug Discovery Today*. **2005**, *10(21)*, 1451-1458.

[59] Mehvar, R. Modulation of the Pharmacokinetics and Pharmacodynamics of Proteins by Polyethylene Glycol Conjugation. *Journal of Pharmacy and Pharmaceutical Sciences*. **2000**, *3(1)*, 125-136.

[60] Harris, J. M.; Martin, N. E.; Modi, M. Pegylation: A Novel Process for Modifying Pharmacokinetics. *Clinical Pharmacokinetics*. **2001**, *40(7)*, 539-551.

[61] Smyth Jr., H. F.; Carpenter, C. P.; Weil, C. S. The Chronic Oral Toxicology of the Polyethylene Glycols*. *Journal of the American Pharmaceutical Association*. **1955**, *44(1)*, 27-30.

[62] Harris, J. M.; Chess, R. B. Effect of Pegylation on Pharmaceuticals. *Nature Reviews Drug Discovery*. **2003**, *2*, 214-221.

[63] Webster, R.; Didier, E.; Harris, P.; Siegel, N.; Stadler, J.; Tilbury, L.; Smith, D. PEGylated Proteins: Evaluation of Their Safety in the Absence of Definitive Metabolism Studies. *Drug Metabolism and Disposition*. **2007**, *35(1)*, 9-16.

[64] Burnham, N. Polymers for delivering peptides and proteins. *American Journal of Hospital Pharmacy*. **1994**, *51(2)*, 210-218.

[65] Nucci, M. L.; Shorr, R.; Abuchowski, A. The therapeutic value of poly(ethylene glycol)-modified proteins. *Advanced Drug Delivery Reviews*. **1991**, *6(2)*, 133-151.

[66] Allen, T. M. Liposomes: Opportunities in Drug Delivery. *Drugs*. **1997**, *54(Suppl 4)*, 8-14.

[67] Gobburu, J. V. S.; Tenhoor, C.; Rogge, M. C.; Frazier, D. E.; Thomas, D. Benjamin, C. Hess, D. M.; Jusko, W. J. Pharmacokinetics/Dynames of 5c8, a Monoclonal Antibody to CD154 (CD40 Ligand) Suppression of an Immune Response in Monkeys. *The Journal of Pharmacology and Experimental Therapeutics*. **1998**, *286(2)*, 925-930.

[68] Davis, F. F.; Abuchowski, A.; van Es, T.; Palczuk, N. C.; Chen, R.; Savoca, K.; Wieder, K. Enzyme-Polyethylene Glycol Adducts: Modified Enzymes with Unique Properties. *Enzyme Engineering*. **1978**, 169-173.

[69] Zalipsky, S.; Harris, J. M. Introduction to Chemistry and Biological Applications of Poly(ethylene glycol). *American Chemical Society*. **1997**, 1-15.

[70] Holtsberg, F. W.; Ensor, C. M.; Steiner, M. R.; Bomalaski, J. S.; Clark, M. A. Poly(ethylene glycol) (PEG) conjugated arginine deiminase: effects of PEG formulations on its pharmacological properties. *Journal of Controlled Release*. **2002**, *80(1-3)*, 259-271.

[71] Turecek, P. L.; Bossard, M. J.; Schoetens, F.; Ivens, I. A. PEGylation of Biopharmaceuticals: A Review of Chemistry and Nonclinical Safety Information of Approved Drugs. *Journal of Pharmaceutical Sciences*. **2016**, *105(2)*, 460-475.

[72] Delman, K. A.; Brown, T. D.; Thomas, M.; Ensor, C. M.; Holtsberg, F. W.; Bomalaski, J. S.; Clark, M. A.; Curley, S. A. Phase I/II trial of pegylated arginine deiminase (ADI-PEG20) in unresectable hepatocellular carcinoma. *Journal of Clinical Oncology*. **2005**, *23(16)*, 4139-4139.

[73] Carter, M. C.; Meyerhoff, M. E. Instability of Succinyl Ester Linkages in O2'-Monosuccinyl Cyclic AMP-Protein Conjugates at Neutral pH. *Journal of Immunological Methods*. **1985**, *81(2)*, 245-257.

[74] Greenwald, R. B.; Choe, Y. H.; McGuire, J.; Conover, C. D. Effective drug delivery by PEGylated drug conjugates. *Advanced Drug Delivery Reviews*. **2003**, *55(2)*, 217-250.

[75] Keating, M. J.; Holmes, R.; Lerner, S.; Ho, D. H. L-Asparaginase and PEG Asparaginase – Past, Present, and Future. *Leukemia & Lymphoma*. **1993**, *10(1)*, 153-157.

[76] Graham, M. L. Pegaspargase: a review of clinical studies. *Advanced Drug Delivery Reviews*. **2003**, *55(10)*, 1293-1302.

[77] Park, Y. K.; Abuchowski, A.; Davis, S.; Davis, F. Pharmacology of Escherichia coli-L-asparaginase polyethylene glycol adduct. *Anticancer Research*. **1981**, *1(6)*, 373-376.

[78] Vertegel, A. A.; Reukov, V.; Maximov, V. Enzyme-Nanoparticle Conjugates for Biomedical Applications. *Enzyme Stabilization and Immobilization: Methods and Protocols*. **2011**, *679*, 165-182.

[79] Sun, T.; Zhang, Y. S.; Pang, B.; Hyun, D. C.; Yang, M.; Xia, Y. Engineered Nanoparticles for Drug Delivery in Cancer Therapy. *Angewandte Chemie International Edition*. **2014**, *53(46)*, 12320-12364.

[80] Bulbake, U.; Doppalapudi, S.; Kommineni, N.; Khan, W. Liposomal Formulations in Clinical Use: An Updated Review. *Pharmaceutics*. **2017**, *9(2)*, 12-44.

[81] Slowing, I. I.; Vivero-Escoto, J. L.; Wu, C. W.; Lin, V. S. Y. Mesoporous silica nanoparticles as controlled release drug delivery and gene transfection carriers. *Advanced Drug Delivery Reviews*. **2008**, *60(11)*, 1278-1288.

[82] Xu, Z. P.; Zeng, Q. H.; Lu, G. Q.; Yu, A. B. Inorganic nanoparticles as carriers for efficient cellular delivery. *Chemical Engineering Science*. **2006**, *61(3)*, 1027-1040.

[83] Piras, A. M.; Chiellini, F.; Fiumi, C.; Bartoli, C.; Chiellini, E.; Fiorentino, B.; Farina, C. A new biocompatible nanoparticle delivery system for the release of fibrinolytic drugs. *International Journal of Pharmaceutics*. **2008**, *357(1-2)*, 260-271.

[84] Reddy, M. K.; Labhasetwar, V. Nanoparticle-mediated delivery of superoxide dismutase to the brain: an effective strategy to reduce ischemia-reperfusion injury. *The FASEB Journal*. **2009**, *23*, 1384-1395.

[85] Dziubla, T. D.; Karim, A.; Muzykantov, V. R. Polymer nanocarriers protecting active enzyme cargo against proteolysis. *Journal of Controlled Release*. **2005**, *102(2)*, 427-439.

[86] Cellesi, F.; Tirelli, N. Enzyme Nanoencapsulation in silica gel based nanoparticles: Towards development of novel nanocarriers for enzyme-mediated therapies. *11th Meeting of the UK Polymer Colloid Forum*. **2006**.

[87] Wang, Y.; Caruso, F. Enzyme encapsulation in nanoporous silica spheres. *Chemical Communications*. **2004**, *13*, 1528-1529.

[88] Volodkin, D. V.; Petrov, A. I.; Prevot, M.; Sukhorukov, G. B. Matrix Polyelectrolyte Microcapsules: New System for Macromolecule Encapsulation. *Langmuir*, **2004**, *20(8)*, 3398-3406.

[89] Kumar, R.; Maitra, A. N.; Patanjali, P. K.; Sharma, P. Hollow gold nanoparticles encapsulating horseradish peroxidase. *Biomaterials*. **2005**, *26(33)*, 6743-6753.

[90] Wang, Y.; Caruso, F. Mesoporous Silica Spheres as Supports for Enzyme Immobilization and Encapsulation. *Chemistry of Materials*. **2005**, *17(5)*, 953-961.

[91] Ortac, I.; Simberg, D.; Yeh, Y. S.; Yang, J.; Messmer, B.; Trogler, W. C.; Tsien, R. Y.; Esener, S. Dual-Porosity Hollow Nanoparticles for the Immunoprotection and Delivery of Nonhuman Enzymes. *Nano Letters*. **2014**, *14(6)*, 3023-3032.

[92] Witucki, G. L. A Silane Primer: Chemistry and Applications of Alkoxy Silanes. *Journal of Coatings Technology*. **1993**, *65(822)*, 57-60.

[93] Haynes, W. M. CRC Handbook of Chemistry and Physics. **2014**, *95 ed*.

[94] Wunsch, J. R. Polystyrene: Synthesis, Production and Applications. *Rapra Review Reports*. **2000**, *10(4)*, 6-18.

[95] Butler, G. H.; Kotani, H.; Kong, L.; Frick, M.; Evancho, S.; Stanbridge, E. J.; McGarrity, G. J. Identification and Characterization of Proteinase K-Resistant Proteins in Members of the Class Mollicutes. *Infection and Immunity*. **1991**, *59(3)*, 1037-1042.

[96] Ebeling, W.; Hennrich, N.; Klockow, M.; Metz, H.; Orth, H. D.; Lang, H. Proteinase K from *Tritirachium album* Limber. *European Journal of Biochemistry*. **1974**, *47(1)*, 91-97.

[97] Bangham, A. D.; Horne, R. W. Negative staining of phospholipids and their structural modification by surface-active agents as observed in the electron microscope. *Journal of Molecular Biology*. **1964**, *8(5)*, 660-668.

[98] Horne, R. W.; Bangham, A. D.; Whittaker, V. P. Negatively Stained Lipoprotein Membranes. *Nature*. **1963**, *200*, 1340.

[99] Bangham, A. D.; Horne, R. W. Action of Saponin on Biological Cell Membranes. *Nature*. **1962**, *196*, 952-953.

[100] Akbarzadeh, A.; Rezaei-Sadabady, R.; Davaran, S.; Joo, S. W.; Zarghami, N. Hanifehpour, Y.; Samiei, M.; Kouhi, M.; Nejati-Koshki, K. Liposome: classification, preparation, and applications. *Nanoscale Research Letters*. **2013**, *8(1)*, 102-110.

[101] Olusanya, T. O. B.; Ahmad, R. R. H.; Ibegbu, D. M.; Smith, J. R.; Elkordy, A. A. Liposomal Drug Delivery Systems and Anticancer Drugs. *Molecules*. **2018**, *23(4)*, 907-923.

[102] Li, J.; Wang, X.; Zhang, T.; Wang, C.; Huang, Z.; Luo, X.; Deng, Y. A review on phospholipids and their main applications in drug delivery systems. *Asian Journal of Pharmaceutical Sciences*. **2015**, *10(2)*, 81-98.

[103] McMullen, T. P. W.; McElhaney, R. N. New aspects of the interaction of cholesterol with dipalmitoylphosphatidylcholine bilayers as revealed by high-sensitivity differential scanning calorimetry. *Biochimica et Biophysica Acta*. **1995**, *1234(1)*, 90-98.

[104] Sada, E.; Katoh, S.; Terashima, M.; Tsukiyama, K. I. Entrapment of an Ion-Dependent Enzyme into Reverse-Phase Evaporation Vesicles. *Biotechnology and Bioengineering*. **1988**, *32(6)*, 826-830.

[105] Bangham, A. D. Liposomes: the Babraham connection. *Chemistry and Physics of Lipids*. **1993**, *64(1-3)*, 275-285.

[106] Malam, Y.; Loizidou, M.; Seifalian, A. M. Liposomes and nanoparticles: nanosized vehicles for drug delivery in cancer. *Trends in Pharmacological Sciences*. **2009**, *30(11)*, 592-599.

[107] Atrooz, O. M. Effects of Alkylresorcinolic Lipids Obtained from Acetonic Extract of Jordanian Wheat Grains on Liposome Properties. *International Journal of Biological Chemistry*. **2011**, *5(5)*, 314-321.

[108] Shehata, T.; Ogawara, K. I.; Higaki, K.; Kimura, T. Prolongation of residence time of liposome by surface-modification with mixture of hydrophilic polymers. *International Journal of Pharmaceutics*. **2008**, *359(1-2)*, 272-279.

[109] Garg, T.; Goyal, A. K. Liposomes: Targeted and Controlled Delivery System. *Drug Delivery Letters*. **2014**, *4(1)*, 62-71.

[110] van der Pol, E.; Boing, A. N.; Harrison, P.; Sturk, A.; Nieuwland, R. Classification, Functions, and Clinical Relevance of Extracellular Vesicles. *Pharmacological Reviews*. **2012**, *64(3)*, 676-705.

[111] Mayer, L. D.; Cullis, P. R.; Bally, M. B. The Use of Transmembrane pH Gradient-Driven Drug Encapsulation in the Pharmacodynamic Evaluation of Liposomal Doxorubicin. *Journal of Liposome Research*. **1994**, *4(1)*, 529-553.

[112] Park, J. W.; Hong, K.; Carter, P.; Asgari, H.; Guo, L. Y.; Keller, G. A.; Wirth, C.; Shalaby, R.; Kotts, C.; Wood, W. I.; Papahadjopoulos, D.; Benz, C. C. Development of anti-p185HER2 immunoliposomes for cancer therapy. *PNAS*. **1995**, *95(5)*, 1327-1331.

[113] Immordino, M. L.; Dosio, F.; Cattel, L. Stealth liposomes: review of the basic science, rationale, and clinical applications, existing and potential. *International Journal of Nanomedicine*. **2006**, *1(3)*, 297-315.

[114] Nohria, A.; Rubin, R. H. Cytokines as potential vaccine adjuvants. *Cytokines in the Treatment of Infectious Diseases*. **1994**, 261-269.

[115] Herzog, C.; Hartmann, K.; Kunzi, V.; Kursteiner, O.; Mischler, R.; Lazar, H.; Gluck, R. Eleven years of Inflexal V–a virosomal adjuvanted influenza vaccine. *Vaccine*. **2009**, *27(33)*, 4381-4387.

[116] New, R. R. C.; Chance, M. L.; Heath, S. Antileishmanial activity of amphotericin and other antifungal agents entrapped in liposomes. *Journal of Antimicrobial Chemotherapy*. **1981**, *8(5)*, 371-381.

[117] Denning, D. W.; Lee, J. Y.; Hostetler, J. S.; Pappas, P.; Kauffman, C. A.; Dewsnup, D. H.; Galgiani, J. N.; Graybill, J. R.; Sugar, A. M.; Catanzaro, A.; Gallis, H.; Perfect, J. R.; Dockery, B.; Dismukes, W. E.; Stevens, D. A. NIAID mycoses study group multicenter trial of oral itraconazole therapy for invasive aspergillosis. *The American Journal of Medicine*. **1994**, *97(2)*, 135-144.

[118] Onyeji, C. O.; Nightingale, C. H.; Marangos, M. N. Enhanced Killing of Methicillin-Resistant *Staphylococcus aureus* in Human Macrophages by Liposome-Entrapped Vancomycin and Teicoplanin. *Infection*. **1994**, *22(5)*, 338-342.

[119] Glantz, M. J.; Jaeckle, K. A.; Chamberlain, M. C.; Phuphanich, S.; Recht, L.; Swinnen, L. J.; Maria, B.; LaFollette, S.; Schumann, G. B.; Cole, B. F.; Howell, S. B. A Randomized Controlled Trial Comparing Intrathecal Sustained-release Cytarabine (DepoCyt) to Intrathecal Methotrexate in Patients with Neoplastic Meningitis from Solid Tumors. *Clinical Cancer Research*. **1999**, *5(11)*, 3394-3402.

[120] Mo, R.; Jiang, T.; Di, J.; Tai, W.; Gu, Z. Emerging micro- and nanotechnology based synthetic approaches for insulin delivery. *Chemical Society Reviews*. **2014**, *43(10)*, 3595-3629.

[121] Morgan, J. R.; Williams, L. A.; Howard, C. B. Technetium-labelled liposome imaging for deep-seated infection. *The British Journal of Radiology*. **1985**, *58(685)*, 35-39.

[122] Williams, B. D.; O'Sullivan, M. M.; Saggu, G. S.; Williams, K. E.; Williams, L. A.; Morgan, J. R. Imaging in rheumatoid arthritis using liposomes labelled with technetium. *British Medical Journal*. **1986**, *293(6555)*, 1143-1144.

[123] Ogihara, I.; Kojima, S.; Jay, M. Differential Uptake of Gallium-67-Labeled Liposomes Between Tumors and Inflammatory Lesions in Rats. *Journal of Nuclear Medicine*. **1986**, *27(8)*, 1300-1307.

[124] Allen, T. M.; Chonn, A. Large unilamellar liposomes with low uptake into the reticuloendothelial system. *FEBS Letters*. **1987**, *223(1)*, 42-46.

[125] Zhang, L.; Granick, S. How to Stabilize Phospholipid Liposomes (Using Nanoparticles). *Nano Letters*. **2006**, *6(4)*, 694-698.

[126] Hoffmann, F.; Cornelius, M.; Morell, J.; Froba, M. Silica-Based Mesoporous Organic–Inorganic Hybrid Materials. *Angewandte Chemie International Edition*. **2006**, *45(20)*, 3216-3251.

[127] Sun, Q.; Vrieling, E. G.; van Santen, R. A.; Sommerdijk, N. A. J. M. Bioinspired synthesis of mesoporous silicas. *Current Opinion in Solid State and Materials Science*. **2004**, *8(2)*, 111-120.

[128] Raman, N. K.; Anderson, M. T.; Brinker, C. J. Template-Based Approaches to the Preparation of Amorphous, Nanoporous Silicas. *Chemistry of Materials*. **1996**, *8(8)*, 1682-1701.

[129] Knecht, M. R.; Wright, D. W. Amine-Terminated Dendrimers as Biomimetic Templates for Silica Nanosphere Formation. *Langmuir*. **2004**, *20(11)*, 4728-4732.

[130] Sila, M.; Au, S.; Weiner, N. Effects of Triton X-100 concentration and incubation temperature on carboxyfluorescein release from multilamellar liposomes. *Biochimica et Biophysica Acta*. **1986**, *859(2)*, 165-170.

[131] Magalhaes, P. O.; Lopes, A. M.; Mazzola, P. G.; Rangel-Yagui, C.; Penna, T. C. V.; Pessoa Jr., A. Methods of Endotoxin Removal from Biological Preparations: a Review. *Journal of Pharmaceutical Sciences*. **2007**, *10(3)*, 388-404.

[132] Anspach, F. B. Endotoxin removal by affinity sorbents. *Journal of Biochemical and Biophysical Methods*. **2001**, *49(1-3)*, 665-681.

[133] Erridge, C.; Bennett-Guerrero, E.; Poxton, I. R. Structure and function of lipopolysaccharides. *Microbes and Infection*. **2002**, *4(8)*, 837-851.

[134] Ogikubo, Y.; Norimatsu, M.; Noda, K.; Takahashi, J.; Inotsume, M.; Tsuchiya, M.; Tamura, Y. Evaluation of the bacterial endotoxin test for qualification of endotoxin contamination of porcine vaccines. *Biologicals*. **2004**, *32(2)*, 88-93.

[135] Vagenende, V.; Ching, T. J.; Chua, R. J.; Gagnon, P. Allantoin as a solid phase adsorbent for removing endotoxins. *Journal of Chromatography A*. **2013**, *1310*, 15-20.

[136] Aida, Y.; Pabst, M. J. Removal of endotoxin from protein solutions by phase separation using Triton X-114. *Journal of Immunological Methods*. **1990**, *132(2)*, 191-195.

[137] Lopes, A. M.; Magalhaes, P. O.; Mazzola, P. G.; Rangel-Yagui, C. O.; de Carvalho, J. C. M.; Penna, T. C. V.; Pessoa Jr, A. LPS Removal from an E. Coli Fermentation Broth Using Aqueous Two-Phase Micellar System. *Biotechnology Progress*. **2010**, *26(6)*, 1644-1653.

[138] Petsch, D.; Anspach, F. B. Endotoxin removal from protein solutions. *Journal of Biotechnology*. **2000**, *76(2-3)*, 97-119.

[139] Kucki, M.; Cavelius, C.; Kraegeloh, A. Interference of silica nanoparticles with the traditional *Limulus* amebocyte lysate gel clot assay. *Innate Immunity*. **2014**, *20(3)*, 327-336.

[140] Yost, R. A.; Enke, C. G. Triple Quadrupole Mass Spectrometry for Direct Mixture Analysis and Structure Elucidation. *Analytical Chemistry*. **1979**, *51(12)*, 1251-1264.

[141] Wiedeman, M. P. Dimensions of Blood Vessels from Distributing Artery to Collecting Vein. *Circulation Research*. **1963**, *12(4)*, 375-378.

[142] Zweifach, B. W.; Kossmann, C. E. Micromanipulation of Small Blood Vessels in the Mouse. *American Journal of Physiology*. **1937**, *120(1)*, 23-35.

[143] Etheridge, M. L.; Campbell, S. A.; Erdman, A. G.; Haynes, C. L.; Wolf, S. M.; McCullough, J. The big picture on nanomedicine: the state of investigational and approved nanomedicine products. *Nanomedicine: Nanotechnology, Biology, and Medicine*. **2013**, *9(1)*, 1-14.